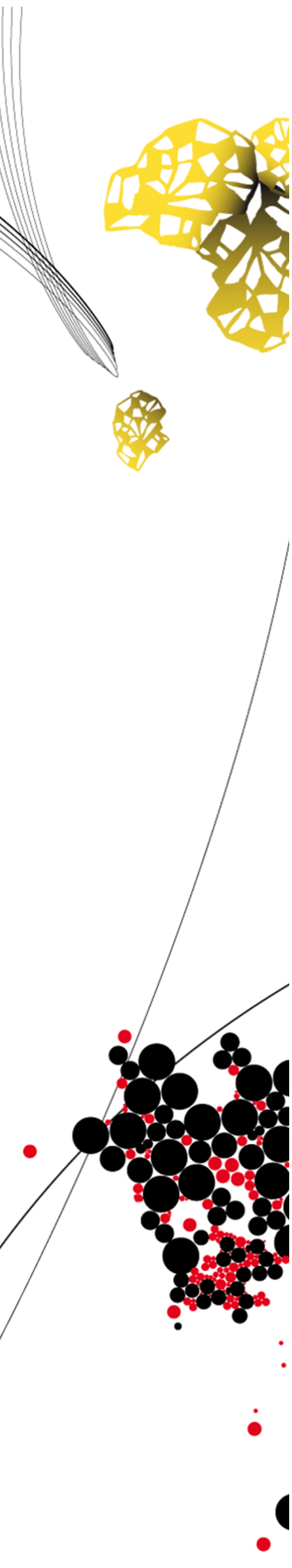

UNIVERSITY OF TWENTE.

Faculty of Engineering Technology
Department of Biomechanical Engineering

The Development of a Cable-driven Variable Stiffness Mechanism Test Bed

Norrasaet Manourat
M-BME
Project done in collaboration with
Robotics & Mechatronics Lab

October 2019
Document number: BW-701

Examination committee:
prof.dr.ir. H.F.J.M. Koopman
A.J. Veale, PhD
dr.ir. G.A. Folkertsma

Acknowledgement

First and foremost, I would like to thank my supervisor and my project coordinator, Allan Veale and Stefan Groothuis for supervising, good advises and assistances in this thesis. Their guidance helped me a lot throughout this master thesis. My sincere thanks also goes to prof. Bart Koopman and dr.ir. Geert Folkertsma for their valuable time to be on my graduation committee. Besides, I would like to prof. Lorenzo Masia and Michele Xiloyannis for their initiation and contribution of this project at the time when they worked in University of Twente. Moreover, I thank all of my friends for their support along my master thesis journey. Last but not least, I would like to thank my family; my dad, mom and brother, for their love and encouragement as always.

Summary

A variable stiffness actuator contributes an interaction with uncertain environment together with substantial robustness of mechanism while a conventional actuator could not carry out. With these benefits, variable stiffness actuators have become an alternative for diverse applications particularly in the field of biorobotics. One design which is usually applied for imitating physiological movement is an antagonistic mechanism. However, bulkiness is a common constraint for the currently used VSA in biorobotics. To reduce size and weight, the cable-driven mechanism has been introduced.The primary goal of this project was to utilize the assistive arm-support exoskeleton, and to that end, both mechanisms have been integrated, proposing a novel cable driven VSA mechanism.

In this study, the development of a cable-driven variable stiffness mechanism test bed is presented. The mechanism is introduced with the cable-driven antagonistic mechanism providing a change of stiffness without varying torque. Variation of stiffness is conducted by a cable-driven system, controlling the pretension of elastic elements which work antagonistically resulting in an equilibrium position. A methodology of design is given along with a primary mathematical model, prototyping and testing. Measurements performed with the test bed show the validity of the theoretical findings, the outcomes satisfy the primary objectives. The stiffness is adaptable with a range of 1.13 Nm/rad to 1.64 Nm/rad. It also brings a constant torque while modulating the stiffness, the measured output displacement for static and dynamic measurement exhibit less than 0.0016 rad and 0.0033 rad, respectively when the stiffness changed by 45.13 %. Moreover, stiffness modulation seems to be qualitatively and quantitatively identical between measurement and simulation (with mean absolute error range of 0.2779 - 0.3355 Nm). Promising results show the possibilities of future work on developing cable-driven variable stiffness actuators by adopting the redesigned this mechanism and applying the actuator to wearable robotic applications.

Contents

Chapter 1

Introduction

Developing a robot that imitates human-like movement is always a challenging task for bio-robotic applications particularly involved with the physiological movement of limbs, i.e., rehabilitation robotics, wearable robotics, exoskeletons, powered prosthetics or bionics. Due to the fact that human movement is complicated by anatomical, physiological and bio-mechanical systems of humans. Furthermore, interaction with human and unpredictable surroundings is also an important concern in the process of development. Therefore, a bio-robot is expected to provide a good and safe performance on assisting users. Considering the safety aspect, in human movement, there is a mechanism to avoid damage from the environment to the human. An adaptability of joint stiffness is a safety mechanism to prevent this unpredictable impact. Keeping in mind the anatomy of humans, the muscles often come and work in pairs called antagonistic muscle pair consisting of antagonist and agonist muscles (as shown in figure 1.1). These muscles work against each other stabilising the position of joint to be at equilibrium position. This balancing muscle's tension also called muscle co-contraction which results in the joint stiffness, the joint is stiffer when the muscles increase their tension. In addition, when the external forces are exerted on the musculoskeletal system, the antagonistic muscle will counteract and make sure the equilibrium position is maintained, compensating disturbances by controlling joint stiffness [1] [2] [3] [4]. With this bio-inspired mechanism, in robotics, joint stiffness control can be duplicated by mechanical implementation. An implementation worth considering is a variable stiffness actuator.

An adjustable compliance actuators or variable stiffness actuators (VSA) have been a recently growing trend in the bio-robotics domain, and this claim is supported by a number of research articles. With the aim of overcoming limitations of the traditional actuators or stiff actuators, VSA has been proposed. The limitation of the stiff actuator is that it lacks of adaptabilities of motion from the external perturbation which can cause a safety issue in human-robot interaction. Human-robot interaction requires advanced adaptability of the springlike presence to mimic biological

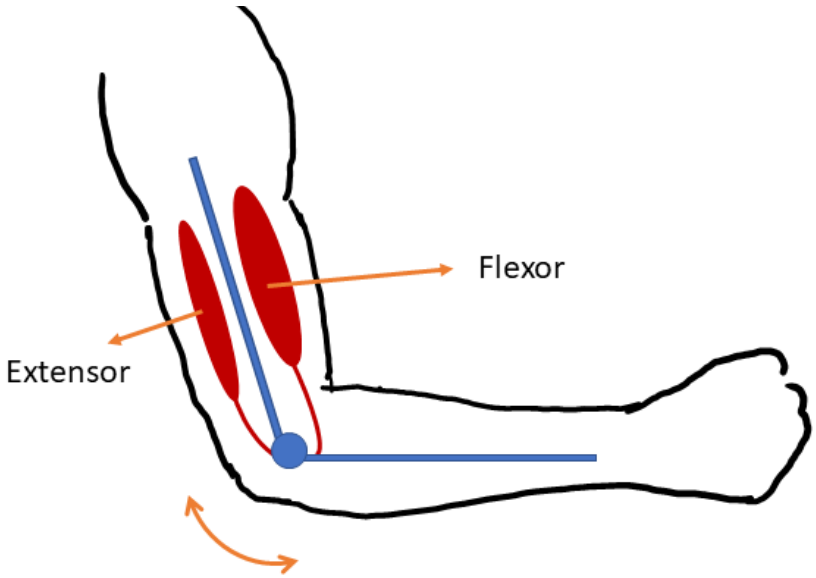

Figure 1.1: Model of antagonistic muscles in musculoskeletal system. To flex the forearm, a flexor muscle acts as an agonist while an extensor muscle is an antagonist.

behaviour preventing adverse events that might arise from this interaction. Additionally, energy efficiency is also another constraint. With the compliance of most of VSAs, the elastic component in its mechanism can store energy. Whereas the classic actuators which are aimed to be as stiff as possible to obtain high accuracy and high bandwidth on trajectory tracking, VSAs have designed and implemented flexible actuation systems allowing a deviation of the equilibrium position due to the external force. The position of the actuator at which the actuator produces zero force or zero torque is described in the equilibrium situation of a compliant actuator, this concept is a specific idea which does not exist for the non-compliant actuators. With this compliance adaptability, therefore, three common advantages can be identified in brief; safety, robustness and energy efficiency. The VSAs offer safety in the operations particularly on co-operating or physically interacting by optimal control and mechanical properties. Moreover, some VSA designs can also minimize the amplitude of impact force from accidental contacts extending the lifetime of components and the intrinsic actuation redundancy increasing their reliability on mechanical failures. Besides, the energy input in the system control can be reduced by imitating a cyclic motion pattern like natural oscillation [5] [6] [7] [8].

Several VSAs have been developed using multiple mechanical designs over the sustained growth of research [5] [6] [9] [8]. In general, VSAs can be roughly separated into two main categories; active and passive compliant actuators. An active compliance type basically uses a stiff actuator implementing the software control varying the stiffness by imitating a spring-like behaviour. The controller will adjust

the calculated compliance during the operation based on measured output states such as external force or torque. When using the classic actuator, the additional component like a sensor is required in this type of compliant actuator together with the designed controller which provides a fast response for the application. The main benefit of using this type of VSAs is online adaptability of stiffness. However, active compliant actuators have some drawbacks for example, continuous energy dissipation, no energy can be stored in the system and there is no absorption of shocks because of lack of passive elastic elements like a spring and bandwidth limitation of the controller. In addition, the controller is complex to develop. On the other hand, to integrate shock absorption and energy storage together with compliance adjustability, a passive compliant actuator which contains an intrinsic compliant or elastic element can be used. This category can be divided into sub-categories on the basis of fixed compliance properties or adaptable compliance properties.

Considering the biological mimicking of muscle co-contraction, one mechanical design of VSAs worth mentioning is the antagonistic mechanism. Antagonist-ism is a biological-inspired mechanism which provides antagonistic forces working against each other, two actuators are mounted in opposed presence at the joint. As a VSA design, this mechanism usually comes with prestressed elastic elements located in the opposite direction, providing encountered forces by pulling back with elastic forces. This elastic element can represent the muscle in the biological context. Using this configuration, stiffness can be adjusted with antagonistic forces from both sides, the magnitude of actuation effect increasing or decreasing the stiffness of the joint or link. This also offers the internal forces/torques to encounter the external forces of mechanism which is impacts or disturbances from the environment. Therefore, it can be seen that the working principle of antagonism reflects the physiology of human musculoskeletal systems mentioned beforeas shown in figure 1.1. [8] [10] [11].

Keeping in mind the primary goal of developing the lower-arm based support exoskeleton (see figure 1.2), an adaptability of joint stiffness cannot be excluded. To duplicate this biological function, the novel VSA which has a cable-driven mechanism associated with antagonistic springs offering the ability to adjust the stiffness is proposed. Owing to the advantages of the cable-driven system, it is commonly used in diverse assisting robotic applications [8] [11]. Not only because of the advantages of compactness and lightness but also because of the possibilities to locate and transmit actuation away from the wearable functional support by the possibilities of cable routing. Thus, this mechanism often comes with antagonistic implementation. As mentioned before, antagonism can provide support on imitating the physiology of human muscle, for example, a co-contraction of the biceps and triceps muscles from the human arm. Inevitably, cable-driven antagonistic mechanism has been adopted for developing the specific-lower arm support VSA, called a cable-driven variable

stiffness actuator.

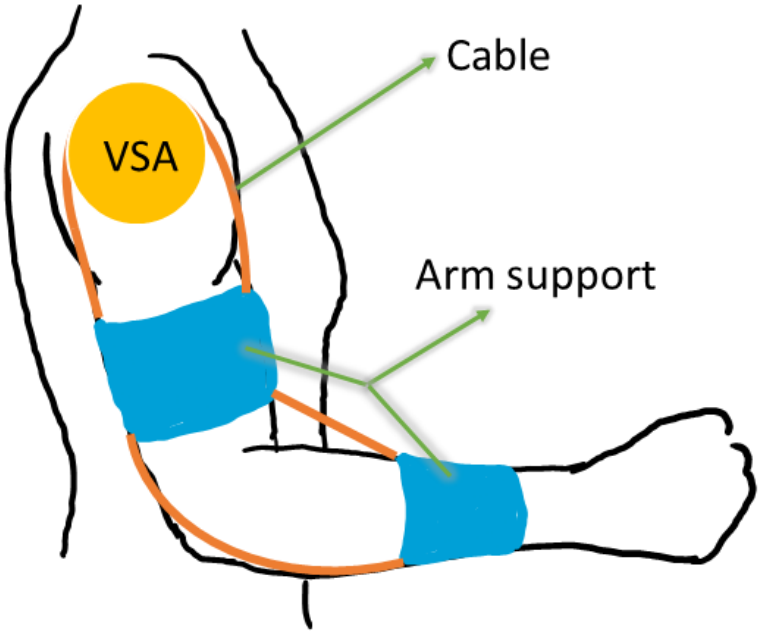

Figure 1.2: Model of conceptual idea for lower-arm based support exoskeleton

1.1 State of the art

In the expanding trend of the bio-robotics applications, there are some VSA designs which implemented with antagonistic mechanism and cable-driven system. An antagonistic VSA can be classified as a subcategory in preloaded spring type according to [5] and [6]. Preloaded spring or pretension spring type is a design which stiffness can be varied by setting the pretension of the elastic element. As a result, the internal energy from the pre-tensioned elastic element will be stored, therefore, offering a large passive angular deflection. Generally, the pretension spring category comes with two elastic elements to balance the deflection, the second spring gives a negative stiffness. The preloaded spring category can also be divided into sub-categories including the antagonistic spring with independent actuators. With antagonistic formation and independent actuation, an equilibrium position and stiffness control happens. The equilibrium position is varied when the stiffness is changed [10]. Therefore, some of the literature which has a related mechanism with the design of cable-driven VSA will be reviewed in this section.

When looking at the antagonistic VSA, one of the studies in [11], introduces the bidirectional antagonism. This mechanism adopted the antagonistic formation by using motors adjusting the springs elastic properties which connected bidirection-

ally to the link to be bidirectional antagonistic design. As a result, the extension of antagonistic joints into bidirectional antagonistic was achieved. A major finding of [11] was that stiffness can be adjusted in a bidirectional way with two operating modes; normal mode and helping mode (as shown in 1.3). In helping mode which is a distinctive feature, the two motor torques actuated alternatively to assist each other resulting in adjusting lower and upper boundaries of stiffness variation. This function showed an advantage on the adaptability of mechanism mimicking the human muscular system. However, with the helping antagonistic mode, two additional actuators are required leading to extra weight on the design. Moreover, to achieve the non-linear realization, one auxiliary is included to modulate the spring length bringing non-linearity. Hence, the main drawback of this design might be the heavy-weight of the system.

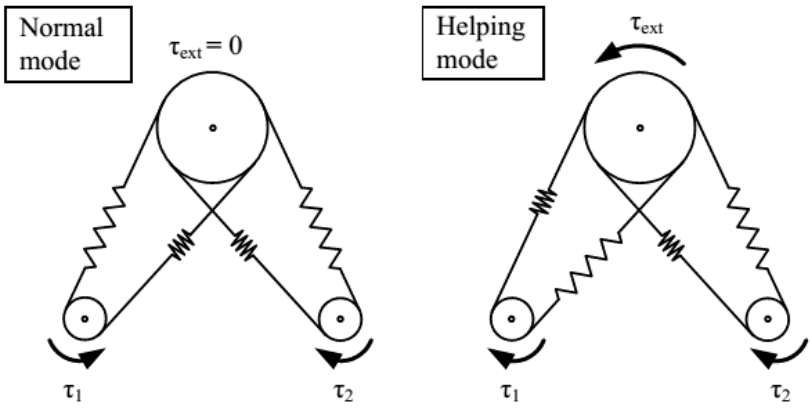

Figure 1.3: Diagram depicting the operating modes of bidirectional antagonistism [11]

Another antagonistic setup was discussed in [12], a triangular formation of pulleys with linear springs was introduced (depicting in figure 1.4). A wide range of stiffness change was combined with inner tension, the stiffness is directly proportional to tension. The design contained two operating modes; active and passive variable stiffness. On the one hand, on a passive mode, the spring attachments were fixed without changing the equilibrium point. On the other hand, an active mode allowed a linear actuator to adjust spring attachment benefiting in higher stiffness with lower tension. This design enabled independent modification of both the desired tension and the comprehended stiffness by independent of cable configuration. Another advantage is that the system has a light-weight structure. The system requires four actuators consisting of two rotary actuators and two linear actuators. With the linear actuators, therefore, the design is bulky by the length of the actuator size.

A tensegrity mechanism was applied to the variable stiffness device in [13]. The

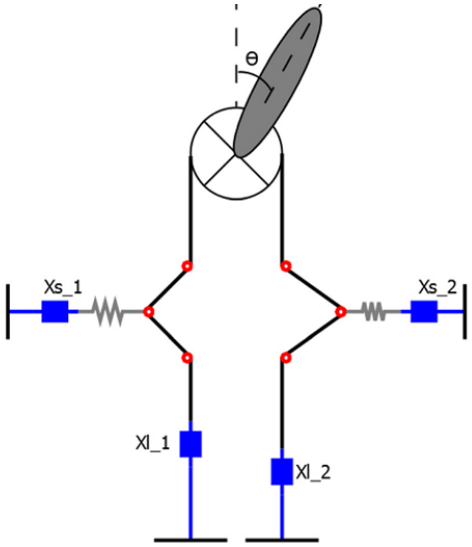

Figure 1.4: Antagonistic mechanism configuration showing triangular formation of pulleys [12]

mechanism was built as a planar tensegrity with cable-driven connected with a non-linear elastic element and pretensioned cable. This mechanism allowed strategies to control an angular position and stiffness as exhibited in figure 1.5. Moreover, the planar structure was designed with parallel-four bar linkage formation, resulting in high dynamics. A planar mechanism consisting of three moving bars and one bar linked to the base actuated by two inelastic cables on two points of the moving bar. Hence, this provides a benefit in lightweight architecture. Moreover, the mechanism is also be re-configurable. Although the parallel structure brings advantages, the drawbacks are also caused by that. The main constraint is the work-space regarding the motion of four-bar linkage, planar motion. Furthermore, the planar motion also limits on implementing multiple degrees of freedom, working in one plane.

In [14], another design with cable-driven mechanism was presented called Actuator with VAriable Stiffness and Torque Threshold or AVASTT. Contrary to the aforementioned works, a pretensioned mechanism with a single actuator configuration was designed in figure 1.6. The actuator regulates the tension of the spring, adjusting the equilibrium position of the output joint. As a consequence, this design provided the feasibility of varying the torque limit is only possible if the external force exceeds a certain level The torque threshold can give an identical equilibrium position without bidirectional mechanism. Nonetheless, the structure of it links reflects the large size together with the heaviness of the system without acknowledging the cable-driven mechanism. Additionally, the motion of joint rotation is limited to only 54 deg.

A single-degree-of-freedom robotics joint which was designed in the antagonistic

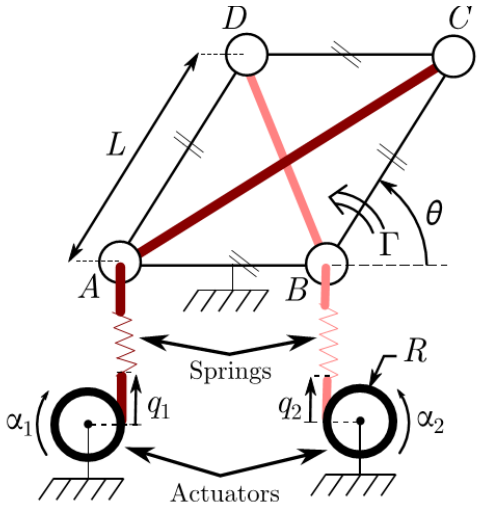

Figure 1.5: Planar tensegrity with cable-driven mechanism [13]

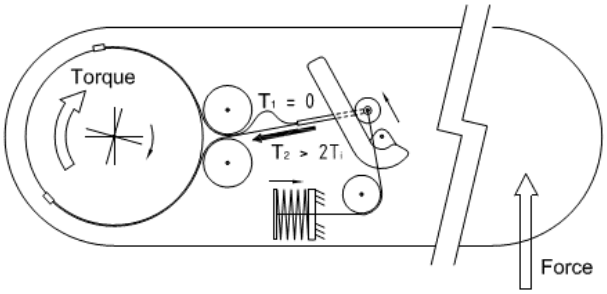

Figure 1.6: Illustration of torque threshold application when the mechanism interacts with the applied force [14]

pattern was presented in [4]. Although it was defined as a series-elastic actuated robotics joint, the working principle of this study can be referred to, as cable/wire-driven VSA (see figure 1.7). It was prototyped to work antagonistically by two actuators which were connected to non-linear elastic devices, producing a quadratic force-length relationship to linear spring. The highlight of this research is the biological imitation of the control system. Not only building the prototype but also implementing the control system. Therefore, it resulted in a high correlation of measurement and estimated result. However, the stiffness seemed to be marginal for the actual work and the feedback from the sensor still need to be improved.

[15] presents a variable stiffness device which was a part for modulating the stiffness through the tension in their cable-driven manipulator. The tensioning device (as shown in figure 1.8) used four torsion springs, winding two of them in clockwise and the others in counter-clockwise resulting in a moment in connecting shafts. With the opposite direction, the pulling forces from both clockwise springs and counter-clockwise spring will cancel each other and also obtain a big displacement-to-force

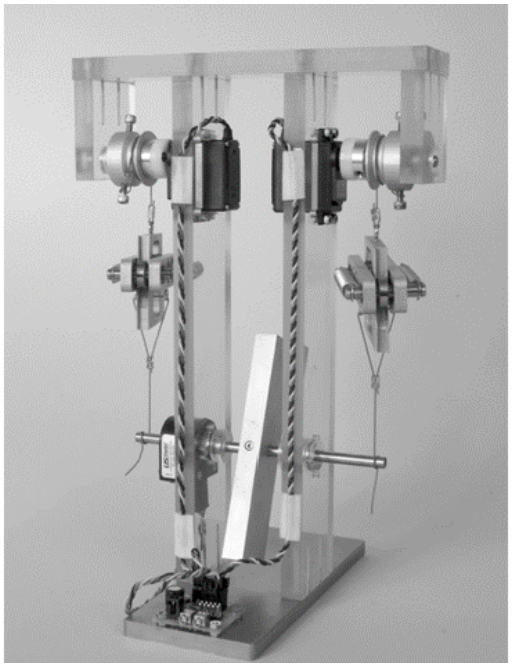

Figure 1.7: Antagonistically actuated single DOF robotic joint with quadratic series-elastic actuation [4]

ratio when the cable tension is low but the displacement-to-force ratio is small when the cable tension is high. However, from the design aspect, it is advantageous on compactness and lightness. On the other hand, the torsion spring hinders the deflection range by specified spring.

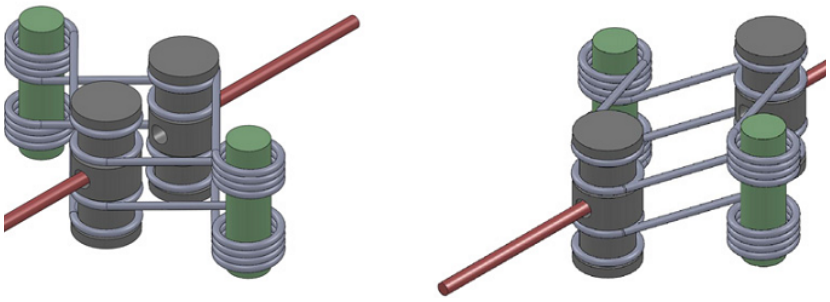

Figure 1.8: Variable stiffness device design from [15]

It can be seen that the features of the various types of VSAs are determined by the particular type of mechanical design used to regulate the actuator's position and stiffness. Although most of them can bring a promising performance on resembling the biological motion of human's limb, limitations can be found. Two main constraints which commonly appeared on most reviewed designs are bulkiness or heaviness and limited range of motion, mostly by applying many actuators to modulate stiffness. Moreover, several VSAs have been developed by the University of

Twente [16] and [17]. Even though they can efficient perform in their function, they still meet the same limitation, the heavy-weight and bulkiness which is might not suitable for implementing on user's elbow.

1.2 Scope of work

To develop the assistive system for lower arm support, it would be better if there were alternative VSAs as an option which could provide safe physical human-robot interaction with light-weight, compact and competent performance. Consequently, the cable-driven VSA is nominated. To ensure that the cable-driven VSA is able to provide high efficiency on wearable robotics, the studies were done. Noted that, the efficiency in this term refers to the ability of the actuator to achieve physiologically stiffness behaviour with competent stiffness control and energy efficiency. It can be noticed that this development is long-period research, can be divided into studies. However, as an initial study for the project, the main focus of this study will be the cable-driven variable stiffness unit or cable-driven variable stiffness mechanism which is a part of VSA design. Considering the VSA has two parts, consisting of a stiffness varying component and an actuation component, the cable-driven VSM is the stiffness varying unit which plays a big role in stiffness variation of VSA.

The contribution of this study is, therefore, a proof of a concept of the new variable stiffness mechanism, understanding the working principle of the stiffness modulation. In this first step, in this case, the cable-driven variable-stiffness unit or variable-stiffness mechanism (VSM) is modelled and designed as a test bed to validate the concept. Additionally, the simulation of the cable-driven VSM is performed in order to realize the effects on altered configurations and to validate of the test bed. Moreover, one notation that needs to be included is that the linear elastic component, spring, will be mainly used in this study. However, the non-linear elastic element also used in the study as an extra task on investigating additional objective (the details will be explained in the next section 1.3).

1.3 Goal(s) of the assignment

To demonstrate the feasibility of resembling the elbow joint motion mechanism of cable-driven VSM is the main purpose of this study. The elbow's motion is controlled by its stiffness, modulating and maintaining the position. For an initial study, the cable-driven variable stiffness mechanism is investigated in section 1.2. A safety interaction from uncertainty and energy efficiency are benefits for implementing physiology of lower arm to a VSM. Hence, the system should give the stiffness variation

without changing torque to follow the physiology of elbow's stiffness. Therefore, various objectives based on physiological stiffness behavior and the basic requirements of VSAs [18] are set to evaluate the performance of the cable-driven variable stiffness mechanism.

The measured stiffness of the cable-driven VSM test bed is equal to the desired stiffness is the first requirement and objective. The desired stiffness need to behave by the design when it performs changing of stiffness ($K = K_{desire}$). This objective refers to the fact that the lower arm support should be adaptable to modulate stiffness as the system requires. The desired stiffness which will be used to compare the test bed performance is done by the simulation. Moreover, to prove adaptability of variable stiffness mechanism by changing characteristics of stiffness, altering elastic element type (linear to non-linear type). Due to the fact that the cable-driven VSM should provide an ability to modulate stiffness with its mechanism for every elastic element, proof of mechanism principle is discussed.

Secondly, another objective is that the design should provide constant torque when varying stiffness ($\dot{\tau} = 0$). When looking at the physical stiffness nature particularly on the lower arm section, one vital application should be pointed out is that a stiffness change can remain no change when the external force or torque is exerted. This physiological mechanism is because of compensation of antagonistic muscles which change the stiffness for a different disturbance or impact, while the torque around the elbow remains constant.

The third objective or requirement is that the internal energy of variable-stiffness unit (summation of energy consumption from all tensioning units) should be equivalent to zero or approximately zero when varying stiffness ($\int_0^t P_{control} \approx 0$, where $P_{control}$ is the power of control units). Noted that, this is determined by an assumption that VSM is unloaded and immovable. One feature that should be on the lower-arm based exoskeleton is energy efficiency. With this objective, the energy efficiency of the cable-driven VSM can be validated. For VSAs, the output energy is the potential energy which is a result of the stored energy, elastic energy from the elastic element. Since the VSAs have the variable stiffness unit for regulating the stiffness, the input energy is the energy that applied to actuators which control the stiffness modulation. So if the stiffness of VSA increases while the deflection has remained, the output energy will increase as its function. However, to increase the stiffness, the actuators need the input energy to adjust the configuration. In the ideal case, the input energy should be equal to the output energy implying the energy efficiency of the mechanism. Therefore, the consumed energy of the system expects to be zero.

Aside from these, an extra objective is also included, studying the cable-driven VSM by a simulation. The simulation is performed for realizing the mechanism principle when its configuration is changed. Since there are several dimension param-

eters which can be affected the behaviour of mechanism, each main parameter will be investigated its roles of this cable-driven VSM.

1.4 Report organization

The remainder of this report is organized as follows. In Chapter 2, the design of the cable-driven VSM is explained in detail including the concept design and elaboration of the design together with the kinematic analysis behind the design. Additionally, the simulations for investigating the test bed's performance when the dimension parameters change is presented in Chapter 3. The experimental protocol to measure the design performance based on the aforementioned objectives is described in Chapter 4. Then, in Chapter 5, experimental results based on the objectives of the study are presented showing the performance of the design from measurements. Thereafter, the discussions of the measurements are deliberated in Chapter 6. Finally, in Chapter 7, conclusions over the results are given along with the recommendations for future implementations.

Chapter 2

Cable-driven variable stiffness mechanism - design of the mechanism

In this chapter, an overview of the design is introduced. Beginning with introduction of design of the cable-driven variable-stiffness mechanism, the conceptual idea are described. Elaborations of design and the kinematics analysis behind the mechanism are presented, explaining the mechanism of the variable-stiffness mechanism (VSM) of cable-driven VSA. Thereafter, to evaluate the performance of the design with three aforementioned objectives of the study, the cabel-driven VSM test bed was designed and prototyped which will be explained in detail.

2.1 Conceptual design

To imitate the physiology of lower arm, a co-contraction of muscles, the antagonistic mechanism was adopted from the cable-driven VSM. Hence, the conceptual idea was designed to be two-sided actuation with two elastic elements working antagonistic to each other.

In the cable-driven VSA mechanism, an antagonistic actuation with four tensioning units (two units for each side) was prototyped to bring about changes of stiffness in non-linearity. Note that nonlinearity is provided by the mechanism's displacement which is results from a rotational transmission ratio between the spring (regulated by the tensioning units) and the output lever.

To clarify it further, in figure 2.1, the diagram of the conceptual design is shown. As it can be noticed, the output of this mechanism were connected by two sides of varying stiffness units. On each side of varying stiffness unit, two tensioning units were placed in order to vary the stiffness of spring which was also located on each

side. The spring acts as the compliant element giving internal mechanical compliance as required for regular VSA. All of the tensioning units, springs and output lever were driven and connected with roped cable, cable-driven mechanism. By translating the tensioning units, the cables were tensioned and springs were stretched which will differ the stiffness on the output. Therefore, there are four degrees of freedom in total considering the tensioning unit solely (a translation motion on each tensioning unit). With this working mechanic, it can be defined that the cable-driven mechanism was adopted in the design showing a balanced pattern of the output. The two-sided varying stiffness units work antagonistically, for instance, the right side will pull back the output lever if the left side is pushed. The two-sided unit works to respond in the opposite direction. This antagonistic mechanism will result in position maintaining, the output will be balanced. Hence, the equilibrium position of output can be found. The equilibrium configuration of output which has equilibrium position results in zero torque and deflection. The equilibrium configuration or default configuration can be done by setting both varying stiffness units in the same position. Note that in this design, the output of cable-driven VSM will be connected between the actuating unit and the load to complete all VSA components which can be done in future development. In this design, all of the movements from the variable-stiffness unit was restricted in two-dimensional motion or in the plane, to avoid the deviation from the vertical direction.

2.2 Mathematical model of cable-driven VSM

In regards the conceptual design, in this section, a model of the system has been made and analysed as shown in figure 2.2. Kinematics of cable-driven VSM will be derived resulting in the spring state derivation which is the initial derivation for further analyses. Secondly, in order to obtain the stiffness calculation, the output torque of the design will be analyzed. Last but not least, the stiffness derivation will be calculated based on the torque and kinematics derivation.

2.2.1 Spring state derivation

When looking at the kinematics of cable-driven VSM, the length of the cable plays a big role in varying the torque and angular deflection of the output lever which results in the varied stiffness. The pulleys' radii were ignored with the reason that the positions of the pulleys are the main concern. As the initial concept, the mechanism was modeled to be simple focusing on the working principle excluding the effect of pulleys' radii. Therefore, the radii were not initially taken into account in the primary

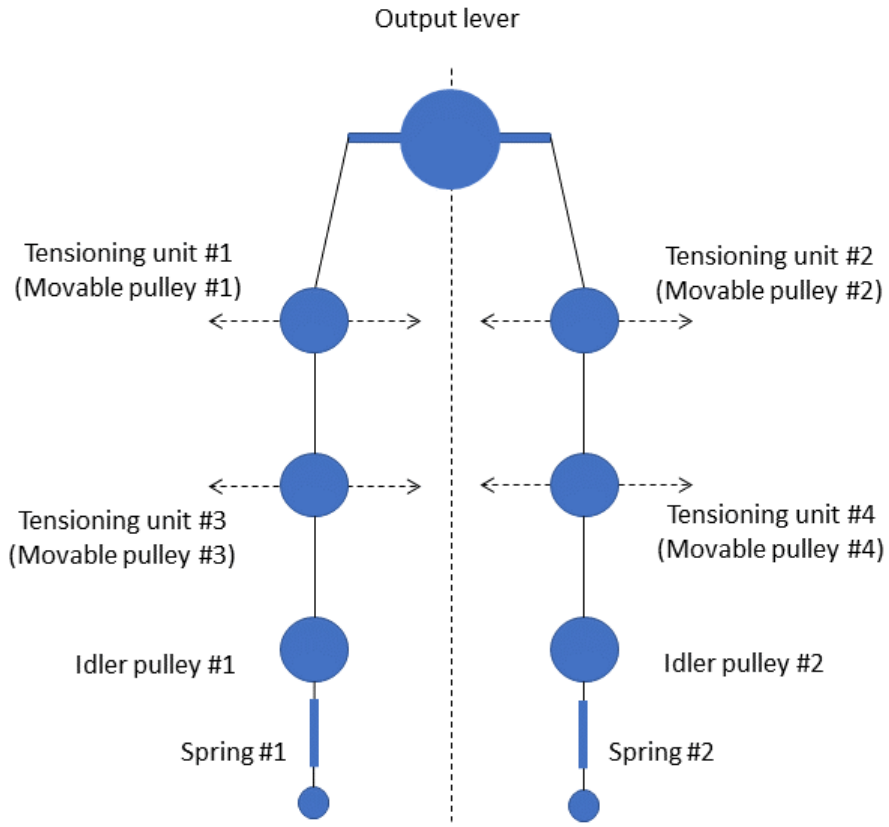

Figure 2.1: Diagram showing the conceptual design of cable-driven VSM

model. As stated below in 2.1, the length of cable implies spring state which is the result of the whole cable dimension.

$$s_n = L_n(q, \theta) - \bar{L} \tag{2.1}$$

where n refers to state, thus s_n is the state of spring, $\bar{L}$ is the equilibrium configuration in which the spring is in a zero-deflection state and the angle of the output lever is zero and L_n is the total length of the cable when the pulleys are moved in the plane. it can be noticed that L_n is a state function of q and θ which are positions of tensioning units and the angular deflection of output.

From the diagram 2.2, the length of the cable can be derived based on dimensions. The calculations which is shown below in 2.2 and 2.3 represent cable's length of left and right side, respectively. It can be noticed that the length of cable is mainly varied by the tensioning units. Hence, the total length of the cable of both side can be expressed as 2.2 and 2.3 for left side and right side, respectively.

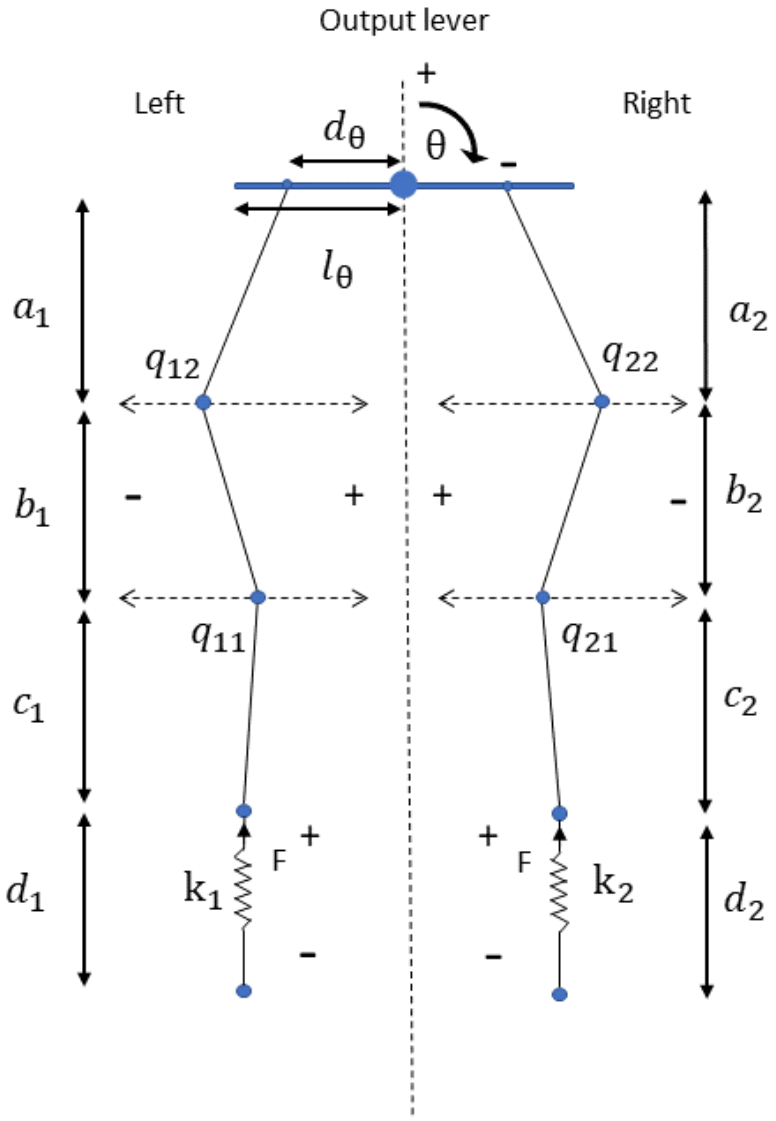

Figure 2.2: Model of cable-driven VSM with cables and pulleys

$$L_1(q,\theta) = L_{Left}(q,\theta)$$
$$= d_1 + \sqrt{{c_1}^2 + {q_{11}}^2} + \sqrt{{b_1}^2 + (q_{11}+q_{12})^2} + \sqrt{\left((d_\theta \cos\theta + q_{12})^2 + (a_1 - d_\theta \sin\theta)^2\right)} \tag{2.2}$$

$$L_2(q,\theta) = L_{Right}(q,\theta)$$
$$= d_2 + \sqrt{{c_2}^2 + {q_{21}}^2} + \sqrt{{b_2}^2 + (q_{21}+q_{22})^2} + \sqrt{\left((d_\theta \cos\theta + q_{22})^2 + (a_2 - d_\theta \sin\theta)^2\right)} \tag{2.3}$$

The positions of the tensioning units from an upper unit and a lower unit (following the diagram in figure 2.2)were presented in q_1 and q_2. As it can be seen, the

tensioning units have upper and lower units which can be indicate by number labels 1 and 2. The lower units are labeled by subscription of '1' whereas the upper units are labeled by '2'. Due to the fact that this design was intended to be re-configurable, the attachments of cable on output lever can also be adjusted. Thus, d_θ is the length where the cable is attached in the output lever. The dimensions of the design are a,b,c and d which are shown in diagram in figure 2.2. a is the length from output lever to the upper tensioning units. b is the length between upper and lower tensioning units. c is the distance from lower tensioning units (q_{11} and q_{21}). While d is the length from idler pulleys to another one which these pulleys will connect cable to the elastic element. By having two side , all parameters can be seperated by the numerical labels, giving '1' and '2' subscription for left and right side.

To convert the length of the cable into the spring state, it can be done by substituting 2.2 or 2.3 in 2.1:

$$s_1 = d_1 + \sqrt{{c_1}^2 + {q_{11}}^2} + \sqrt{{b_1}^2 + (q_{11} + q_{12})^2} + \sqrt{\left((d_\theta \cos\theta + q_{12})^2 + (a_1 - d_\theta \sin\theta)^2\right)} - \bar{L} \tag{2.4}$$

$$s_2 = d_2 + \sqrt{{c_2}^2 + {q_{21}}^2} + \sqrt{{b_2}^2 + (q_{21} + q_{22})^2} + \sqrt{\left((d_\theta \cos\theta + q_{22})^2 + (a_2 - d_\theta \sin\theta)^2\right)} - \bar{L} \tag{2.5}$$

2.2.2 Torque derivation

The total torque or output torque (τ_θ) is a summation of left-sided and right-sided torque, which can be derived from the storage energy of elastic element (H) with respect to the state of spring as shown in equation 2.8. Prior to looking at the equation of output torque (equation 2.8), an equation 2.6 shows the elastic potential energy of spring when spring is compressed or stretched which is an initial equation for deriving output torque. The output torque was derived based on the port-based and bond graph model which have a benefit in domain-independent energy flow coupling converting one domain of energy to another domain of energy in the system [19] [20] [21] [22]. In this present case, the derivative of storage energy was converted to torque as these two variables are the effort in port-based model.

Prior to looking at the derivation of the output torque, one thing should be determined is the free body diagram of the design to define the direction of each forces. As it can be seen in diagram 2.2, the positive and negative sign show the direction of each interacted forces. The torques have a positive sign to account for $F = k \cdot s_n$. The direction of torque and stretched spring has the same direction. Where k rep-

resents the spring constant of the spring which used in the design.

$$H\left(s_n\right) \;=\; \frac{1}{2}k_n s_n^2 \tag{2.6}$$

$$H\left(s_1, s_2\right) \;=\; \frac{1}{2}k_1 s_1^2 + \frac{1}{2}k_2 s_2^2 \tag{2.7}$$

In the port-based model, the output torque can be determined by the storage energy which is the elastic energy on this scenario as shown in equation 2.6. As it can be noticed, the elastic energy is varied by the spring state (s_n) that means the output torque is also affected by s_n. When the configuration changes, the output torque would be affected by the differed spring state. In equation 2.6, it represents internal potential energy of the spring for a single-sided VSM. Hence, in equation 2.7, the total storage energy of VSM can be found by addition of both sides of VSM as exhibited in equation 2.7. Therefore, the output torque (τ_θ) can be derived by H in equation 2.7 into equation 2.8. The variables can be used for both sides of VSM by substituting different dimensions (in this case, the dimensions of both sides have the same lengths).

$$\begin{aligned}\tau_\theta\left(q,\theta\right) &= \frac{\partial H\left(s_1, s_2\right)}{\partial\theta} \\ &= k_1(L_1\left(q,\theta\right) - \bar{L})\,\frac{\partial(L_1\left(q,\theta\right))}{\partial\theta} + k_2(L_2\left(q,\theta\right) - \bar{L})\,\frac{\partial(L_2\left(q,\theta\right))}{\partial\theta}\end{aligned} \tag{2.8}$$

From the model, it can be seen that the torque of one-sided VSM is zero at the default configuration. Consequently, the total torque of the two-sided VSM is also zero when both VSM's side are at default configuration which the angular deflection is also zero. However, when the output angular position deviates from the zero-configuration (the springs are not in the default configuration, and they are elongated or compressed), a torque is acquired. However, in the situation that linear springs and pulleys hover the projection of cable force to remain constant, the torque and angular deflection will be zero. In this way, the forces or torques for two sides will eliminate each other due to the antagonistic design.

2.2.3 Stiffness derivation

The stiffness (K) of the cable-driven VSM can be derived from torque and angular deflection of the output lever since stiffness is related with the change of torque and the change of angular deflection as shown in 2.9.

$$K = \frac{\partial\tau_\theta\left(q,\theta\right)}{\partial\theta} \tag{2.9}$$

Therefore, the derivative of torques from two-sided VSM which given in equation 2.8 by angular deflection, resulting in stiffnesses of cable-driven VSM. It can be seen that the stiffness can be differed by the change of the tensioning units's positions or stroke length of tensioning units. The change of the stroke length can be referred to the change of length of the cable which affects the change of the storage energy which consequently determining the output torque and the stiffness.

2.3 Cable-driven VSM test bed

A testbed of the cable-driven VSM has been developed according to the mathematical model and conceptual design described in section 2.2 and 2.1, respectively. This testbed was used in the measurements for validating the concept. To illustrate the details of the testbed, the figure is showed below with the description.

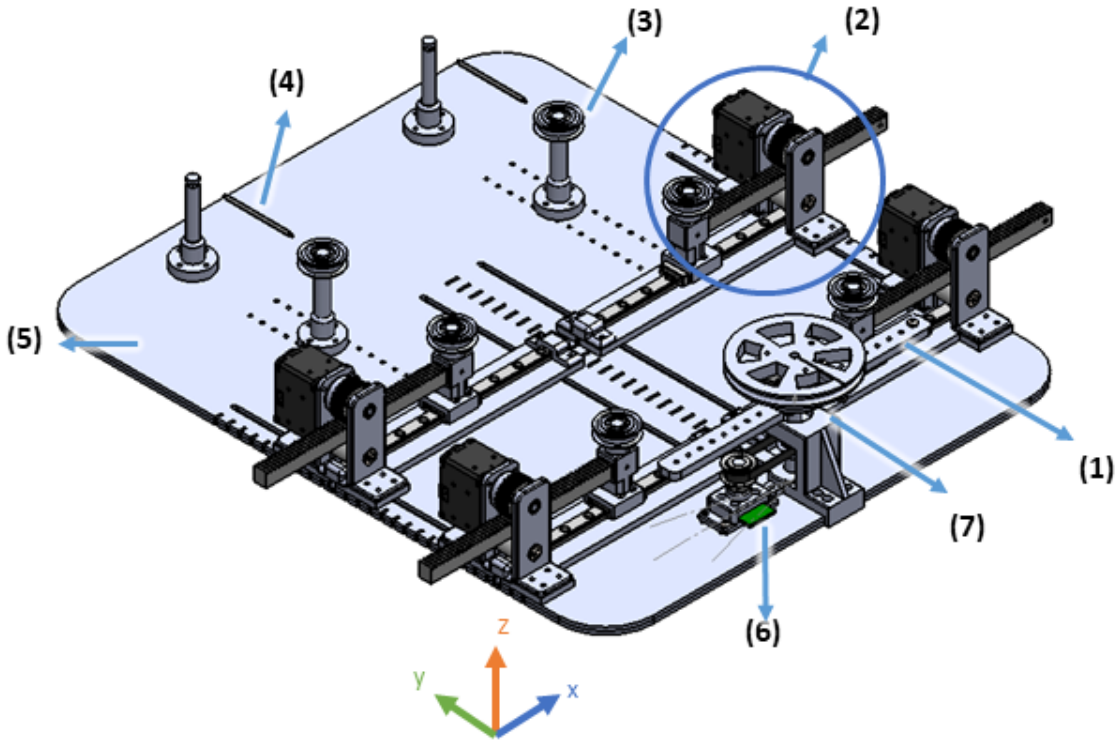

Figure 2.3: CAD of cable-driven VSM test bed with the scale 1:5, (1) shows the output lever, (2) is a tensioning unit, (3) is an idler pulley, (4) presents a spring, (5) is a base of test bed, (6) is a magnetic rotary encoder and (7) is a force/torque sensor

Figure 2.3 showed a CAD of cable-driven variable-stiffness mechanism testbed. The testbed was designed to be a test bed in order to study the mechanism of the cable-driven variable stiffness mechanism design. To make the test bed compliant with the conceptual idea, four tensioning units (figure 2.3(2)) (the detail will also be shown in figure 2.7) were prototyped applying rack and pinion driving mechanism which have attached pulleys to tension the cable. The output was made to be a lever (figure 2.3(1)) which has a magnetic rotary encoder (figure 2.3(6)) and a force/torque sensor (figure 2.3(7)) attached on it. The force/torque sensor was located and connected under the output lever due to its function to measure torque when the output

lever is interacted with user. The rotary encoder was settled aside the output lever to make it less complicated when setting up the test rid and also prevent an accident which can damage the sensor. To transfer the rotation of output, the belt and pulley were applied with transmission ratio 1:1 over the encoder which will read the angular position of a shaft with magnet. In figure 2.4, it shows the close-up view of the output which can illustrate the mechanism on the output. Regarding cable-driven design, the string was wired connecting the spring with other pulleys (figure 2.3(3)) which are idler pulleys and the output lever on both sides. The string was used to be cable in the test bed since it can complied with the curvature of pulleys, steel wire cable is stiffer which can not curve along with the small diameter of pulleys in this test bed. The elastic element in the set-up is linear spring which has spring constant equal to $100 N/m$ (figure 2.3(4)). Moreover, the design particular base of test bed (figure 2.3(5)) was built to be re-configurable to serve the investigation on the effect when relocating tension units. Therefore, the idler pulleys and the tensioning unit can be re-positioned.

The test bed was mainly made by the rapid prototyping technique, i.e., laser cutting and 3D printing. The base and output lever were created by laser cutting. For the pulleys, racks, gears and some supporting parts were fabricated by 3D printing.

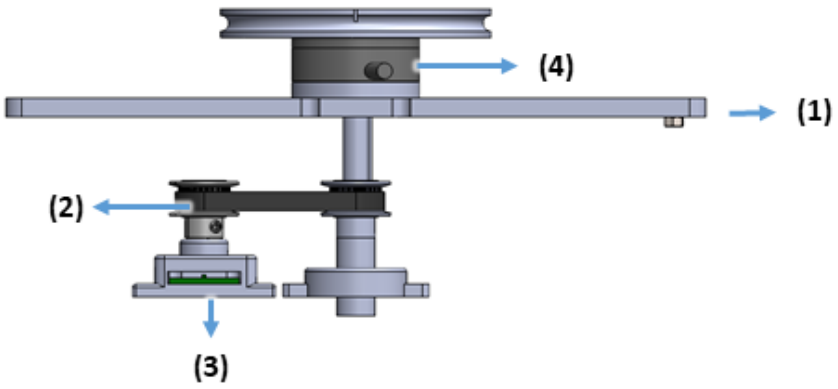

Figure 2.4: CAD of output in close-up showing in front view with 1:2 scale;(1) output shaft, (2) pulley and belt mechanism, (3) encoder and (4) force/torque sensor

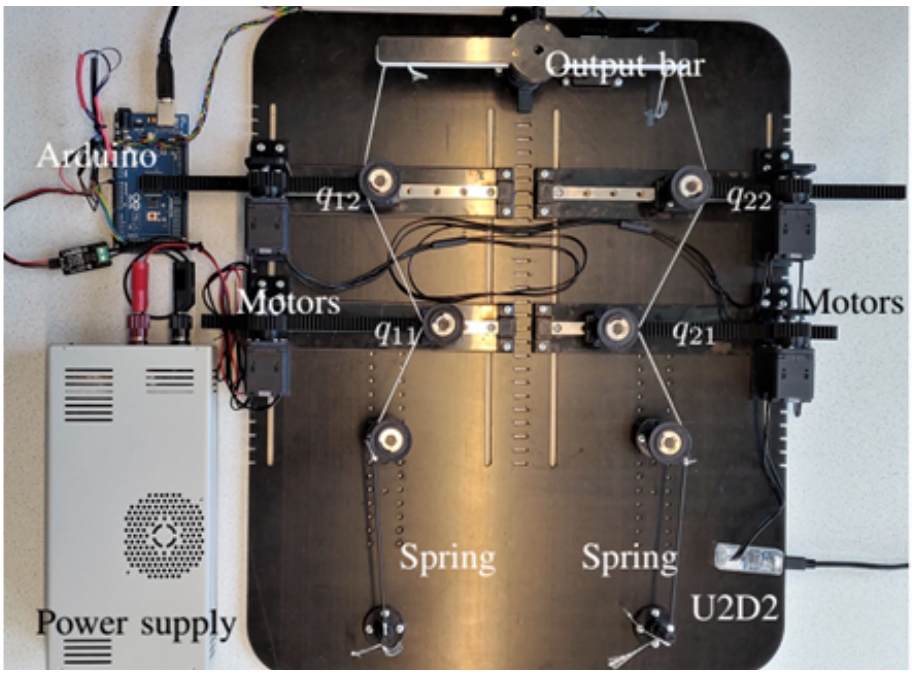

Figure 2.5: Cable-driven VSM test bed

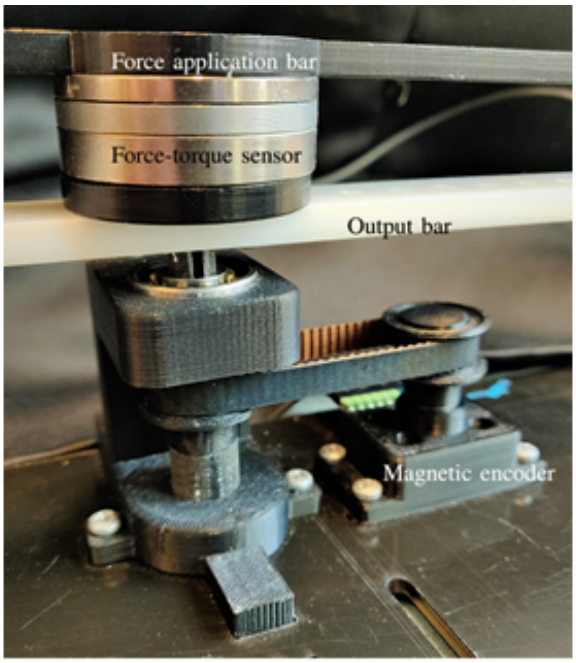

Figure 2.6: close-up view of output lever from the test bed

2.3.1 Tensioning unit

Considering the main function of the test bed which was to modulate the stiffness, the tensioning unit plays a big role on this. In figure 2.7 below, the CAD of tensioning unit is presented. The pinion and rack mechanism is used to tension the cable, eventually resulting in varying stiffness. Figure 2.7(5) and 2.7(4) showed rack gear and pinion gear which were fabricated by 3D printing, respectively. Servomotors (Dynamixel XL430-W250-T) in figure 2.7(3) were selected to drive pinions and racks. To actuate the tensioning units, the servomotors are controlled by using Dynamixel U2D2 USB-interface and are powered with a 24 V power supply. The controller was developed based on the ROBOTIS Dynamixel SDK 3.6.0 which is the software developing kit by ROBOTIS. In every unit, there is a pulley (figure 2.7(2)) which has wired cable and connected with linear slider (figure2.7(1)), providing less friction when driving. To prevent the backlash caused by gears and racks, the supporting roller (figure 2.7(6)) was added in each unit. Due to the positioning function is the main purpose of these units, the rack and gear ratio is designed to be 0.0125 rad/m (converting rotation to translation motion). Additionally, the stroke range of the tensioning unit has designed to be 0.1 m in total, 0.05 m length for both left and right side.

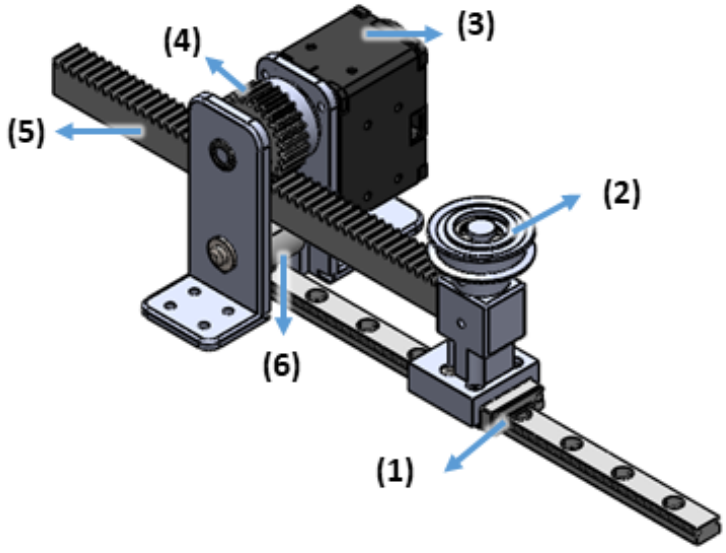

Figure 2.7: CAD of tensioning unit with the scale 1:2, (1) is linear slider,(2) is movable pulley,(3) is actuator which is servo motor,(4) is a pinion gear,(5) is a rack gear and (6) is supporting roller

Chapter 3

Simulations

Prior to performing the measurement with a prototyped test-bench, the effect of the test rigs setting must first be understood. As it can be seen in figure 2.2 and 2.3, the test bed is designed to be re-configurable. Therefore, many parameters, e.g., 'a', 'b', 'c' and 'q_{ij}', can be relocated. The changes in these parameters can also affect the output by changing the length of the cable, as can be seen in 2.4 and 2.5. By changing the length of cable, the output torque will be altered as shown in 2.8 which also results in varied stiffness. Hence, based on the equations in section 2.2, the output torque and stiffness of the cable-driven VSM test bed can be simulated to realize the roles of each dimension parameter.

In the simulation, the initial setting of dimension parameters are set as seen in figure 3.1 and table 3.1 which are shown below. The dimension parameters in the table and figure are stated before in the equations in chapter 2. These dimensions are based on the actual setting from the test bed. The dimension parameters which will be simulated are described in the next sections.

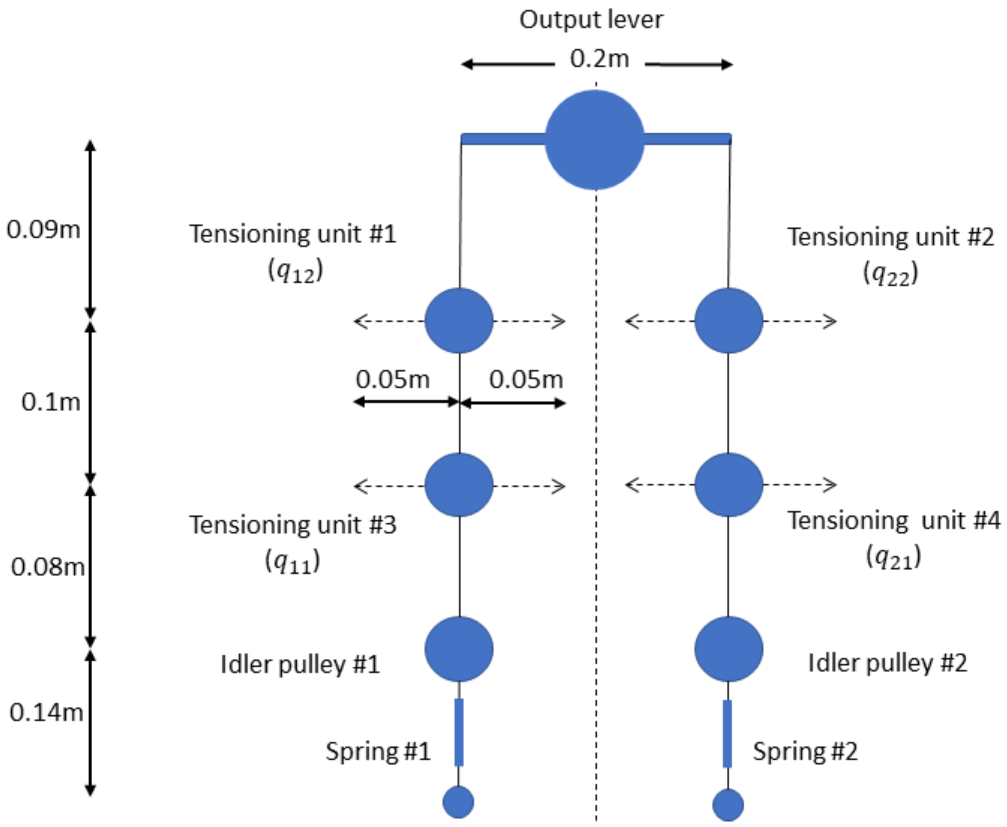

Figure 3.1: Diagram of test-bench dimension on experiments

parameter	d_θ	a	b	c	d	q_{ij}
length (m)	0.1	0.09	0.1	0.08	0.14	-0.05 - 0.05

Table 3.1: Dimension parameters of test bed

Noted: i and j subscription represent position of tension units; i indicates left(1) or right(2) side and j is for upper(2) or lower(1) unit

3.1 Effects of dimension parameters

To consider the effect of dimension parameters, on these simulations, each parameter is varied once at the time, the rest of the parameters are kept the same at that time. The aforementioned dimension parameters; 'q_1', 'q_2', 'a', 'b' and 'c', will be included in varying their length. The outcome of each parameter will focus on the output stiffness, some of the parameters might be shown together with the output torque as supplementary information.

3.1.1 Effects of lower versus upper tensioning units

One parameter which is interesting to consider is the tensioning unit since it plays an important role in varying stiffness. The tensioning unit has four units which can be grouped as upper and lower units. The upper and lower group influence the output stiffness differently when considering a position as shown in figure 2.2. Therefore, in this section, simulations of torque-deflection and stiffness to investigate the effect of tensioning units is elaborated upon.

Four configurations are set on these simulations following two groups of tensioning units; upper and lower unit. The first configuration is the default configuration in which all tensioning units are aligned at 0m position. At 0.05m for only upper units is the second configuration whereas when the third configuration is at 0.05m only lower units are positioned. The last configuration is when all units are located at the 0.05m position.

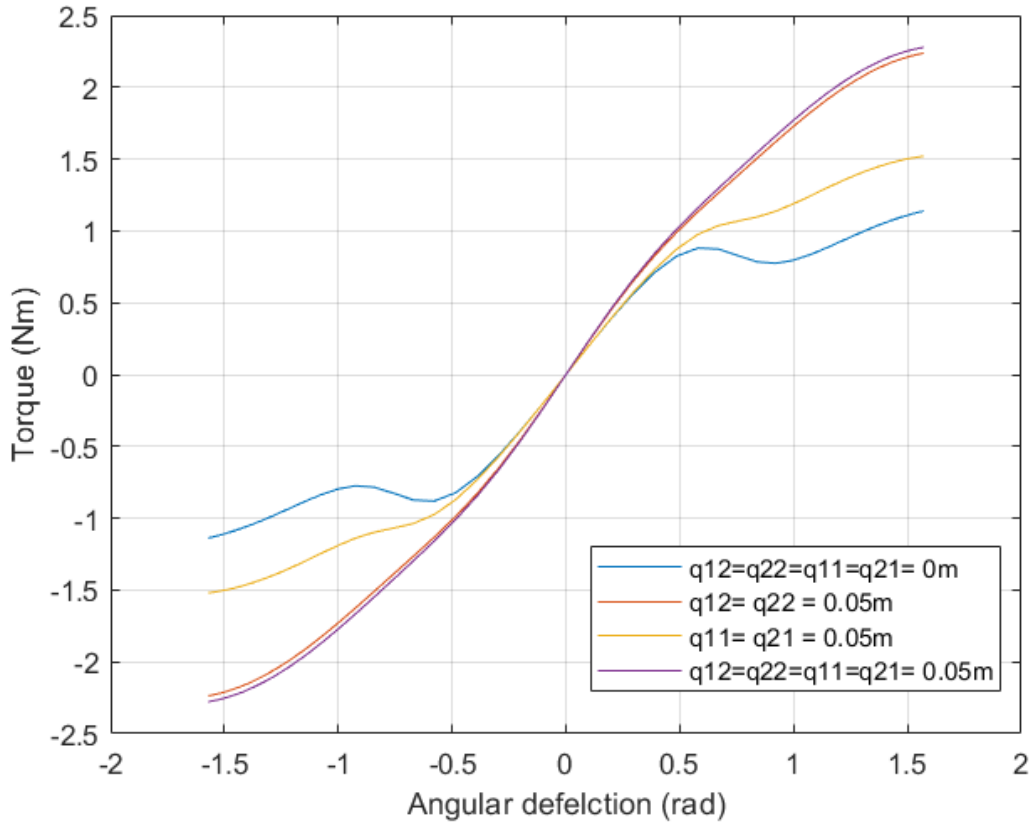

Figure 3.2: Torque-deflection plot of three different configurations at $-\pi/2$ to $\pi/2$ rad from the simulation. Four configurations consist of default configuration (all tensioning units at 0m), only upper tensioning unit (q_{12} and q_{22}) at 0.05m, only lower tensioning units (q_{11} and q_{21}) at 0.05m and all tensioning units at 0.05m which are labeled with blue, red, yellow and purple color, respectively.

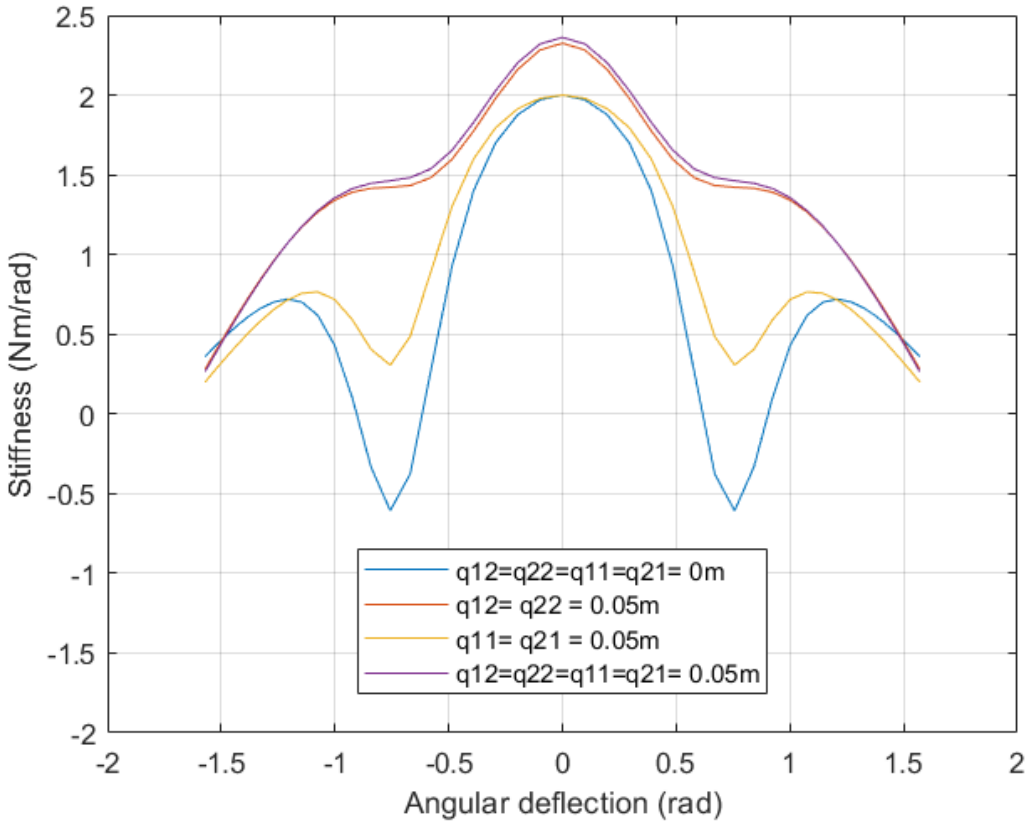

Figure 3.3: Stiffness-deflection plot of three different configurations at $-\pi/2$ to $\pi/2$ rad from the simulation. Four configurations consist of default configuration (all tensioning units at 0m), only upper tensioning unit (q_{12} and q_{22}) at 0.05m, only lower tensioning units (q_{11} and q_{21}) at 0.05m and all tensioning units at 0.05m which are labeled with blue, red, yellow and purple color, respectively.

The outcomes of output torque and stiffness show in figure 3.2 and 3.3. As it can be noticed, the lower units (q_{11} and q_{21}) provide a marginal effect on modulating stiffness in this test-bed. In comparison to the default configuration (red line in both plots), it shows a small increase for output torque which also affects small changes in stiffness, presenting the range of torque from -1.5 Nm to 1.5 Nm. The purple lines (all units at 0.05m position configuration) show a minor rise of output torque and stiffness with the red lines (configuration which only upper units actuated). The torques for both configurations show a range from -2.35 Nm to 2.35 Nm and from -2.3 Nm to 2.3 Nm, for all units at 0.05m position configuration and the upper units at 0.05m when varying angular deflection, respectively. This means that the lower units do not influence major stiffness to this test-rig. Therefore, by the upper units alone, it can regulate the output torque and stiffness of this design.

3.1.2 Effects of the lengths of parameters a,b and c

Not only tensioning units can determine the output stiffness of this test-bed but also the dimension parameters also have an influence on the cable length. In this section, therefore, the dimensions of a, b and c are varied to observe their roles on the output. The simulations are done with two configurations at 0 rad angular deflection; the default and at 0.05m position for the upper tensioning units acknowledge to the previous section (section 3.1.1) which shows that only the upper tensioning units can mainly regulate the output stiffness. The length of each parameter is varied from 0m to 0.1m with an increment of 0.01m.

Effects of a parameter

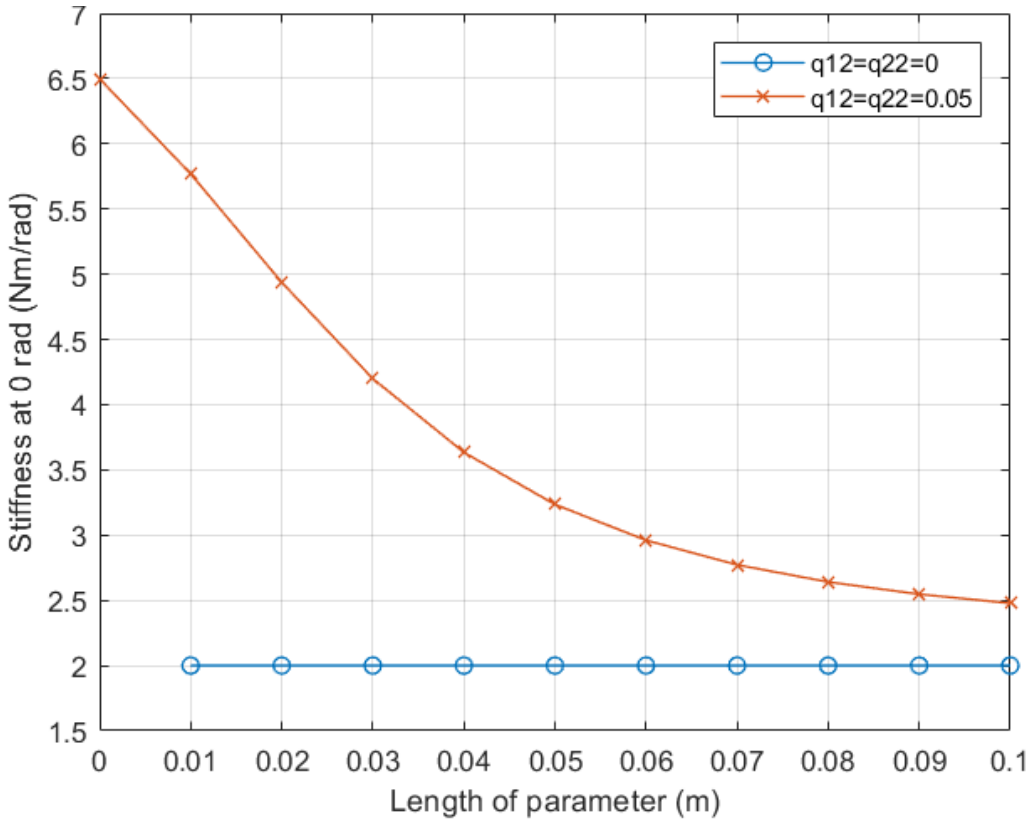

Figure 3.4: Stiffness plot of 0m and 0.05m configurations from simulation at 0 rad. Stiffnesses of each varied 'a' length (0 to 0.1 m length) from both configurations are compared. The blue 'o'-points and red 'x'-points represent the stiffness from 0m and 0.05m configuration respectively.

In figure 3.4, the output stiffness at 0 rad deflection shows stable stiffness at 2 Nm/rad for the default configuration. Whereas, for the 0.05m configuration, it shows a tendency of stiffness non-linear decreasing when the a parameter is longer. The

stiffness of the 0.05m configuration starts at approximately 6.5 Nm/rad for 0m length then gradually dropping to 2.5 Nm/rad for 0.1m varied length.

Effects of b parameter

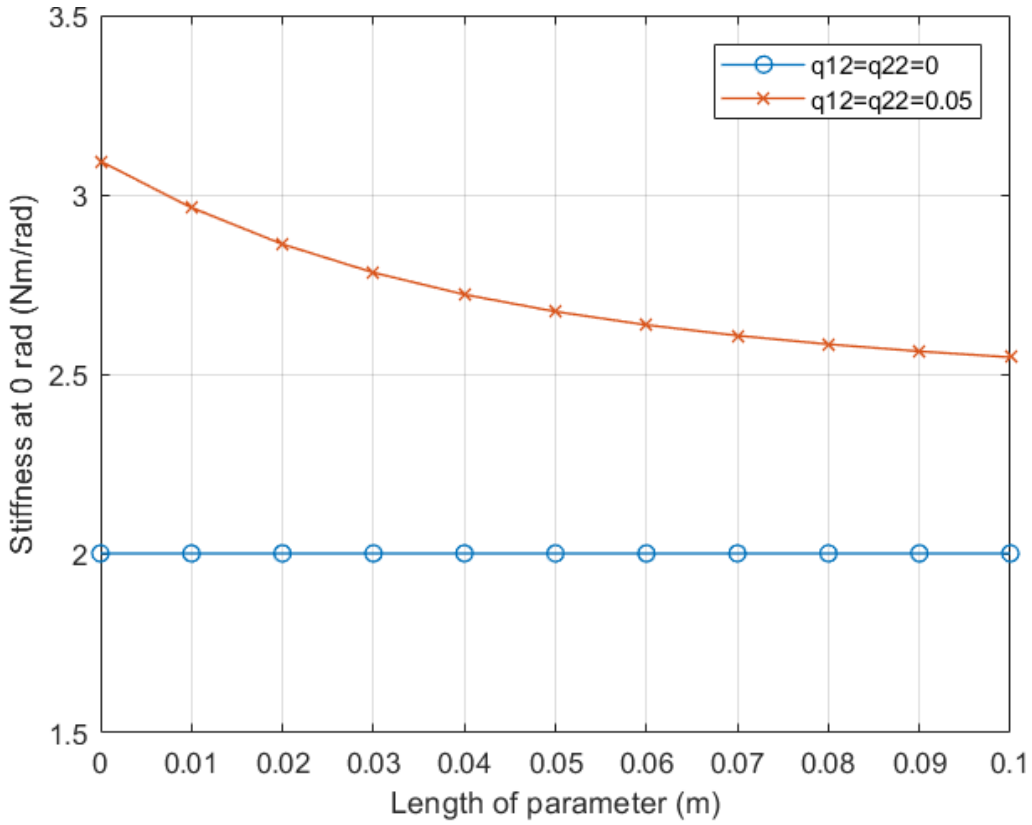

Figure 3.5: Stiffness plot of 0m and 0.05m configurations from simulation at 0 rad. Stiffnesses of each varied 'b' length (0 to 0.1 m length) from both configurations are compared. The blue 'o'-points and red 'x'-points represent the stiffness from 0m and 0.05m configuration respectively.

As it can be seen, in figure 3.5, the output stiffness at 0 rad deflection also exhibits constant stiffness at 2 Nm/rad for the default configuration as the same with varying a parameter dimension. For the 0.05m configuration, once again, it presents a decline of stiffness when the dimension of b is lengthened, starting from proximate 3.1 Nm/rad at 0m varied length and droping down to 2.6 Nm/rad at 0.1m varied length.

Effects of c parameter

As seen with the parameters mentioned prior, the output stiffness at 0 rad deflection shows stable stiffness for the default configuration. While for 0.05m configuration, it

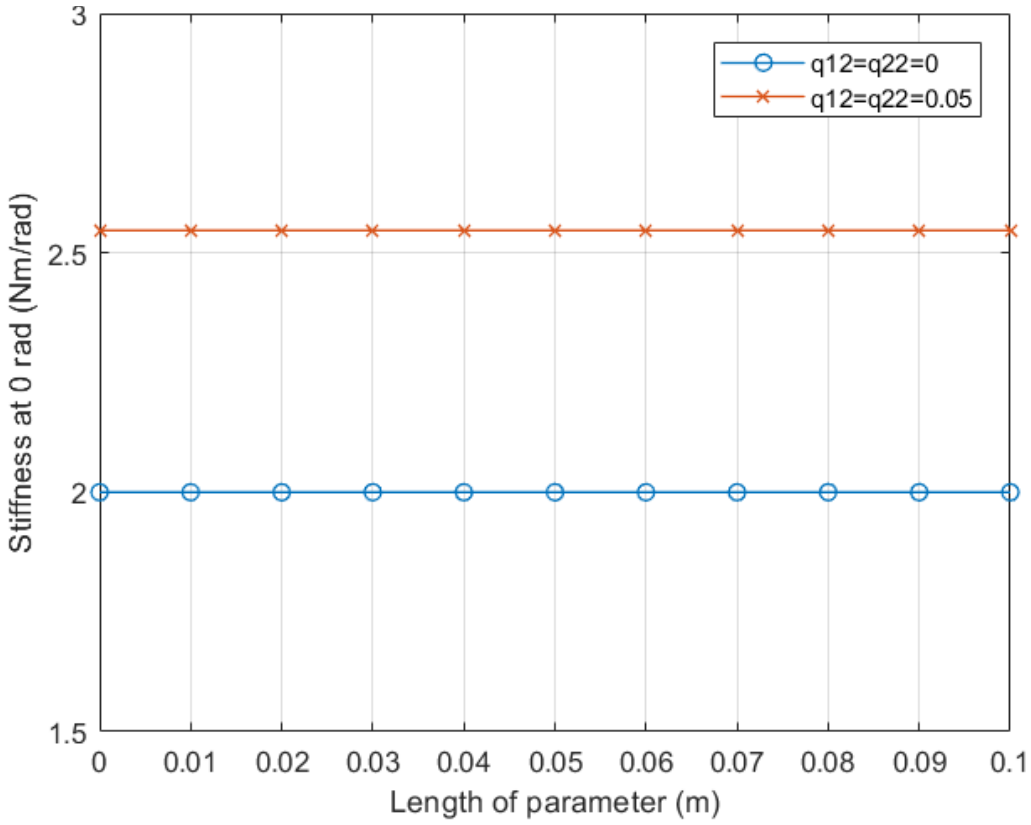

Figure 3.6: Stiffness plot of 0m and 0.05m configurations from simulation at 0 rad. Stiffnesses of each varied 'c' length (0 to 0.1 m length) from both configurations are compared. The blue 'o'-points and red 'x'-points represent the stiffness from 0m and 0.05m configuration respectively.

appears to be stable when c parameter is increased, as shown in figure 3.6. This means that c parameter does not affect the output torque or stiffness of the test bed. The stiffness is found to be higher at the 0.05m configuration than the default configuration, because the cable is tensioned by tensioning units. The outcome has higher than the default configuration results for approximately 0.6 Nm/rad.

Overall for the effect of these three parameters, the same trend of the output stiffness is presented for a and b parameters, longer the length, lower is the provided stiffness. A reason behind this trend can be referred back to the equations in section 2.2 (equation 2.4, 2.5, 2.8 and 2.9, The length of the cable can be correlatively adjusted by the magnitude and pattern by these dimension parameters especially a and b parameters. By determining the angular position at the same value, the only factor that can influence the stiffness could be torque which is a result of the cable's length. Unlike a and b parameters, the c parameter does not affect stiffness.

3.2 Torque and stiffness of cable-driven VSM test bed

After understanding the roles of each parameter on varying the stiffness, the test bed is set according to the dimension parameters as previously shown in figure 3.1. Thereafter, the output torque and stiffness are simulated to examine the capability of test bed on providing stiffness. Furthermore, these outcomes can be compared with the actual performance of the test bed in the measurement.

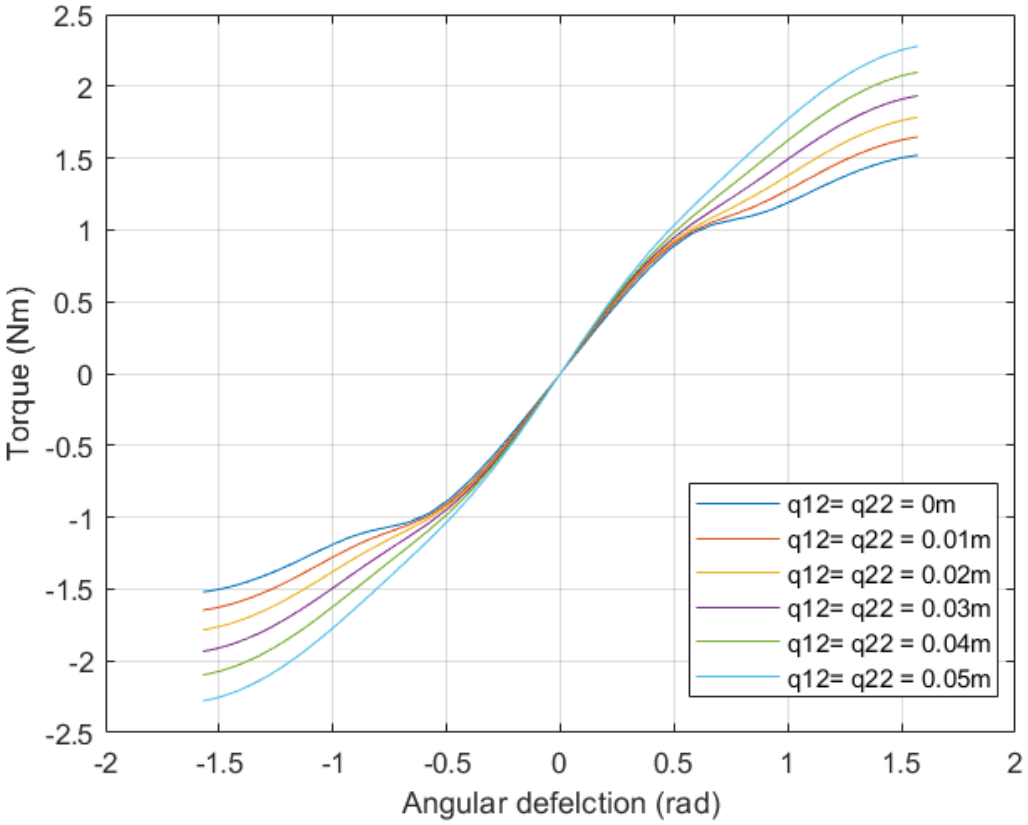

Figure 3.7: Torque-deflection plot of all configurations; 0m to 0.05m with 0.01m increment at $-\pi/2$ to $\pi/2$ rad from the simulation.

In figure 3.7, the torque-angular deflection is plotted for all configuration of the upper tensioning unit position around the angular deflection of $-\pi/2$ to $\pi/2$ rad. The pattern of the output torque presents the higher tension on cable (tensioning units moved further), the higher torque and stiffness can be obtained. The simulated results are also reflected in each configuration in figure 3.8. The stiffness plot shows the maximum and minimum of stiffness. As observed, for the stiffness change of all configuration, at 0 rad angular deflection, the stiffness change can be noticed. The maximum stiffness change can be observed at approximately 0.75 rad while he minimum stiffness change of all configuration shows at 1.6 rad.

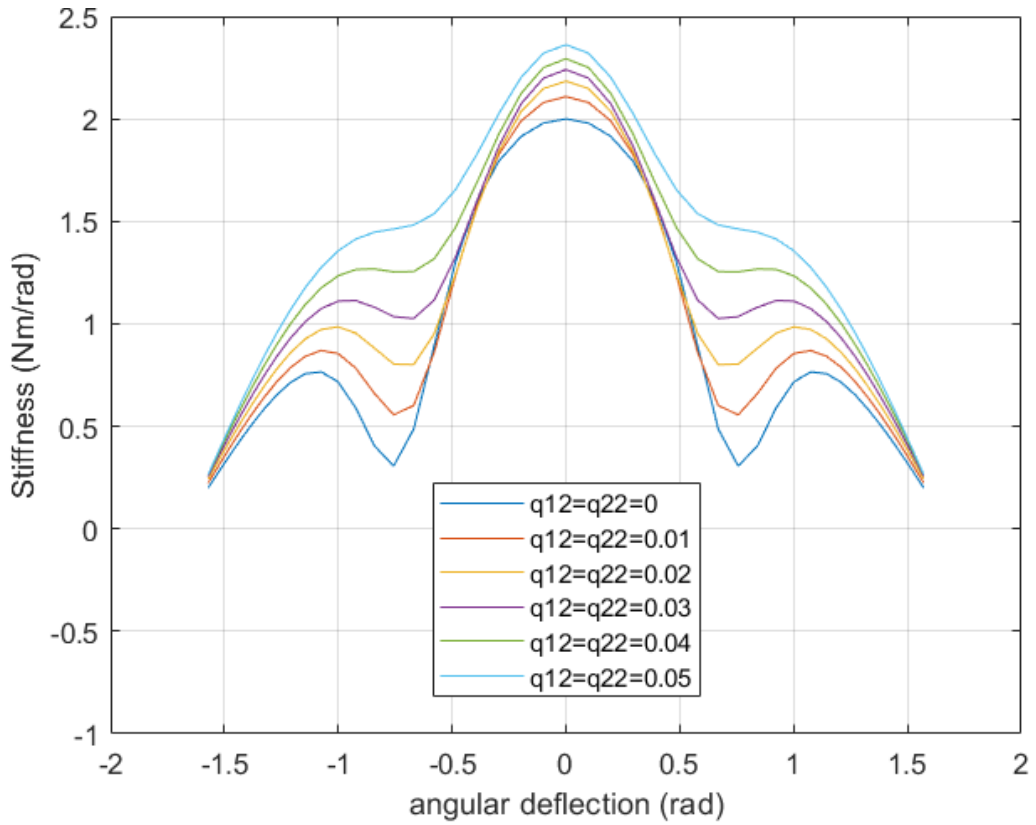

Figure 3.8: Stiffness-deflection plot of all configurations; 0m to 0.05m with 0.01m increment at $-\pi/2$ to $\pi/2$ rad from the simulation.

3.3 Effects of an elastic element

Apart from the dimension parameters, the effect of the elastic element which was also applied on the test bed might be intriguing to understand. By changing the type of elastic element, which outcome of the test bed will be altered is a question that will be answered in this section. Moreover, the additional objective as mentioned in section 1.3 is also planned to perform with a different elastic material.

In this simulation, therefore, rubber bands are chosen to be used since it has nonlinear stiffness property. Unlike the linear stiffness material which has constant stiffness, the nonlinear stiffness material has a unique nonlinear stiffness. The stiffness of rubber band is calculated by performing regression calculations over its tensile force-elongation plot which shown in appendix A.

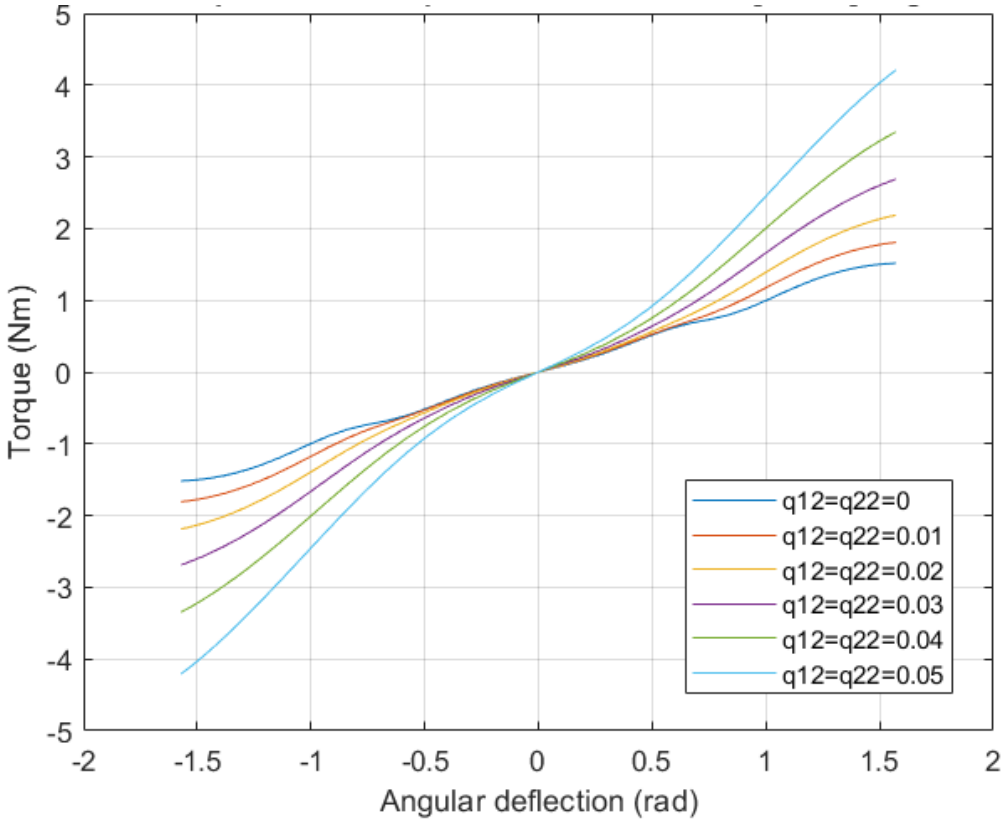

Figure 3.9: Torque-deflection plot of all configurations; 0m to 0.05m with 0.01m increment at $-\pi/2$ to $\pi/2$ rad from the simulation with non-linear stiffness element

In figure 3.9, the torque-deflection plot for all configurations at $-\pi/2$ to $\pi/2$ rad is shown. The plot profile is different from figure 3.7. The profiles of figure 3.7 have 's'-shaped curves, the end of curves curling inward. While in figure 3.9, the profiles align straighter than in figure 3.7 with some deviations at the end of curves diverging outward. In addition, the torque magnitudes of each configuration are also different.

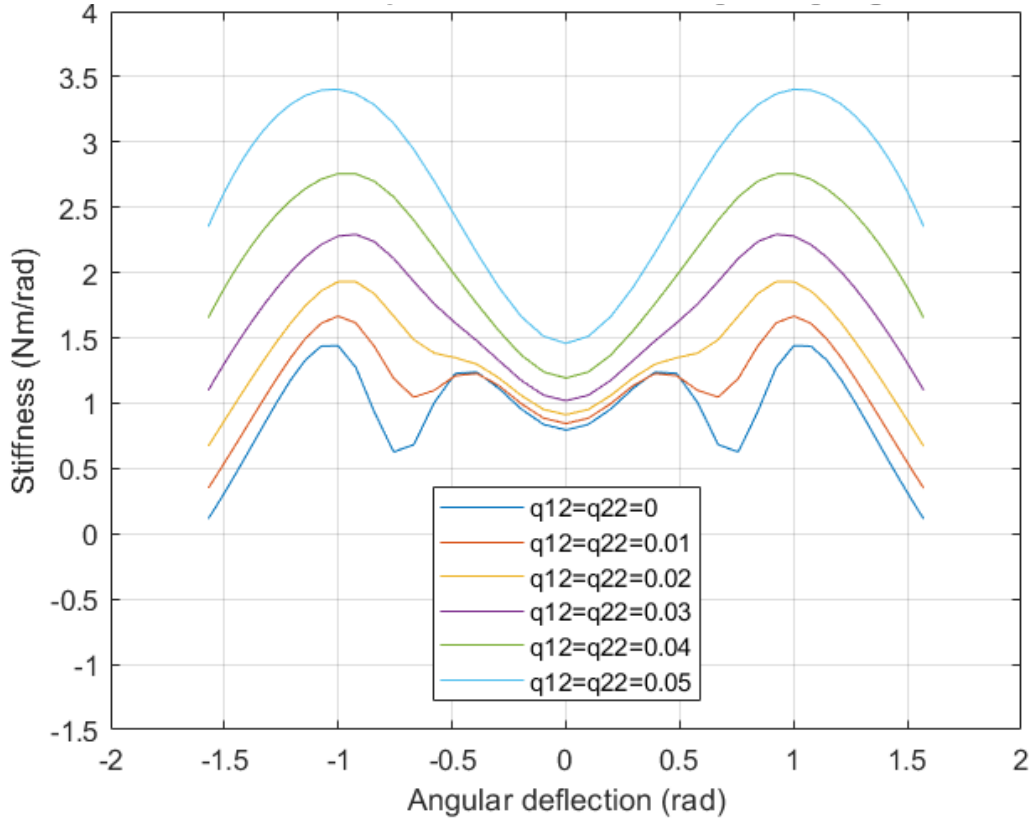

Figure 3.10: Stiffness-deflection plot of all configurations; 0m to 0.05m with 0.01m increment at $-\pi/2$ to $\pi/2$ rad from the simulation with non-linear stiffness element

The nonlinear stiffness element have higher torque than the linear stiffness element, for instance, the range of torque presents -4.2 to 4.2 Nm for nonlinear stiffness element which is higher than the range of torque for linear stiffness element (-2.35 to 2.35 Nm) at 0.05m configuration. Likewise, the stiffnesses of all configurations around $-\pi/2$ to $\pi/2$ rad which exhibits in figure 3.10 show different profiles. The stiffness of linear stiffness element in figure 3.8 exhibit a bell-shaped profile while figure 3.10 has a wave-shaped profile. At the 0 rad angular deflection, the stiffness of nonlinear material presents lower stiffness than linear material.

Chapter 4

Measurement of cable-driven variable stiffness mechanism

As mentioned before in section 1.3, to prove that the design meets the objectives of the study, three measurements were set up. The test bed which has been prototyped according to Chapter 2 was used in these measurements. The details of each measurement is described, the procedure and experimental setup in each case of measurement is explained. Furthermore, the hardware and software used for this study is specified. Lastly, data processing techniques that were used and analysis of the measured data is elaborated upon.

4.1 Measurement procedures

Prior to performing measurements, one notice that should be mentioned is the default configuration of the test bed. it was configured as shown in figure 3.1 as the default setting. Additionally, an extra measurement was also done in order to investigate the stiffness of the design with a non-linear elastic element. Therefore, there were four experiments in total. Each experiment is explained in detail.

Proving that measured stiffness is equal to the desired stiffness is the first objective. In this experiment, the stiffness was measured by acquiring torque and deflection of output from the encoder and sensor stated in figure 2.3 with no load applied on the output lever. During measurement, the output lever was moved back and forth with a certain deflection from - 0.436 to 0.436 rad (or -25 to 25 deg) which is limited by a marker in the set-up. Therefore, the stiffness can be determined about the default angle of zero. The different tensioning pulleys stroke length was varied. In each varied stroke length, the pulley in the upper tensioning units (q_{12} and q_{22}) will move symmetrically outward as shown in figure 4.1. The stroke length started from default configuration and increased in increments of 0.01m and went upto 0.05m

position measuring five repetitions for each configuration. The measured stiffness will be collected and compared with the desired stiffness which simulated from the derivation based on kinematic analysis (section 2.2).

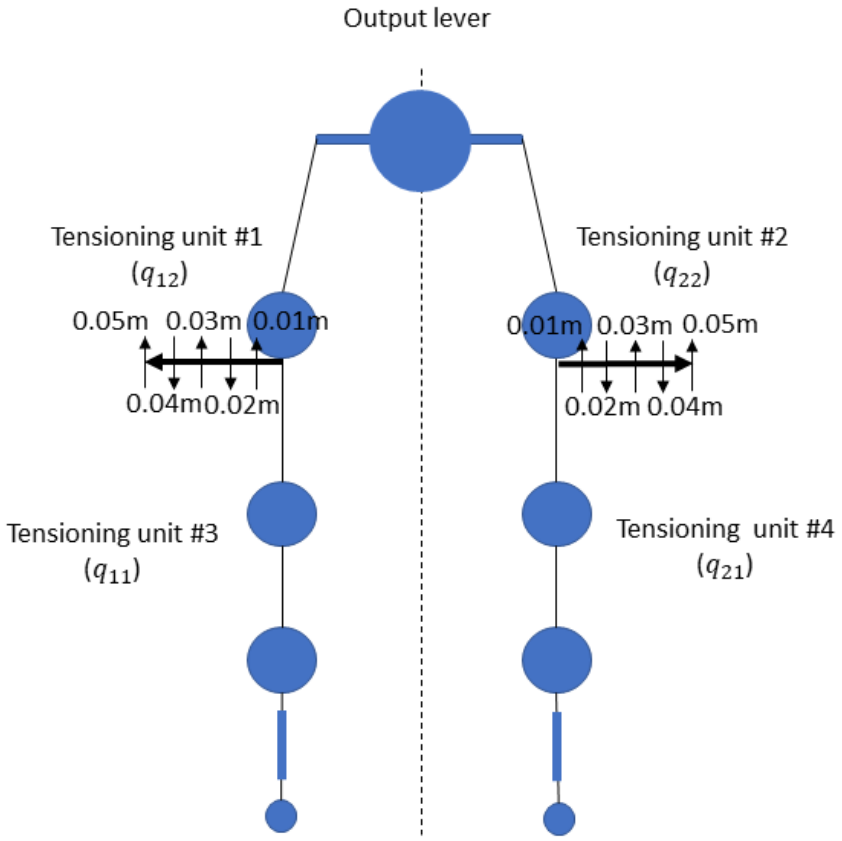

Figure 4.1: Scheme shows configuration for varying stroke length during measurement

The next objective is to prove that the mechanism can provide constant torque when varying the stiffness of mechanism. Due to the non-linearity of the transformation between the cable mechanism and the attachment to the output lever which causes different force projections of the cable on the perpendicular and parallel axes, the output lever should remain at the equilibrium position. Thus, the constant torque which can be referred to the consistency of angular position was expected to remain at the equilibrium position when stiffness changes for every applied torque conditions. During the experiment, varied loads were applied to the output lever by changing calibration weights, exemplifying the constant torque. To keep the applied toque constant, the calibration weights will be weighted under the gravity and routed it with the cable and an additional pulley which mounted on the output lever. Measuring the angular position of output by the encoder, the measured angle should remain constant when the stroke length of tensioning pulleys change. Furthermore, in the same manner with the first experiment,repetiitons were done five times for

each varied weight. However, in this objective, two measurements are done; static and dynamic measurement. Both measurements are done with the same setting. The only difference is the motion and number of movable pulleys. For the static measurement, the stroke length of two tensioning units (same configurations with the first experiment as shown in figure 4.1) are varied every 10 seconds from 0.01 m to 0.05 m long. On the other hand, the dynamic measurements are performed with specific trajectories of four tensioning units for a 10-second period. In figure 4.2, the trajectories are shown indicating the equation of motions for upper tensioning units(q12 and q22) and lower tensioning units(q11 and q21) were derived from the simulation-based on the analytical model which were shown in sinusoidal form but differ in phase. As it can be noticed, the upper tensioning units were moved in the opposite direction with the same equation, exhibiting dynamic motion which is periodic (sinusoidal waveforms). Likewise, the trajectories of both lower units were actuated in the same manner.

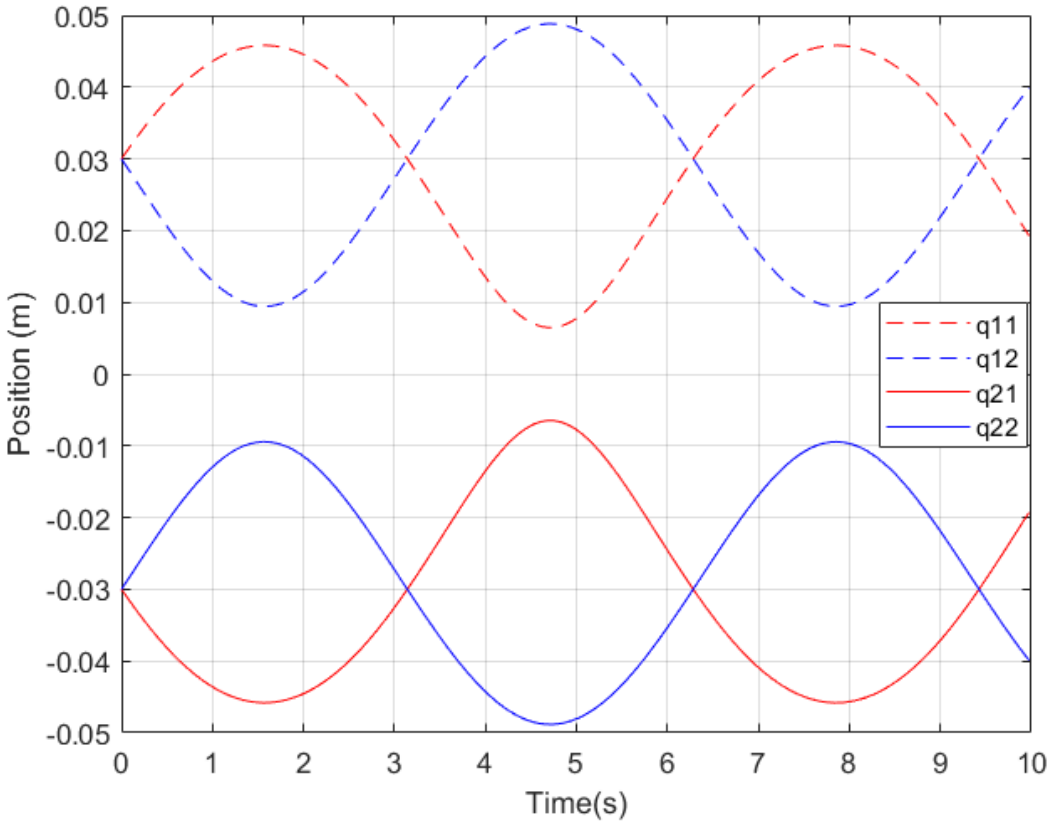

Figure 4.2: Trajectories of tensioning units for dynamic motion

The third objective was to prove that total energy consummation of the variable-stiffness unit is equal to zero or approximately to be zero by compensation. The power consummation was tracked by measuring the present current by connect-

ing the current sensor to the power supply, recording power consumption (current). This measurement can be performed during the second-objective measurement in both static and dynamics which means all setting was the same with those measurements. The setting includes the varied parameters, stroke length (in statics) and the trajectories (in dynamics). The trajectories shown in figure 4.2 is applied again on this measurement. It is because of the trajectories are the compensation in motion of each pulleys from the simulation. Five repetitions are performed for this measurement.

Apart from the three main objectives, one additional measurement is included to prove that the mechanism can vary its stiffness in any case. By substituting from linear stiffness spring to non-linear stiffness spring (rubber band), different characteristics of stiffness (due to the altered springs compliance) will be presented. The profile of rubber band was given in A(will be added after getting the result from tensile machine). As was the case for the first experiment, stiffness by torque and deflection angle were measured by varying stroke length following the order from the first experiment. The measured stiffness profile between linear and non-linear springs was compared. In the same manner with the first measurement, the interaction bar was rotated with periodic movement, backward and forward, providing the deflection amplitude and frequency (approximate) of the cycle. As a result of this, the hysteresis profile of both springs types was obtained. The rotation will be limited by the marks on the set-up. Once again, this measurement were done with five-time repetitions.

4.1.1 Measurement setup

All of the measurements were done with the cable-driven VSM test bed which has a force/torque sensor and an encoder. To obtain the output torque on the z-axis (torsion torque), ATI Mini40 force/torque sensor is connected with a computer over ethernet. The angular deflection is measured by using an AMS magnetic encoder (AS5048A). Additionally, a current sensor (RobotDyn ACS712ELCTR-20A-T) was added in order to perform the third objective (proving energy consumption), measuring the servo motors current. To acquire the data from sensors, a microcontroller (Arduino mega 2560) was used and connected with sensors. The encoder and current sensor are interfaced directly with the microcontroller. For the force/torque sensor, it was individually connected to the computer with a separate port, ethernet as mentioned before. All data from three sensors are simultaneously acquired in Matlab Simulink for further processing.

4.1.2 Data processing

The data from each measurement are processed with Matlab(2017b), the processed data will be shown in the next chapter, chapter 5. Regard to the measurements procedure in section 4.1, four measurements were done. When considering about post-processing, therefore, it can be classified into three approaches:

1. Stiffness of the cable-driven VSM

   In this method, stiffness modulation and individual torque-deflection profile for both the linear and nonlinear elastic elements are included. The acquired torque and angular deflection were extracted by segmentation. Thereafter, for illustrating the result, all the segmented data from every trial (5 trials for each configuration) were included to calculate averaged data. The averaged data of torque and angular deflection were together plotted. With the relationship between stiffness, torque and angular deflection($K = \frac{\partial \tau}{\partial \theta}$) as shown in equation 2.5, the stiffness can be found from the slope of torque and angular deflection plots. For computing the stiffness from the slope of the plot, linear regression is applied. The linearization covers all the data ranges of torque and angular deflection then selecting two points in the line for calculating slope or stiffness. Lastly, the averaged data of torque and angular deflection of every configuration will be plotted in the individual and overlaid presentation. The overlaid plot can exhibit the modulation of stiffness when configuration changed. Furthermore, a statistical test will be done with Mean Absolute Error (MAE) to compare the similarity of both measured and simulated data in quantitative term.

2. Angular position when changing stiffness

   To meet the second objective of the study, showing equilibrium position when changing stiffness, five repetitions of each varied load are averaged and displayed in the time frame. The measured data, the angular position and current, are averaged. The current represents the moment of stiffness changing actuation. The angular position together with the current allows observation of the change of equilibrium position of each constant load condition. Be noted that, the equilibrium position indicates the constant torque and angular position. To obtain the quantitative result of the consistency of equilibrium position, the angular position data are subtracted with the offset resulting in angular displacement. The offset is the initial angular position which occurred before starting measurement when applying loads on the output lever. The initial position was acquired by collecting data of angular position over the resting period (10-second interval after applying weight and before varying stiffness). Then,

these extractions from every varied load were calculated the average of angular displacement with standard deviation. Besides, this approach is used for both static and dynamic measurement of the second objective.

3. Energy consumption

   The energy consumption can be derived by the power usage of the system. With the relationship between power and current, the data of current for both static and dynamic measurement can be calculated into power consumption. Eventually, the energy consumption can be also computed form the power consumption. All repetitions from each varied parameters are averaged and presented.

Chapter 5

Results

In this chapter, the results of the measurements are discussed. These results indicate the characteristics of the design as the proofs of concept based on the research objectives. First, the characterization of the mechanisms stiffness will be presented based on the first objective, proving the change of stiffness should be controlled as desired (following section 1.3). Then, the profile of the change of output deflection when the tensioning units actuated will be displayed, verifying the objective that the mechanism should provide the constant torque when the mechanism adapting the stiffness. Lastly, the stiffness profile when replacing the elastic component will be shown.

5.1 Stiffness of the cable-driven VSM

5.1.1 Measured data

Figure 5.1 shows the results of three measurements for different configurations of tensioning units position, namely 0, 0.03, 0.05 m. The increment of stiffness can be found from 1.13 Nm/rad to 1.64 Nm/rad when inflecting tensioning units from zero position to q_{12} and q_{22} =0.05m, indicating a capability of stiffness modulation. As it can be seen, the output torques go from negative to positive value (-0.4 Nm - -0.5Nm to 0.45Nm - 0.55Nm) varied as the change of angular deflection from approximately -0.4 rad to 0.4 rad. Moreover, the curves recognize the hysteresis profile which was plotted by the measured torque and angular deflection from different configurations of the upper tensioning units (q_{12} and q_{22} as follow in diagram figure 2.2). The hysteresis loops showed particular slopes or stiffnesses. The color-dashed lines are linearized slope over the whole data representing stiffness. The plot shows averaged curves of each configuration. Be noted that, in this figure, three of configurations' results were displayed with the reason for an explicit visualization. However, in

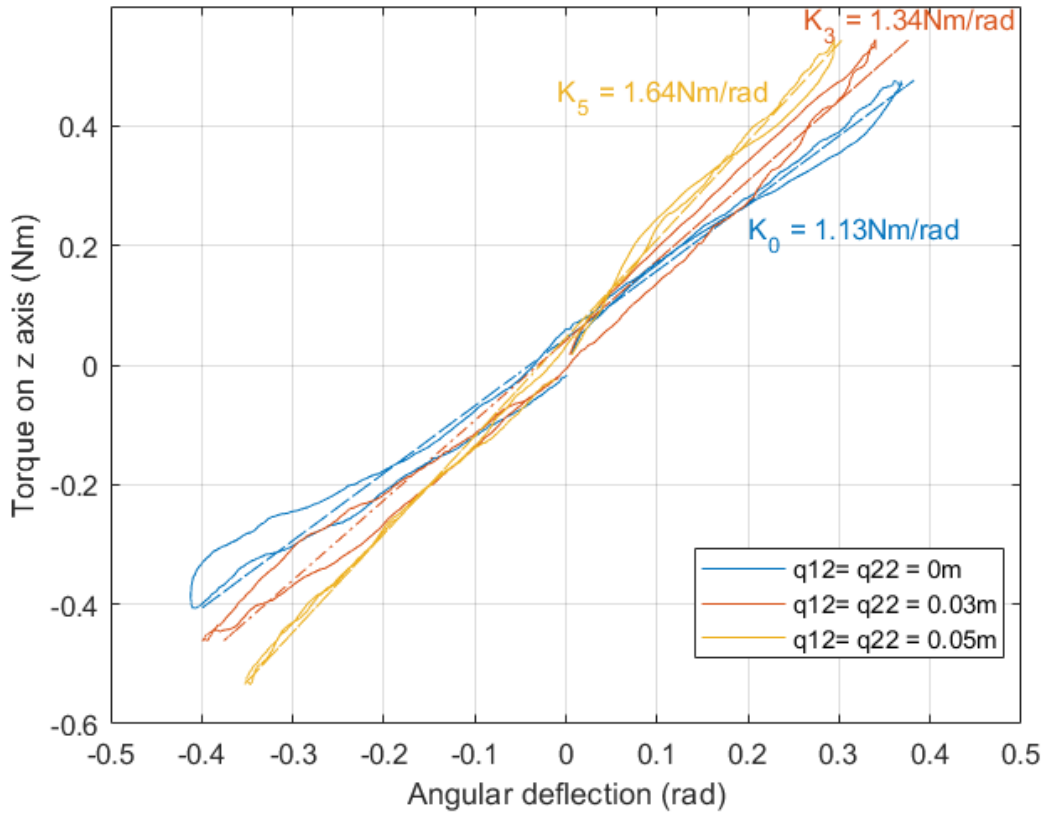

Figure 5.1: Torque-deflection plot of various configurations; 0m, 0.03m and 0.05m from measurements. Approximate stiffnesses of each configuration are shown in dash-colored lines with labelled stiffnesses values

appendix B, a torque-deflection plot which includes every configurations' data overlaying in one plot is presented.

To clarify the characterization of each configuration, the plots of all distinctive hystereses have been presented in appendix B.1. However, in this section, only one example is shown. In figure 5.2 displayed below, the characterization of stiffness from 0.01m configuration is exhibited with 1.19 Nm/rad of stiffness from -0.4 to 0.4 rad angular deflection. To calculate the stiffness, the same method shown in figure 5.1 was applied. The averaged curve was shown in blue color with dashed lines. The dashed lines represent stiffnesses, as follows the data processing in section 4.1.2. As it can be noticed, there are two stiffnesses from this configuration. Throughout, all results for individual torque and angular deflection plots, some of configurations showed diverged curve out of the linearized line. Hence, the diverged part was performed the segmented linear regression to bring out the diverged stiffness as shown in the purple-colored line. In this case, the secondary stiffness shows 2.43 Nm/rad with the same angular deflection range. As mentioned before, the hysteresis

can be found for all measured results. Therefore, in this example, it also shows hysteresis.

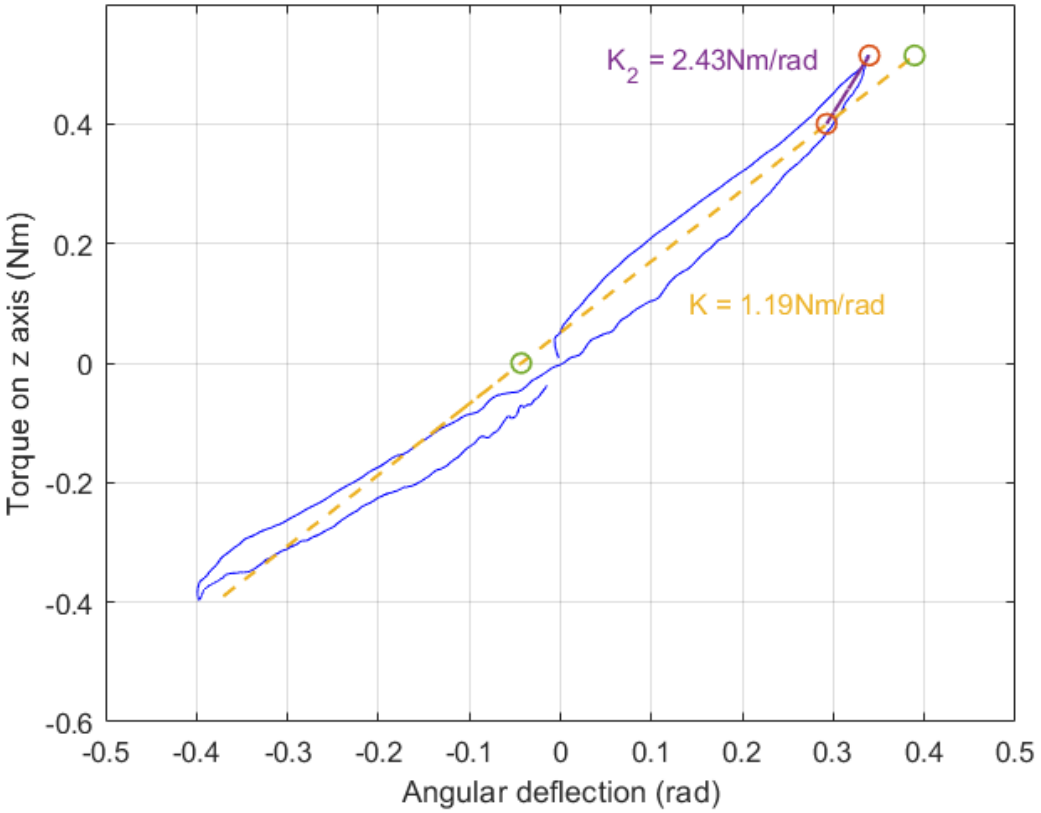

Figure 5.2: A representative torque-deflection plot of 0.01m configuration with segmented stiffnesses. The yellow line depicts the estimated stiffness in overall with the color-labelled stiffness value. The secondary stiffness is shown as the purple line and value, indicating the diverged segment of the curve.

5.1.2 Simulated data

Simulated result for some configurations is displayed in figure 5.3. As can be observed, the stiffness varying is appeared when the configuration of q_{12} and q_{22} was changed with the range from 1.96 Nm/rad to 2.21 Nm/rad. The plots show the same pattern with the result in section 5.1.1, the stiffness increases when the tensioning unit position rise. Unlike in figure 5.1, the output torques are higher than the measured result (-0.85 - -0.76 Nm to 0.85 - 0.76 Nm at angular deflection from -0.4 to 0.4 rad). Moreover, in figure 5.3 showed no hysteresis. This simulated result is the extraction of figure 3.7, showing some configurations for the reason for clear visualization. Each curves represented each configuration outcome. The individual slopes which can be referred to as the stiffness are exhibited. Similarly, with the measured results in section 5.1.1, three curves for three configurations; 0m, 0.03m and 0.05m, are displayed. For all configurations' results, they were displayed in appendix B.

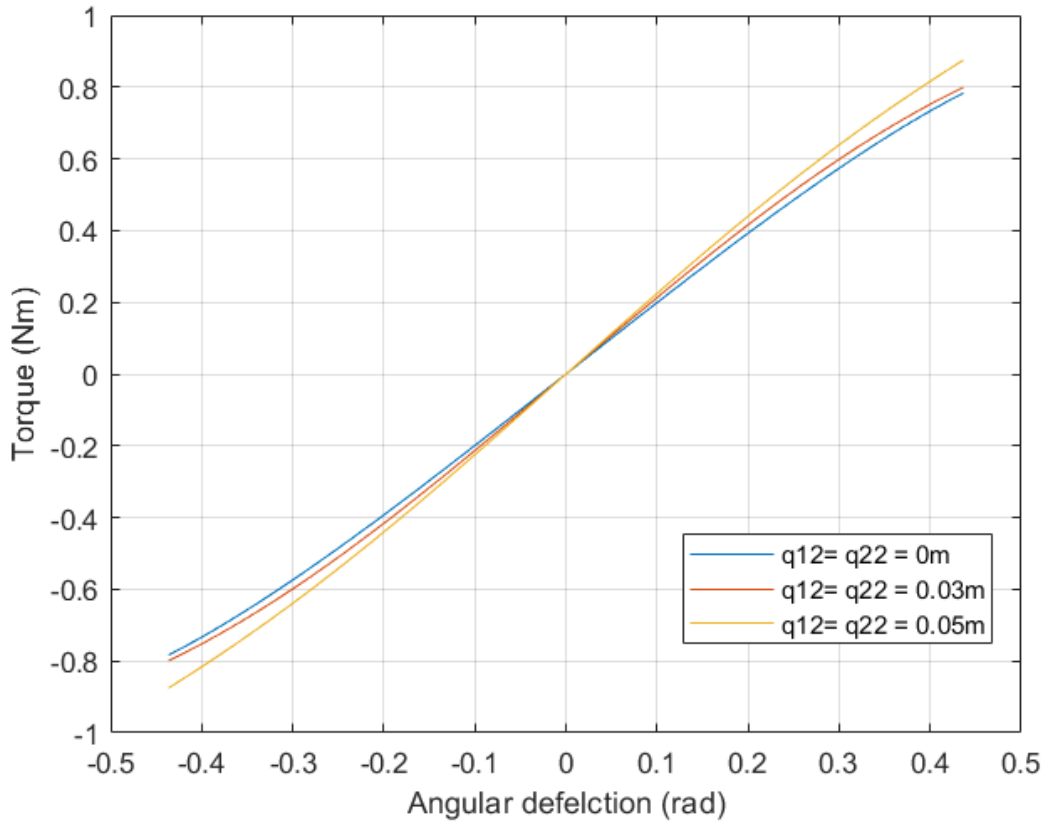

Figure 5.3: Torque-deflection plot of various configurations; 0m, 0.03m and 0.05m from simulation with the colored lines indicating each configuration

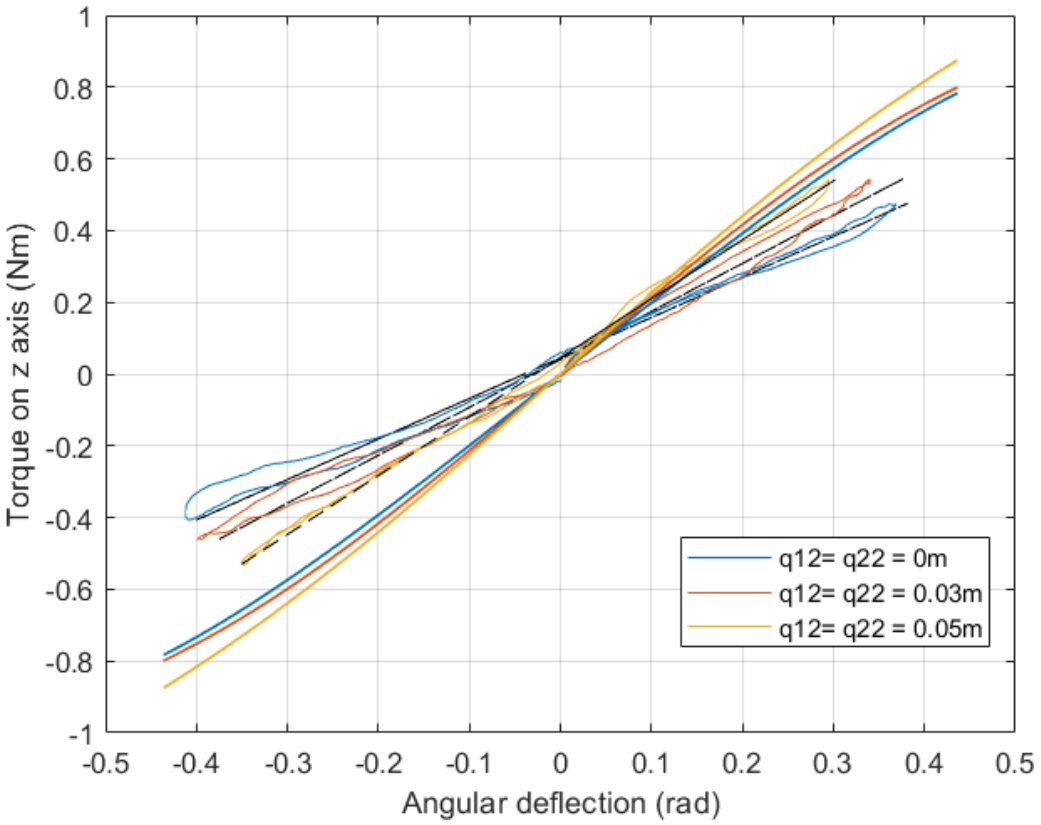

Figure 5.4: Torque-deflection plot of several configurations comparing between measurement and simulation. The measured data are illustrated as an approximate linearized stiffness (dashed black lines). Simulated data are shown as solid curves.

Configuration (m)	**0**	**0.01**	**0.02**	**0.03**	**0.04**	**0.05**
MAE (Nm)	0.3027	0.2911	0.2779	0.3068	0.2883	0.3355

Table 5.1: Statistical results of comparison between measurement and simulation showing with Mean Absolute Error (MAE)

For comparison, figure 5.4 shows the result of both measurement and simulation overlaid on each other. Although both of the results were arranged in the same pattern, differences in stiffness can be found when comparing both simulation and measurement. The slopes which represent the stiffness of simulation seems to be steeper than measurement on every configuration. In table 5.2, MAE calculations are performed between the simulation and measurement for each configuration. The result is exhibited the range of 0.2779 - 0.3355 Nm for MAE which means a marginal dissimilarity of both data can be found. For each type of results, data from three configurations were shown, labelling by colors; blue, red and yellow which identify 0, 3

and 5 cm configurations, respectively. The simulated data is presented in solid lines with colored labels as mentioned. For the measurement, the colored hystereses of each configuration has been illustrated with the black-dashed lines symbolizing stiffnesses. The dashed lines represent proximate stiffness by linear regression.

5.2 Output angular position when changing stiffness

5.2.1 Static measurement

As the results of the second measurement shows, performing the change of tensioning units configurations in order to vary stiffness, figure 5.5 shows the change of output position by time. As can be seen, in figure 5.5(A) exhibits the angular deflection of the output bar over time for every condition of the applied load. The changes of angular position leave unchanged for most of the constant load conditions. For the 0.4Nm-condition, slight differences between initial and last position can be noticed. The average of angular displacement have complied with the aforementioned observation, the first three conditions show marginal angular displacement (0.001, 0 and 0.003 rad) and the last condition (0.4Nm condition) reveal a higher angular displacement than the other. Likewise, when looking at the standard deviation, the variation in average displacement change of the 0.4Nm condition is largest value over the other. Deviation is exhibited after actuating the 0.01m-configuration stiffness relating to the middle plot (figure 5.5(B)) which represents the current use indicating actuation of tensioning units for all conditions. As demonstrated, the actuation shows around every 10-second as follow the procedure in section 4.1. In figure 5.5(c), The bar chart reveals the angular displacement throughout all time in quantitative results. The chart shows the average difference of angular position with standard deviations of every condition.

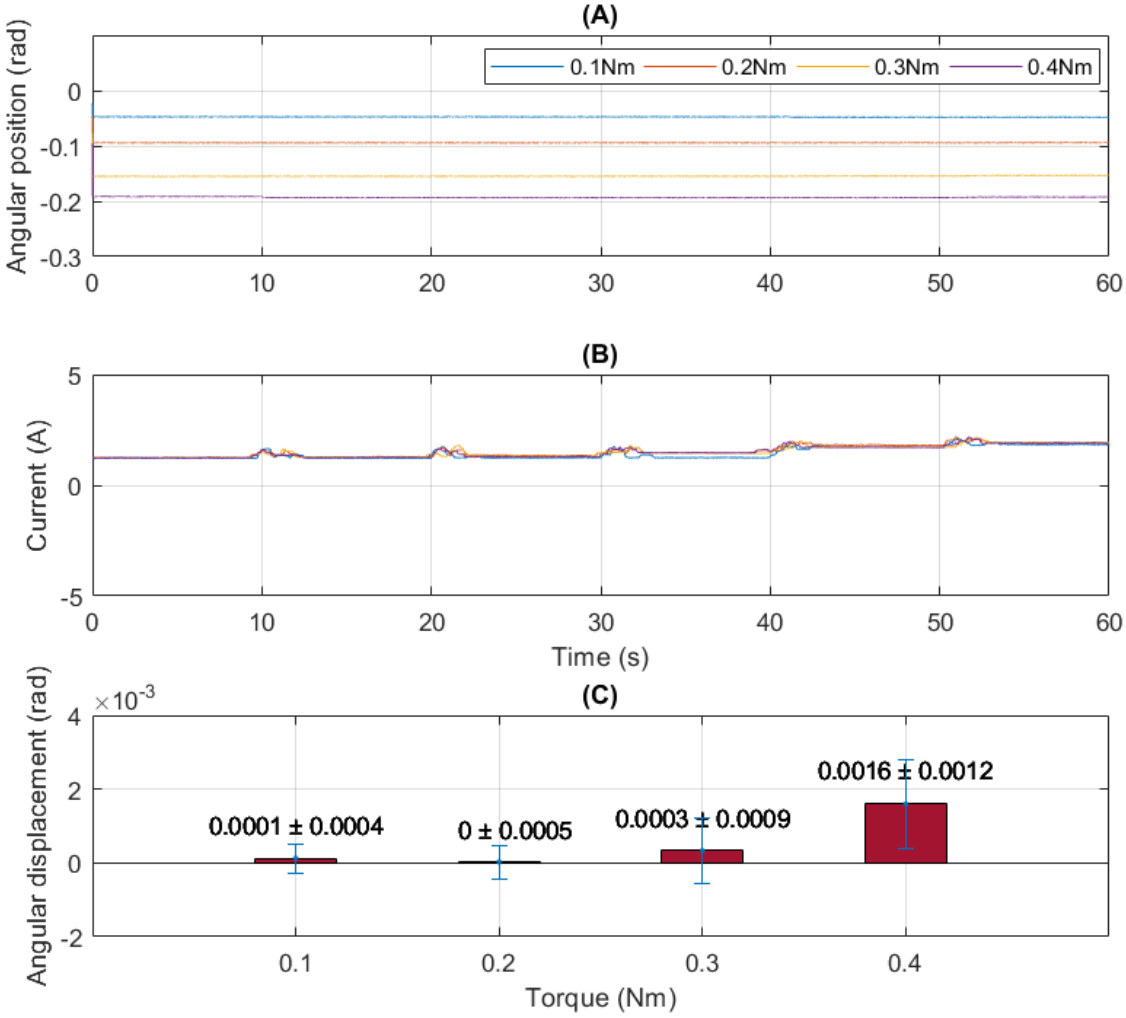

Figure 5.5: The output angular position when changing stiffness with holding constant load in static measurement.(A): the change of angular position of each constant load condition in measured duration.(B): the actuation of stiffness modulation are represented by motor's current in the same measured duration. (C): the quantitative results of the angular displacement of each constant load

5.2.2 Dynamic measurement

Figure 5.5, figure 5.6 presents the outcome of output angular position when the stiffness of mechanism was varied in dynamic motion respecting the trajectories (figure 4.2). When looking at the result, the output positions of all conditions through the period of time were collected and displayed in the top plot (figure 5.6(A)), slight changes are displayed when the stiffness changed in dynamic of every condition. At around 12-second to 22-second time, the minor deviation of output can be observed. The angular position show larger fluctuation for 0.1Nm and 0.4Nm conditions than the 0.2Nm and 0.3Nm condition. In figure 5.6(B) exhibits the operating time period which complies to the aforementioned inspection, the current use of all conditions also show fluctuations at approximate 12-second to 22-second time. To show measurable results, in figure 5.6(C), the deviation of angular displacement and the average angular displacement are presented. In the bar chart presents the higher displacements for the 0.1Nm and 0.4Nm conditions and lower number for 0.2Nm and 0.3Nm conditions, values support the observation.

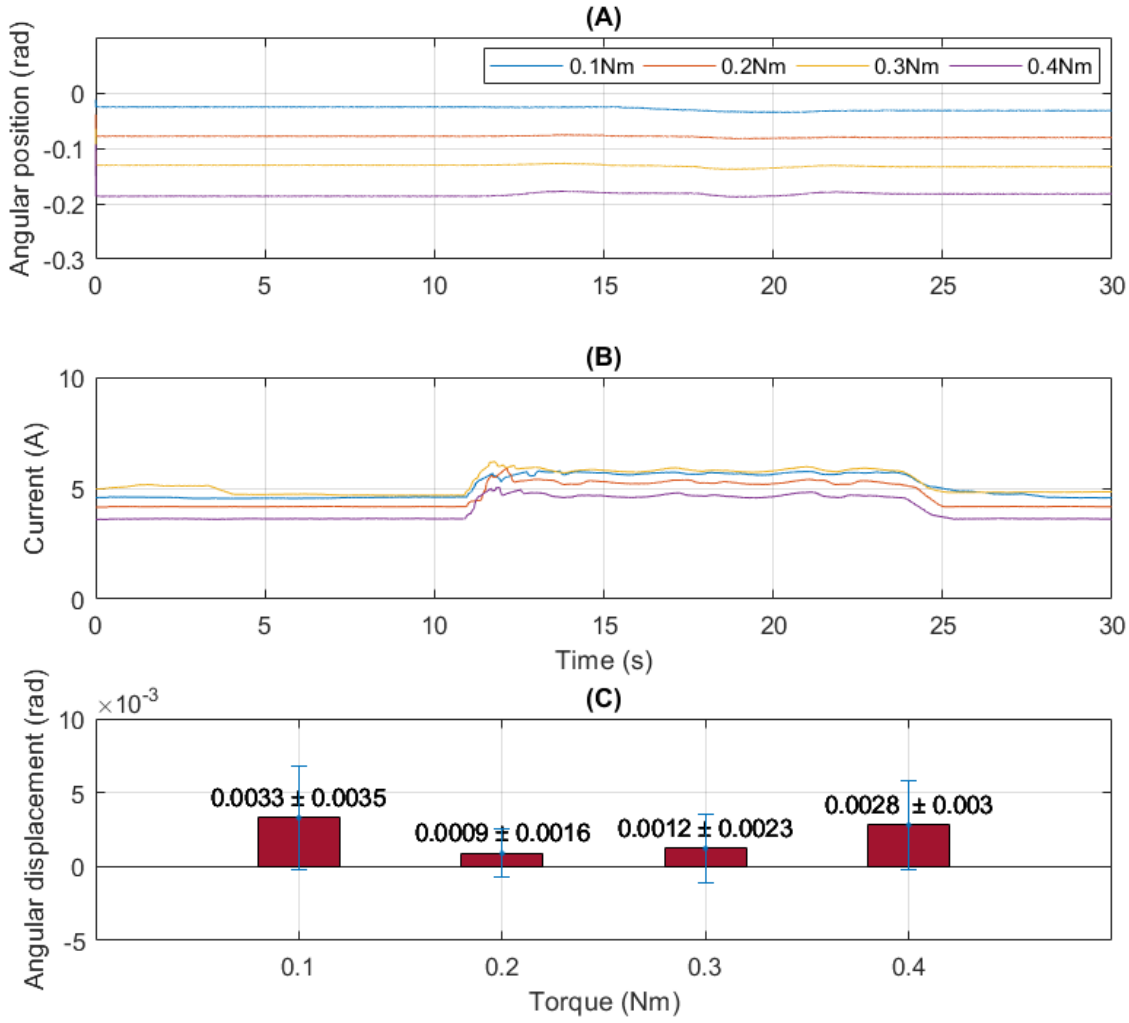

Figure 5.6: The output angular position when changing stiffness with holding constant load in dynamic measurement. (A): the change of angular position of each constant load condition in measured duration. (B): the actuation of stiffness modulation are represented by motor's current in the trajectories duration. (C): the quantitative results of the angular displacement of each constant load

5.3 Stiffness of the cable-driven VSM with non-linear stiffness elastic element

To ensure that the cable-driven VSM is promising on varying stiffness, the different elastic element like a rubber band, is used, which provides nonlinear stiffness. The nonlinear stiffness of rubber bands can be found by performing the regression over its tensile force - elongation profile which is shown in appendix A.

5.3.1 Measured data

In figure 5.7 shows the result of the change of stiffness over various configurations. It can be seen that the stiffnesses were modulated when configuration was changed, showing an increment of stiffness when the tension of cable risers, from 0.47 Nm/rad to 0.63 Nm/rad for the default configuration and 0.05m configuration. When looking at the torques, they are also varied from negative to positive value as the angular deflection changed from -0.4 to 0.4 rad. One remark on this result, the slopes of the plot showed differences with figure 5.1 since the elastic material has distinct properties. The differences are the the magnitude of torque and also the hysteresis profile. The hystereses are wider than the linear stiffness material. Whereas, the output torques are lower than the linear stiffness elastic element. Once again, each configuration is labeled by the color with linearized slope which is shown as a dashed line.

Similar to figure 5.2, in figure 5.8 as an example, an individual curve of 0.01m configuration with stiffness (K is represented). By applying linear regression, the slope or stiffness is shown 0.52 Nm/rad. As a measured data, the hysteresis can be found. The yellow-dashed line indicates an approximate stiffness on this configuration as mentioned method in 4.1.2. The rest of the nonlinear elastic elements result from the other configurations were presented in appendix B.

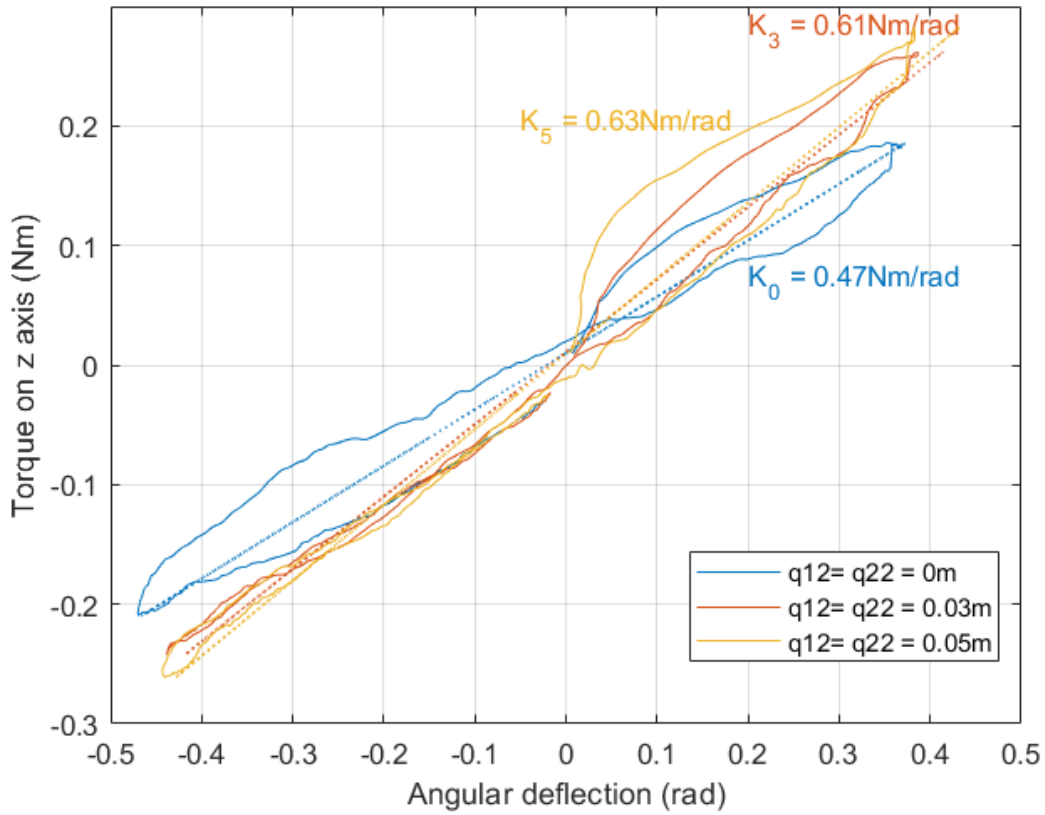

Figure 5.7: Output torque versus angular deflection of rubberband for various configurations of q_{12} and q_{22}

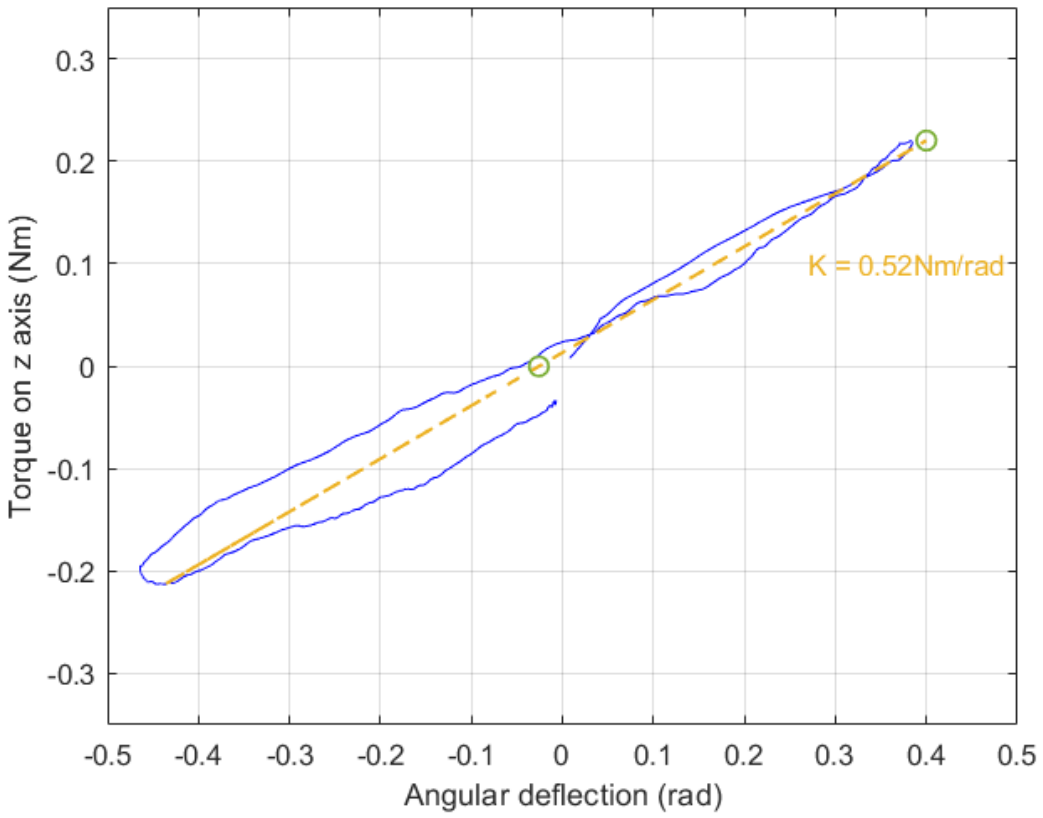

Figure 5.8: Output torque versus angular deflection for 1cm configuration with segmented stiffnesses

5.3.2 Simulated data

Simulation of nonlinear stiffness elastic element is performed in section 3.3 which can be used to compare the simulated and measured result. Apart from the additional objective, changing the type of elastic element to prove the mechanism performance, this comparison can assist on reflecting clues of factors behind the differences between the measured result and simulation. In figure 5.9, it is a extracted traces of some configurations (0, 0.02 and 0.05 m configuration) from figure 3.9 for the clear display of comparison. The simulated outcome shows the increment of stiffness (considering on steepness of traces) when the tension of the cable following the position of tensioning units grow. This means that the modulation of stiffness can be found when configuration has changed, similar to another results previous mentioned.

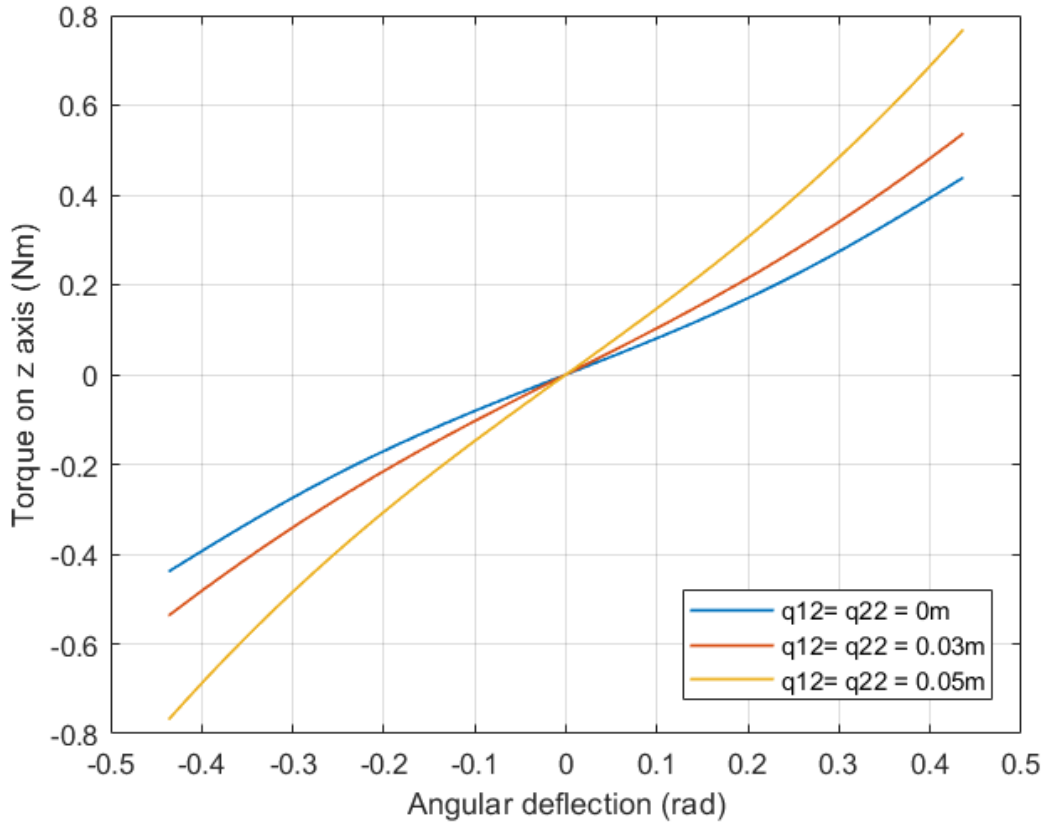

Figure 5.9: Torque-deflection plot of various configurations; 0m, 0.03m and 0.05m from non-linear stiffness elastic element simulation with the colored lines indicating each configuration

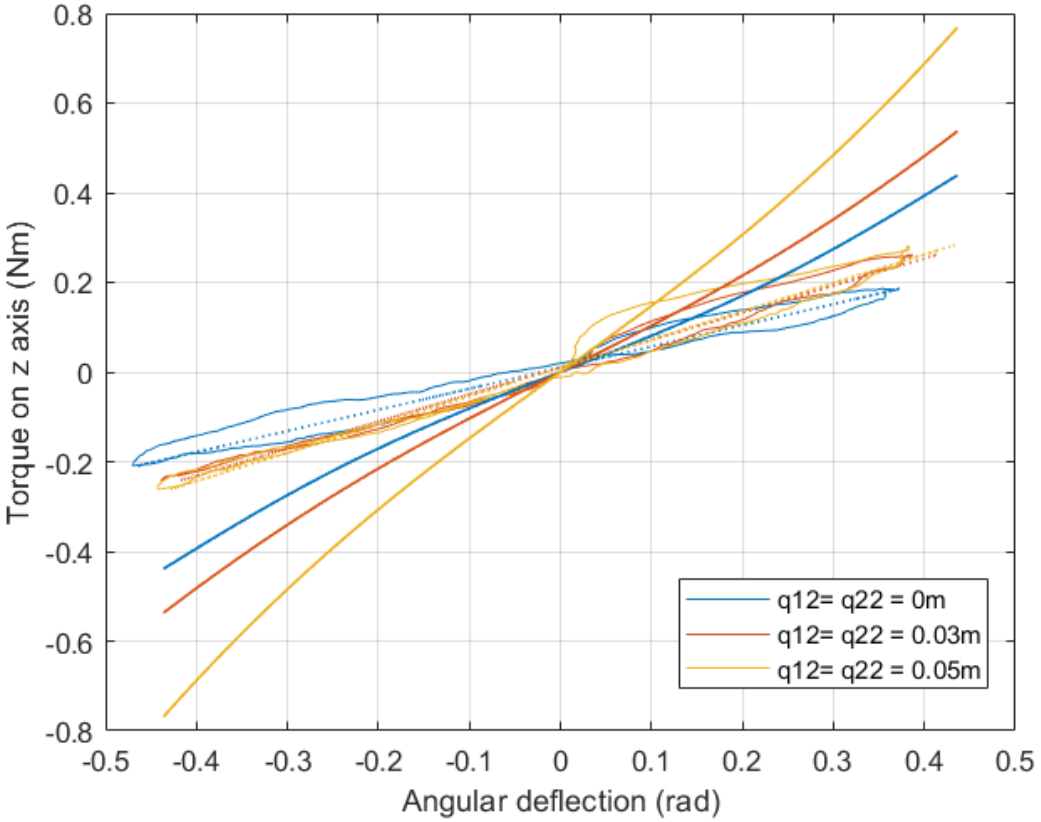

Figure 5.10: Torque-deflection plot of several configurations comparing between measurement and simulation for non-linear stiffness elastic element. The measured data are illustrated as an approximate linearized stiffness (dashed black lines). Simulated data are shown as solid curves.

Configuration (m)	**0**	**0.01**	**0.02**	**0.03**	**0.04**	**0.05**
MAE (Nm)	0.1619	0.1652	0.1784	0.2193	0.2489	0.3261

Table 5.2: Statistical results of comparison between measurement and simulation from non-linear stiffness elastic element showing with Mean Absolute Error (MAE)

When comparing both simulation and measurement outcomes, in figure 5.10, it can be seen the similarity of plots' pattern. The higher tension configuration shows higher steepness of stiffness of the outcomes. However, there is an appearance of difference on the magnitude of the traces on the same configuration like showing in linear stiffness elastic element (section 5.1.2). In statistical result, in table 5.2, MAE is calculated between the simulation and measurement for each configuration showing the range of 0.1619 - 0.3261 Nm. The low values of MAE show the minimal disparity when compare both results.

5.4 Energy injection of cable-driven VSM

As mentioned in objectives of this study, the energy injection of cable-driven VSM should be proved in the measurement. However, it could not be measured for individual current draw of each servo motor. Due to the limitation of servo motor, it has not provided port or wire that can connect the current sensor, only total current consumption of four servo motors can be acquired. Therefore, the energy injection which required individual current consumption to prove the compensation of energy injection could not be conclusive in this measurement.

Chapter 6

Discussions

As a proof of concept, to prove the cable-driven VSM has complied with the aforementioned objectives (following section 1.3), this study is preliminary validations of the conceptual system. The three measurements based on three objectives; $K = K_{desire}$, $\dot{\tau} = 0$ and $\int_0^t P_{control} \approx 0$, show persuasive working when considering on the outcomes. The variable stiffness property can bring the promising modulation of stiffness when compared with the simulation together with remaining output torque constant when output stiffness changed. Moreover, the cable-driven VSM also presents its variable stiffness property with an alternative elastic element. These indicate that the cable-driven VSM has the potential for the further development of VSA which is applicable for a specific feature, as an actuator for lower-arm based support exoskeleton. However, there are some remarks on the results and the limitations of this test bed which should be discussed following the presented outcomes. Therefore, the discussion of the results will be addressed first and following by the discussion of the test bed's limitations with suggestions of improvement.

On the variable stiffness property of the test bed, the measurements of the stiffness of both different elastic elements (springs and rubber bands) are taken into account. As it can be seen, the stiffness of cable-driven VSM can be varied as following its working principle on varying stiffness whether it used spring or rubber band as elastic components. The stiffness is changed when the tension of the cable is adjusted by the tensioning units. However, when focusing on the simulated and the measured result (figure 5.4), it is noticed that the dissimilarity of torque-deflection profile between both results on every configuration. One reason behind the difference of stiffness might be the offset of pulleys' radii. The simulation modelled the pulleys to be as points (zero radius). With this discrepancy of pulleys' dimensions, it deviates the kinematics of cable from both simulation and measurement, the width of pulleys in the test bed extends the length of cable resulting in slight different stiffness in output lever when performing the same configuration. The extension of cables' length causes an extra tension to test bed which leads the stiff-

ness of output to be higher than estimation (please refer to the mathematical model in section 2.2). The output torque drops for positive deflection and becomes higher for negative deflection. This shows contrary to a result even if it affects the difference. The difference of the stiffness is caused by radii, nonetheless; the marginal growth of stiffness is presented. Thereby, there might be another cause that lower the stiffness of the measurement instead of the offset from pulleys' radii. Another factor of this might be compliance of test bed, the material in the test bed, i.e., cable or output lever, also influences the output stiffness. For the cable, each cable has its individual properties including their compliance [23]. In this experimental setup, the string was chosen to be the test bed's cable. Unlike the test bed, in the simulation model, the rigid cable was applied. In addition, the output lever which was used for applying back and forth motion during the measurement can also cause less stiffness. Owing to the observation from the measurement, the output lever showed compliant under push and pull force. Be noticed that, the output lever was fabricated with Delrin, POM (polyoxymethylene) which is the polymer that has elasticity allows the deformation when exerts force. The long-shaped lever can be compliant with the applied force. Hence, the compliance of the actual test bed has more compliant than the model. This causes more stiff to the simulation than the test bed. Besides, one cause which might be worth to consider is the concurrent force. When applying force to the output interaction bar on the stiffness measurement, the interacted force might not completely transfer to be torque solely z-axis but also aberrate in the other axis. Therefore, the torque on z-axis which is the consequence was reduced. Lastly, the friction from the mechanism might also be a factor of this stiffness magnitude discrepancy. In this case, regarding the structure of the test bed, friction can be caused by the output which can lower the output torque when the output lever was rotated. One observation on the stiffness profile of measurements it can be noticed that some of the configurations have two stiffnesses. The stiffnesses can be found by the linearized line. On 0.01m, 0.02m and 0.03m configurations, the slope of the line which refers to stiffness show distinct slopes which are not followed linearized line at the angular deflection around 0.26 rad to 0.43 rad (15 deg to 25 deg) on three configurations. This dissimilarity can be found only for the measurements but not in the simulation. Owing to the fact that in some trials of the measurements, the spring was overextended and winded into the pulley. Hence, this differed the output torque which is the result of the length of cable showing alternatives of stiffness.

Another remark on stiffness characteristics is the dissimilarity of the plot profile between the simulated data and the measured data. As noticed the results (figure 5.4 and 5.10), the measured data exhibited the hysteresis loop in contrast with the simulation which showed the only curve. When looking at the statistical result, in table 5.1 and 5.2, low values of MAE are found for every configuration which re-

flect that the dissimilarities of both elastic element compared with simulations are marginal. However, the factors that caused this dissimilarity between the actual outcome from test bed and the estimated outcome from the simulation would be worth to discuss about. The explanation on this might be that the simulation was done without including some factors which could affect the actual working. In addition, hysteresis is often related to intrinsic energy storage. Thus, all of the factors which can dissipate the internal energy of the setup should play a role in this. With this reason, the aforementioned factors in the previous paragraph which affect on decreasing stiffness also influence the hysteresis. One factor which did not be considered in simulation is the friction of components in test bed. Since the simulation did not take the external force into account, the unexpected force from the friction causes a decrease of output torque and oscillate plots. The energy storage, therefore, is deferred by this. As mentioned before, the compliance of the cable which is modelled to be rigid has differed in the experimental setup. For that reason, the measured torque has diverged from the simulated aspect. Likewise, with modelling the pulleys to be points, the differences of a dimension slightly change the measured output by altering the length of cable. Perhaps, the effect of the type of stiffness element can also be included on this. As mentioned in 4, two measurements were done for stiffness modulation which used a different type of elastic materials; tensile spring for linear stiffness element and rubber band for nonlinear stiffness element. Although the main objective of both measurements is not for investigating this effect, the results can compare the differences. Apart from the amplitude difference of output torque, the hysteresis of both type reflects the difference. The nonlinear stiffness (rubber band) element shows wider range of hysteresis than the linear type which is metal tensile spring. Due to the fact that the rubber band has an intrinsic stiffness which metal spring has none. The intrinsic stiffness is the result of the structure of the material which also indicates the stiffness of material, i.e. how difficult to compress/stretch the material. The natural of rubber band's structure is a worm-like chain model allowing the material to stretch out easier than the metal. In consideration of these factors, as can be seen in section 2.2, these factors relate to affecting the internal energy. Thus, the hysteresis on measured data could be induced by them, unlike the simulated data which exclude these.

Referring to literature in chapter 1.1, [12], [13], [14] and [15], the result of modulation of stiffness showed the increment of tension on the cable influencing the raise of output stiffness. Zhou et al. [12] are selected for comparison with the reason that their design is similar to our work in term of design and mechanism. To compare with, our test bed shows a range of modulation from 1.13 Nm/rad to 1.64 Nm/rad with the stiffness changed by 45.13 %

which is lower than the result of Zhou et al. showing the range of 0.5 to 5 N/m,

900% of stiffness change. However, in our design, the angular position was limited at 0.43 to -0.43 rad. Even though the studies were designed by applying the cable-driven mechanism, each study has its own specific design varying by set-up dimension. Therefore, the results of the stiffness of our design has complied with the previous studies and can modulate the stiffness as desired. One limitation which another research found on affecting the stiffness characteristic is the unexpected force, i.e., friction or concurrent forces. Another factor is the cable type. As mentioned before, each cable has different properties which could cause tension of the cable. The aforementioned factors support the modulation of stiffness's result to be reliable.

When looking at the output angular position on stiffness varying, the result shows agreement to the expectation, maintaining output position. As shown in figure 5.5 and 5.6, the angular positions appear constant on every stiffness condition. However, there are small variations of angular position when looking at the angular displacement of both static and dynamic measurements (figure 5.5(C) and 5.6(C)). The static result shows marginal differences on every condition with the trend of angular displacement increasing when the applied load raise, except for the first condition. The reason behind this trend might be the actuation of tensioning units when varied stiffness. During the actuation, it might cause swing of the applied weight which is connected with the output lever by the cable. Thereby, this swing may affect the output lever rotating (deflecting in angular motion). The heavier load that applied on the setup induces the larger motion of the swing, reflecting the trend. On the other hand, the dynamic measurement presents greater deflection than the static measurement when comparing on the same condition. The same reason for the variation with the static measurement can be applicable to this, the relationship of the swing motion and the applied weight. Since the trajectories of the movable pulleys were moved continuously in periodic motion, the output lever was affected by this dynamic movement. The rotation of the output lever was observed minimal oscillation which seemed to be greater than the static measurement. Therefore, it reflects in the quantitative result as the variation of displacement for dynamics is greater than the statics. When looking back at dynamic measurements respecting the difference in each condition, the 0.2 and 0.3-Nm conditions present lower values than the 0.1 and 0.4-Nm conditions as stated in 5.6(C). In addition, a tendency can be seen in the bar chart, the increment of angular displacement can be found from 0.2Nm to 0.4Nm conditions except in the first condition (0.1Nm) showing a distinct result. It can be assumed that the cause of this might be from the actuation of servomotors. During the measurement, the servomotor with the applied trajectories exhibited a higher speed of driving than the static measurement. Consequently, the aggressiveness from the motor could affect the output lever on swinging around. With the lightness of the output lever, it can be easily disturbed. The heavier load

on output lever can provide more counterbalancing on this disturbance. However, as mentioned, the higher weight could also cause the larger swing of the load presenting the higher displacement.

In [12], the same measurement of varying stiffness while holding the load was done. On comparison, it was found that the outcome of the study was different, the corresponding angular position could not hold the initial position when stiffness was varied. The reason behind this difference might be the configuration of the mechanism. For comparison, the angular displacement from Zhou et al. [12] shows approximate 0.24-0.14 rad with 100g of a load when stiffness varying which is higher than the output displacement of every condition in our work presenting less than 0.0016 rad and 0.0033 rad for static and dynamic measurement. Although the design of [12] is similar to our design, the mechanism works slightly distinct. One of stiffness motor of their design is for pre-tensioning the elastic element since the study aimed to have two working modes, low and high range of stiffness. Thus, the goal of the measurement to holding the angular position while varying stiffness is modelled to be different.

Prior to moving in to the limitation of the cable-driven VSM, it would be helpful to discuss about the mechanism its operating principle. From the simulations in chapter 3, it established that which dimension parameters are influential or redundant in this mechanism. It is obvious that not all of tensioning units need to be included. The lower units (q_{11} and q_{21}) show trivial effect on modulating the stiffness of this mechanism reflecting redundant units for tensioning the cable. Contrastingly, the upper units (q_{12} and q_{22}) noticeably influence the stiffness output. However, the lower units are able to modulate the pattern of the output torque. For the lengths of a and b, they show the same trends exhibiting the longer length, the lower stiffness can be reachable. Whereas, c seems to be redundant for stiffness modulation, presents a constant stiffness. This might be because of the simulation was performed by moving only the upper tensioning units. Thus, c is expected to show non-influence on the stiffness unlike a and b which are directly related to the actuated tensioning units as depicted in figure 2.2. Changing the type of elastic element also affect the stiffness and torque output on their pattern and magnitude (not the capability of modulation). In terms of the magnitude of both variables depend on the stiffness of the elastic elements, the nonlinear stiffness material shows wider range of stiffness with nonlinearity pattern than linear stiffness element. When the default configuration is considered, the nonlinear stiffness material presents stiffness approximately 0.2 - 1.48 Nm/rad while the linear stiffness element shows range of 0.25-2 Nm/rad at $-\pi/2$ to $\pi/2$. Oppositely, for 0.05m configuration, the non-linear stiffness element has 1.5 - 3.4 Nm/rad whereas the liner stiffness material exhibits the range of 0.25 - 2.3 Nm/rad at $-\pi/2$ to $\pi/2$. As mentioned above in result discussion, the differ-

ent intrinsic stiffness of the elastic elements would be the reason for affecting the stiffness magnitude and pattern.

Considering the limitations of the cable-driven VSM test bed, there are few remarks that should be presented. The measurement of motor current might be the first remark. Although the outcomes of the current use (can be noticed in figure 5.5 and 5.6) seem to be agreeable on computing the energy consumption of the test bed, they are not accurate and sufficient to conclude the zero energy consumption objective. In the static measurement, the processed result exhibits proximate zero for the power usage which results in approximate zero energy consumption. Additionally, the measurement of current through the motors seems to be constant during the actuated pulleys trajectories. However, these current data are not the individual current use of each motor. Since the servo motor has limited support on the connecting port, the motors could not measure individual motor current. Therefore, the passive balancing of the internal energy which needs the individual motor current in calculation cannot be analysed. To overcome this issue, the substitution of the new motor which can provide the possibility of detecting the individual motor current can be done. Another restriction should be that in this test bed, the backdrivable motor was used. The backdrivability can cancel force from spring extension with the movable pulleys, much electric energy is required to hold the pulley in a certain place. However, in this setup, the backdrivability was designed to turn the motor into a generator creating electrical energy in the first idea. To solve this, the non-backdrivable motor can be replaced in the test bed. Another constraint of this test bed is the limited range of stiffness. In general, the actual application of VSA has to serve wider range for biorobotic feature. Therefore, the reachable range of stiffness should be considered in the further study. The mechanism can be redesigned based on the desired range of stiffness. the major limitation on stiffness modulation could be working space of tension unit. To increase the range of stiffness, the design which could couple and manipulate each tensioning unit motions by only one actuator might be an alternative which provides compactness and more working space of each unit. The possible future designs are presented in figure 6.1 and 6.2. For the simulation, some assumptions on the simulations can be improved, i.e, the offset from radii of the pulleys, cable's compliance or assumed friction, since the current simulation is still missing some actual setting parameters. One remark that should be included is the cable type. Owing to each cable has their own compliance, the study of cable that suits for the actual application might be interesting for further step.

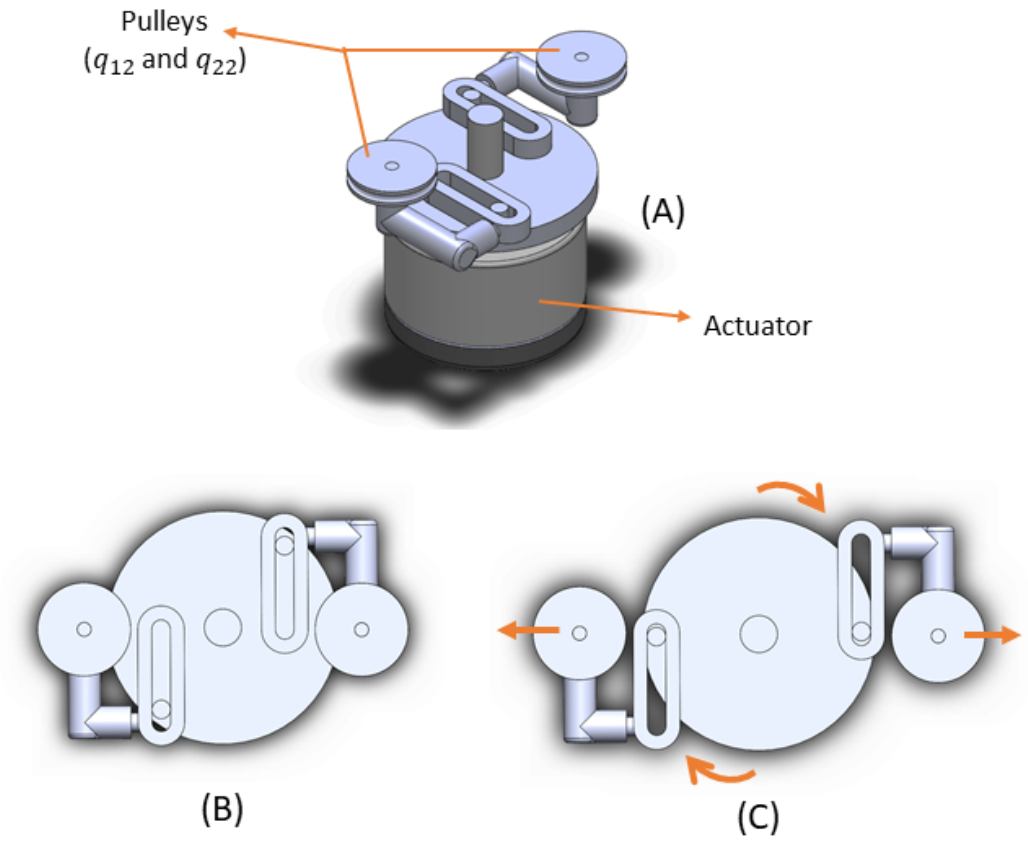

Figure 6.1: First conceptual design for future development. (A) Perspective view of tensioning unit,(B)Top view of tensioning unit and (C) Top view of tensioning unit when the actuator rotate resulting in tensioning action in translation

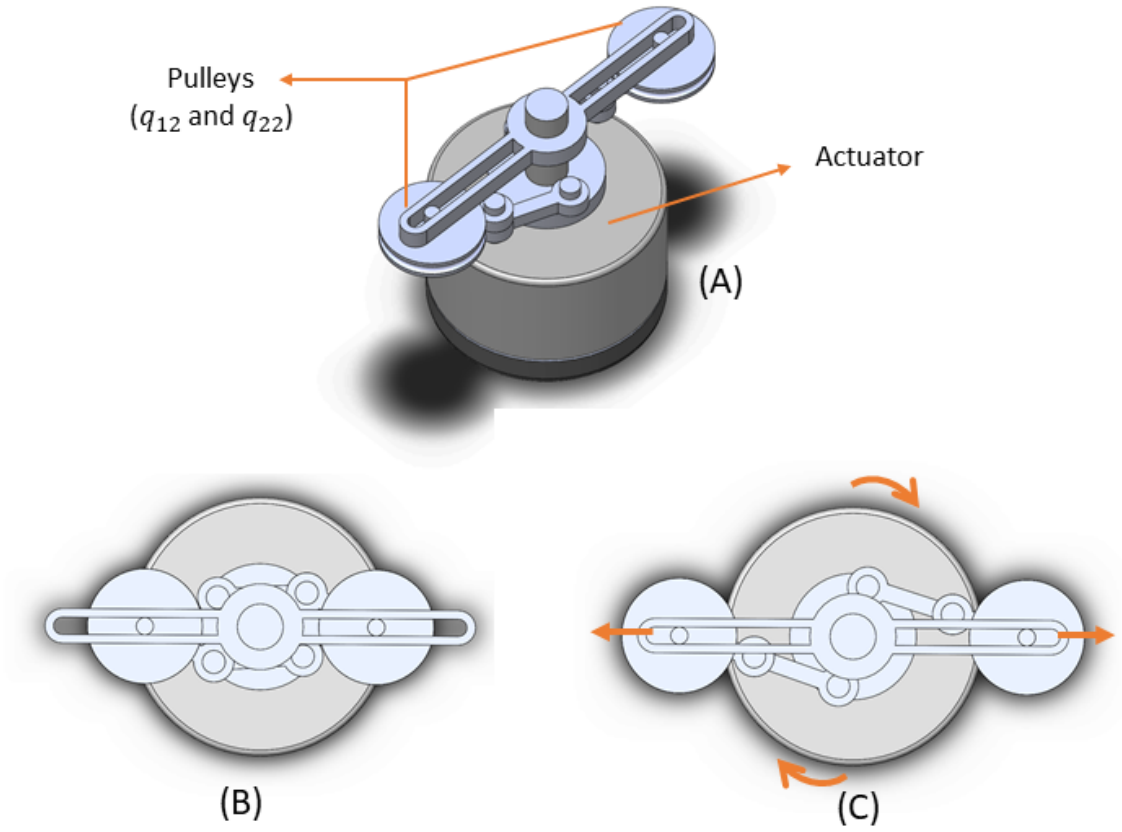

Figure 6.2: Second conceptual design for future development. (A) Perspective view of tensioning unit,(B) Top view of tensioning unit and (C) Top view of tensioning unit when the actuator rotate resulting in tensioning action in translation

Chapter 7

Conclusions and recommendations

In this chapter, the conclusions and the recommendations of this study are included. In the conclusion section, the study will be concluded from the aspect of the determined objectives. Thereafter, the suggestions on the future development of this project will be summarized based on the aforementioned remarks in Chapter 6.

7.1 Conclusions

As proof of the concept, the cable-driven VSM can achieve the objectives. With the objectives to apply this mechanism for supporting biorobotic applications, three theoretical working principles, i.e.,$K = K_{desire}$, $\dot{\tau} = 0$ and ensuring energy injection to the system is zero ($\int_0^t P_{control} \approx 0$), has been presented. A testbed of cable-driven VSM has been developed based on the model of system from the collaborated study. Measurements based on three main objectives were performed to demonstrate and validate the discoveries based on the theory.

Therefore, the result was shown that the modulation of stiffness, with the range of 1.13 Nm/rad to 1.64 Nm/rad, was exhibited proximate with the desired stiffnesses as follows the simulation (with mean absolute error range of 0.2779 - 0.3355 Nm). Moreover, the adaptability of stiffness while generating a constant torque was presented the output displacement less than 0.0016 rad and 0.0033 rad for static and dynamic measurement respectively when the stiffness changed by 45.13 % establishing the potential of the system for the expectation. However, further measurements for the objective of ensuring zero power consumption of the system should prove whether zero energy consumption is obtainable.

7.2 Recommendations

To improve the study, several remarks can be done as a future work. Recommendations are not only for the cable-driven VSM test bed development but also for overall study.

1. The further measurement of motor current should be done to prove the zero energy consumption is possible. Therefore, the alternative motor which can give the individual current use should be used.

2. The non-backdrivable motor should be substituted in the system preventing the possibility of unintentional movement of tensioning unit.

3. Further implementation of mechanism should be fulfilled, providing the desired stiffness range which suits the exo-skeletal application in term of performance and size.

4. the cable type used in the mechanism should be studied more. The property of each cable particularly the compliance affects the stiffness outcome. Therefore, the type of cable might be suited of the application.

5. the simulation can be included some parameters which affect the mechanism in actual set up, improving its realism which provide more efficiency on comparison or performance's simulation in the future.

For extensions of this study, two possibilities might be worth considering. One study would be the development of the cable-driven VSA. To complete the VSA, findings of this study based on both outcomes and recommendations can be adopted in developing and studying the VSA. To give a instance for developing cable-driven VSA, the possible designs (in figure 6.1 and 6.2) of variable stiffness mechanism which presented in 6 could be applied. These designs can provide more compactness to the future VSA, removing some redundant components and adding more range of working space and stiffness with the similar working principle. Thereafter, the lower-arm exoskeleton could be implemented with the cable-driven VSA, fulfilling the ultimate goal of the project.

Bibliography

[1] N. Hogan, "Adaptive control of mechanical impedance by coactivation of antagonist muscles," *IEEE Transactions on automatic control*, vol. 29, no. 8, pp. 681–690, 1984.

[2] S. Wolf and G. Hirzinger, "A new variable stiffness design: Matching requirements of the next robot generation," in *2008 IEEE International Conference on Robotics and Automation*. IEEE, 2008, pp. 1741–1746.

[3] T. Sonoda, Y. Nishida, A. A. F. Nassiraei, and K. Ishii, "Development of antagonistic wire-driven joint employing kinematic transmission mechanism," *Journal of Automation Mobile Robotics and Intelligent Systems*, vol. 4, pp. 62–70, 2010.

[4] S. A. Migliore, E. A. Brown, and S. P. DeWeerth, "Biologically inspired joint stiffness control," in *Proceedings of the 2005 IEEE international conference on robotics and automation*. IEEE, 2005, pp. 4508–4513.

[5] B. Vanderborght, A. Albu-Schäffer, A. Bicchi, E. Burdet, D. G. Caldwell, R. Carloni, M. Catalano, O. Eiberger, W. Friedl, G. Ganesh *et al.*, "Variable impedance actuators: A review," *Robotics and autonomous systems*, vol. 61, no. 12, pp. 1601–1614, 2013.

[6] R. v. Ham, T. Sugar, B. Vanderborght, K. Hollander, and D. Lefeber, "Compliant actuator designs," *IEEE Robotics & Automation Magazine*, vol. 3, no. 16, pp. 81–94, 2009.

[7] G. Grioli, S. Wolf, M. Garabini, M. Catalano, E. Burdet, D. Caldwell, R. Carloni, W. Friedl, M. Grebenstein, M. Laffranchi *et al.*, "Variable stiffness actuators: The users point of view," *The International Journal of Robotics Research*, vol. 34, no. 6, pp. 727–743, 2015.

[8] M. Azadi, S. Behzadipour, and G. Faulkner, "Antagonistic variable stiffness elements," *Mechanism and Machine Theory*, vol. 44, no. 9, pp. 1746–1758, 2009.

[9] J. Guo and G. Tian, "Conceptual design and analysis of four types of variable stiffness actuators based on spring pretension," *International Journal of Advanced Robotic Systems*, vol. 12, no. 5, p. 62, 2015.

[10] N. L. Tagliamonte, F. Sergi, D. Accoto, G. Carpino, and E. Guglielmelli, "Double actuation architectures for rendering variable impedance in compliant robots: A review," *Mechatronics*, vol. 22, no. 8, pp. 1187–1203, 2012.

[11] F. Petit, M. Chalon, W. Friedl, M. Grebenstein, A. Albu-Schäffer, and G. Hirzinger, "Bidirectional antagonistic variable stiffness actuation: Analysis, design & implementation," in *2010 IEEE International Conference on Robotics and Automation*. IEEE, 2010, pp. 4189–4196.

[12] X. Zhou, S.-k. Jun, and V. Krovi, "A cable based active variable stiffness module with decoupled tension," *Journal of Mechanisms and Robotics*, vol. 7, no. 1, p. 011005, 2015.

[13] Q. Boehler, S. Abdelaziz, M. Vedrines, P. Poignet, and P. Renaud, "From modeling to control of a variable stiffness device based on a cable-driven tensegrity mechanism," *Mechanism and Machine Theory*, vol. 107, pp. 1–12, 2017.

[14] J. L. Martínez, J.-L. Blanco, D. G. Vallejo, J. Torres, and A. G. Fernández, "Avastt: A new variable stiffness actuator with torque threshold," in *ROBOT2013: First Iberian Robotics Conference*. Springer, 2014, pp. 573–583.

[15] S. Yeo, G. Yang, and W. Lim, "Design and analysis of cable-driven manipulators with variable stiffness," *Mechanism and Machine Theory*, vol. 69, pp. 230–244, 2013.

[16] S. S. Groothuis, G. Rusticelli, A. Zucchelli, S. Stramigioli, and R. Carloni, "The variable stiffness actuator vsaut-ii: Mechanical design, modeling, and identification," *IEEE/ASME transactions on mechatronics*, vol. 19, no. 2, pp. 589–597, 2013.

[17] M. Fumagalli, E. Barrett, S. Stramigioli, and R. Carloni, "The mvsa-ut: A miniaturized differential mechanism for a continuous rotational variable stiffness actuator," in *2012 4th IEEE RAS & EMBS International Conference on Biomedical Robotics and Biomechatronics (BioRob)*. IEEE, 2012, pp. 1943–1948.

[18] A. Jafari, H. Q. Vu, and F. Iida, "Determinants for stiffness adjustment mechanisms," *Journal of intelligent & robotic systems*, vol. 82, no. 3-4, pp. 435–454, 2016.

[19] P. Breedveld, “Port-based modelling of multidomain physical systems in terms of bond graphs,” in *Simulation Techniques for Applied Dynamics*. Springer, 2008, pp. 141–190.

[20] R. Carloni, L. C. Visser, and S. Stramigioli, “Variable stiffness actuators: A port-based power-flow analysis,” *IEEE Transactions on Robotics*, vol. 28, no. 1, pp. 1–11, 2011.

[21] L. C. Visser, R. Carloni, and S. Stramigioli, “Variable stiffness actuators: A port-based analysis and a comparison of energy efficiency,” in *2010 IEEE International Conference on Robotics and Automation*. IEEE, 2010, pp. 3279–3284.

[22] ——, “Energy-efficient variable stiffness actuators,” *IEEE Transactions on Robotics*, vol. 27, no. 5, pp. 865–875, 2011.

[23] S. Grosu, C. Rodriguez-Guerrero, V. Grosu, B. Vanderborght, and D. Lefeber, “Evaluation and analysis of push-pull cable actuation system used for powered orthoses,” *Frontiers in Robotics and AI*, vol. 5, p. 105, 2018.

Appendix A

Nonlinear stiffness elastic element's tensile profile

In this appendix, the profile of tensile force- elongation plot of the nonlinear elastic element is shown. To ensure that the elastic material for substituting the spring in the test bed has non-linear stiffness, the rubber band which is chosen as a replacement is measured the tensile strength. The measurement is done with the tensile testing machine from 0m to 0.1m elongation of the material. The tensile testing is selected for obtaining the tensile profile since the elastic elements in the test bed is also stretched regards to its task. Therefore, the result of this test is shown below in figure A.1. In figure A.1, the rubber band is elongated from 0m to 0.1m. The tensile force increases non-linearly from zero to approximate 8.5 N. In figure A.2 presents the basic dimension of the rubber band; thickness, width and length, which are 1.3 mm, 1.35 mm and 25mm, respectively.

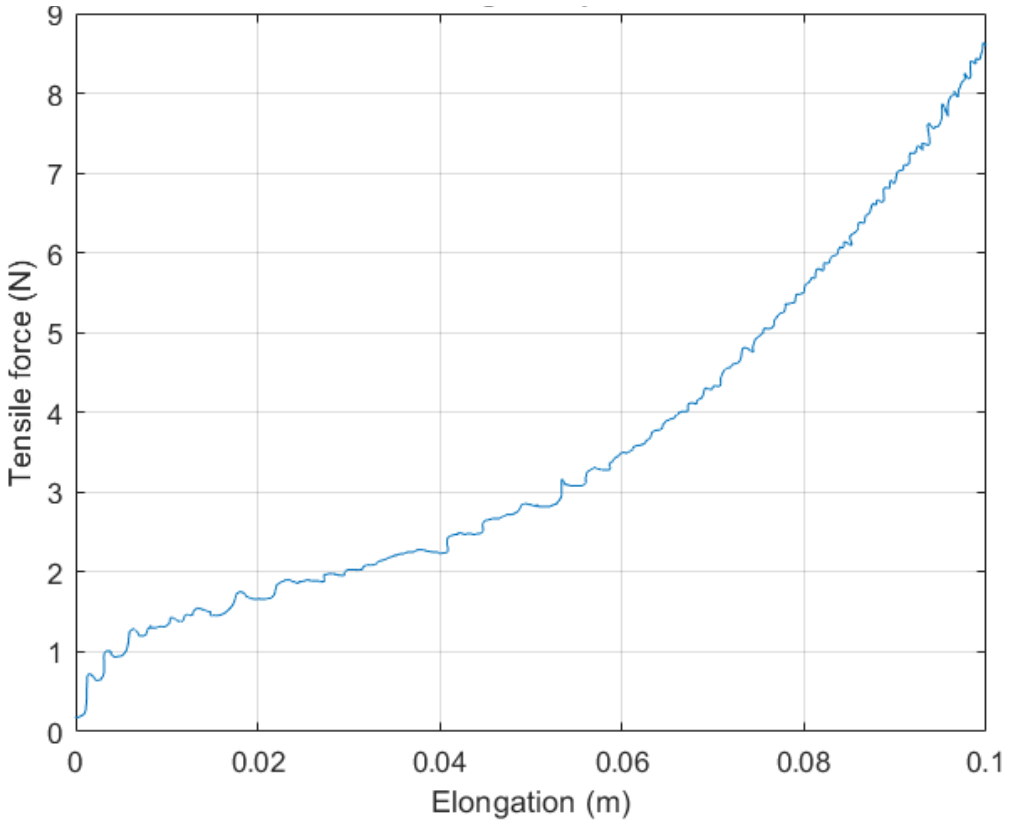

Figure A.1: Tensile force- elongation plot of the chosen rubber band is presented. The measurement was done with the range of elongation of material from 0m to 0.1m.

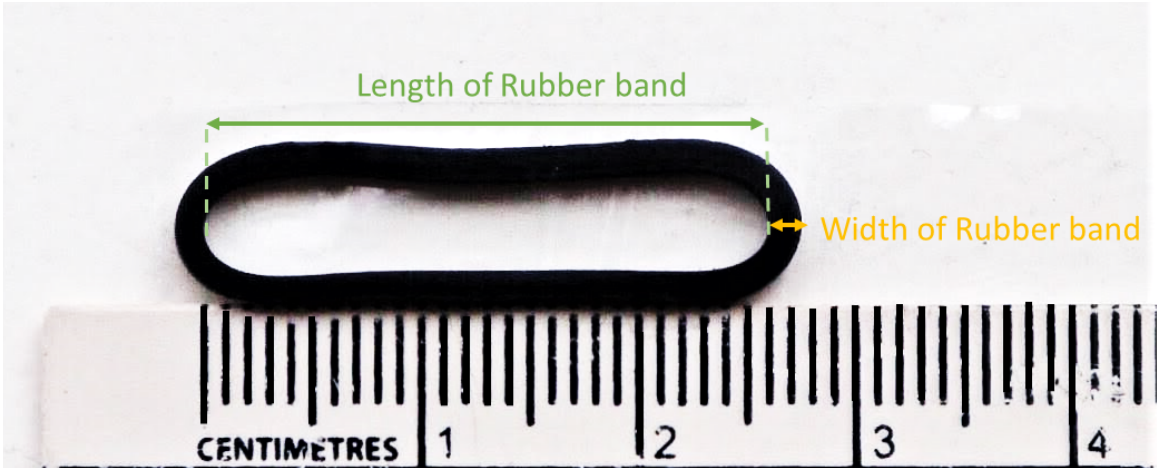

Figure A.2: The dimension of the chosen rubber band. The length shows 25 mm long. The width is 1.35 mm with the thickness of 1.3 mm. Noted that, in this figure , the thickness is obscure.

Appendix B

Torque and stiffness from measurements

All torque-deflection and stiffness profiles from the linear and nonlinear stiffness elastic element are exhibited in this appendix. The modulation of stiffness which is presented as the overlaid torque-deflection plot is shown in addition to the individual torque-deflection plot for every configuration. The torque-deflection plots are averaged data from 5 measurement trials for each configuration.

B.1 Modulation of stiffness and torque from linear stiffness elastic element

In figure B.1, it can be seen that the modulation of stiffness can be found together with hysteresis. The stiffness is altered when the cable has more tension by changing the tensioning units configuration.

The torque- deflection plots of each configuration are shown below. On each plot, the averaged data of torque and angular deflection which acquired from the five measurements is exhibited with the labelled stiffness and stiffnesses in some cases.

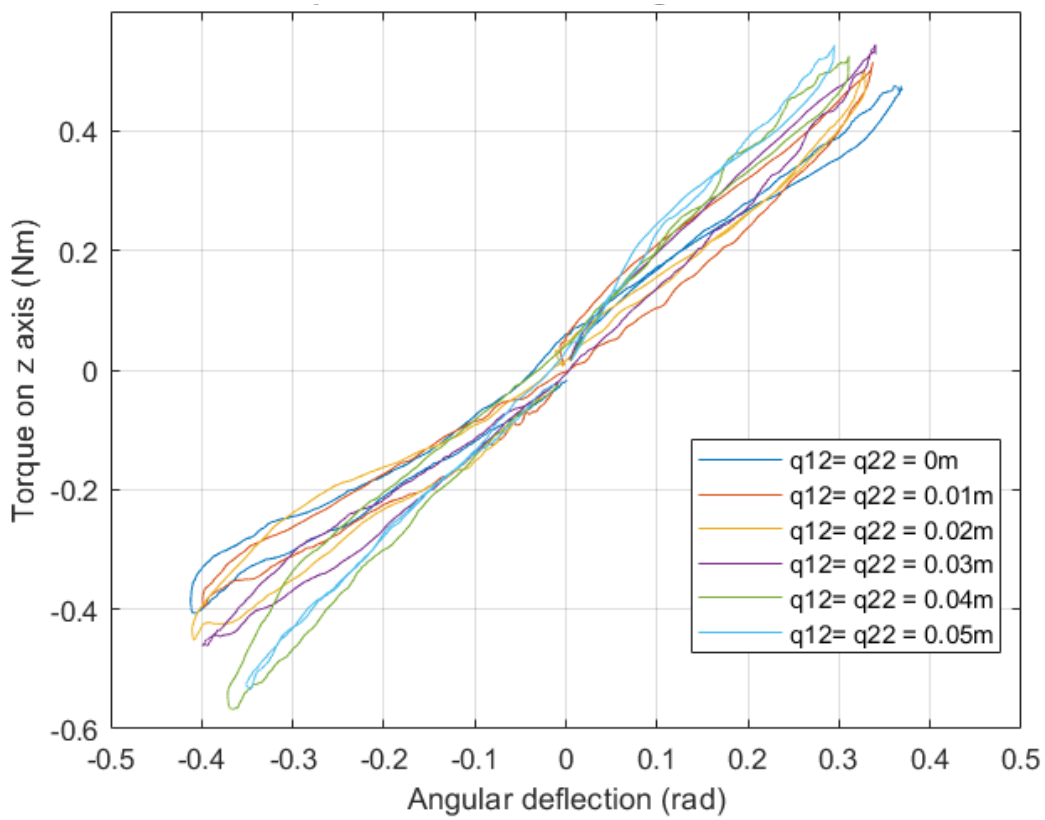

Figure B.1: The modulation of stiffness which presented as the overlaid torque-deflection plot. Each configuration is labelled by colors

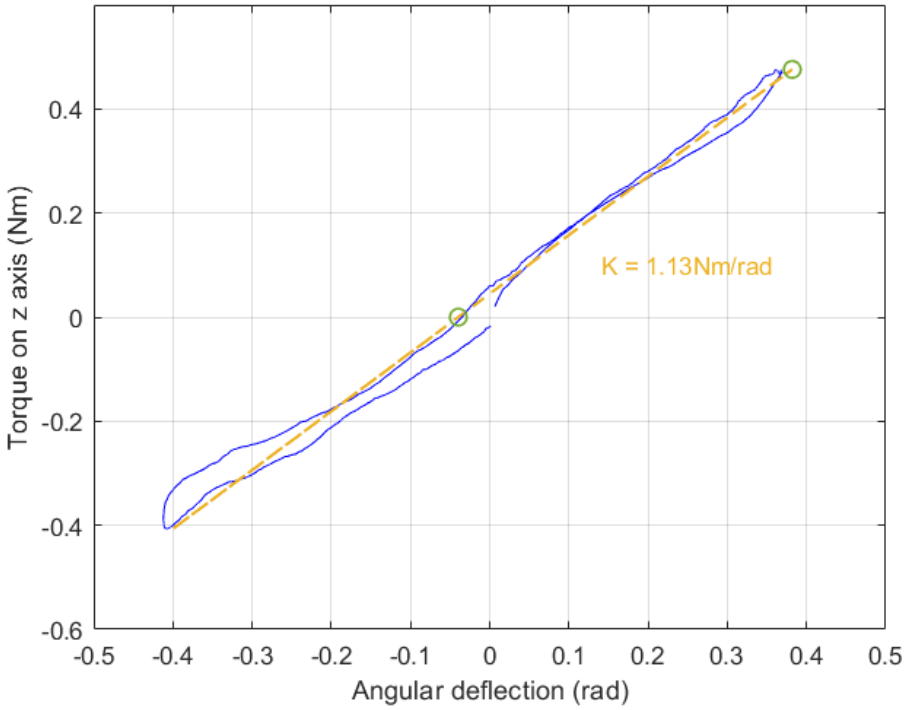

Figure B.2: Torque-deflection plot of 0m configurations from measurements.

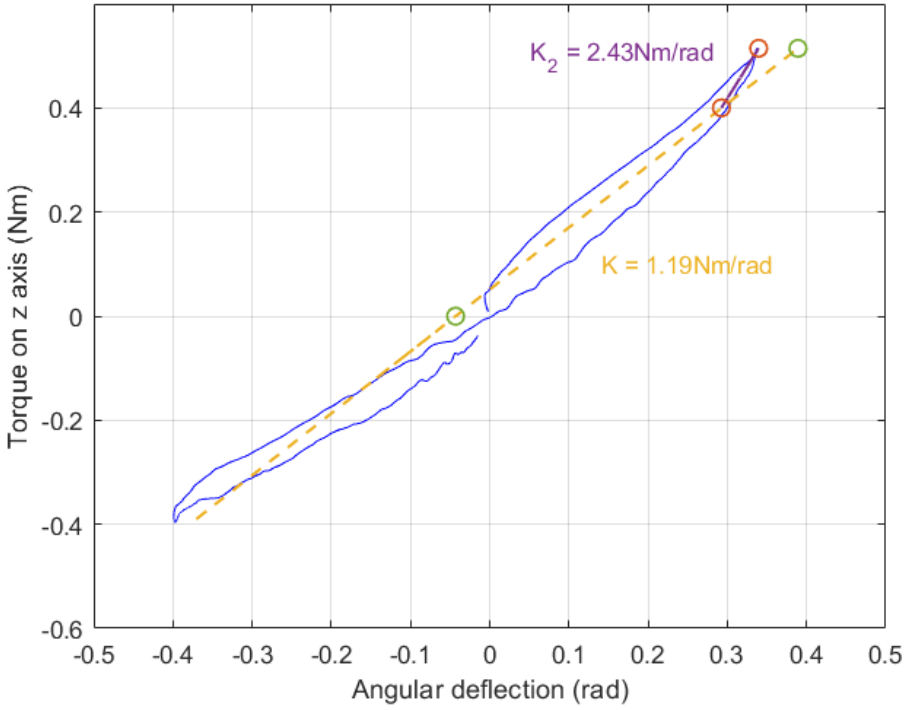

Figure B.3: Torque-deflection plot of 0.01m configurations from measurements.

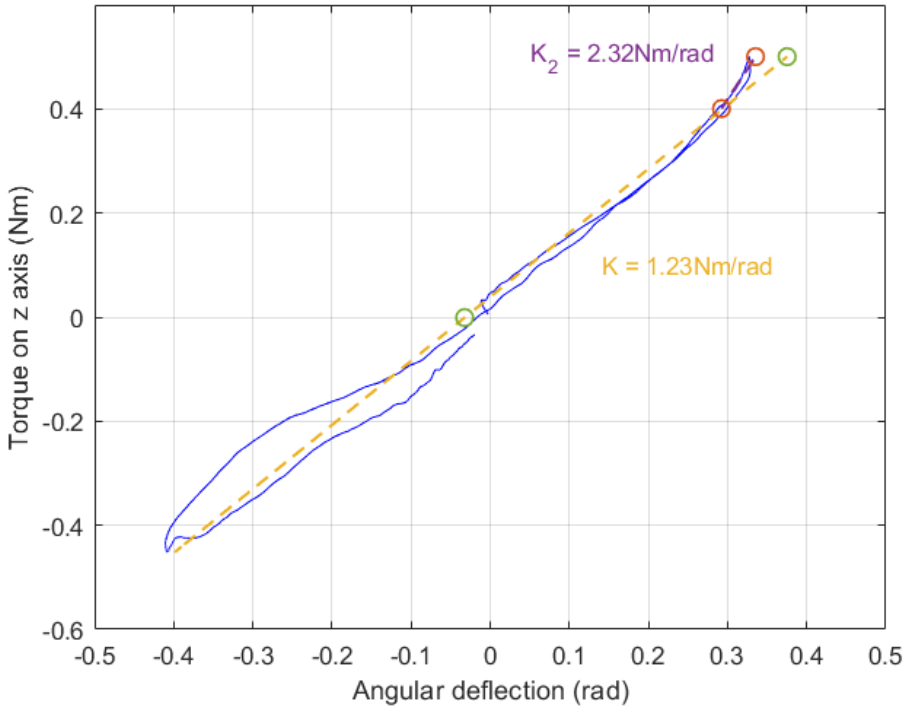

Figure B.4: Torque-deflection plot of 0.02m configurations from measurements.

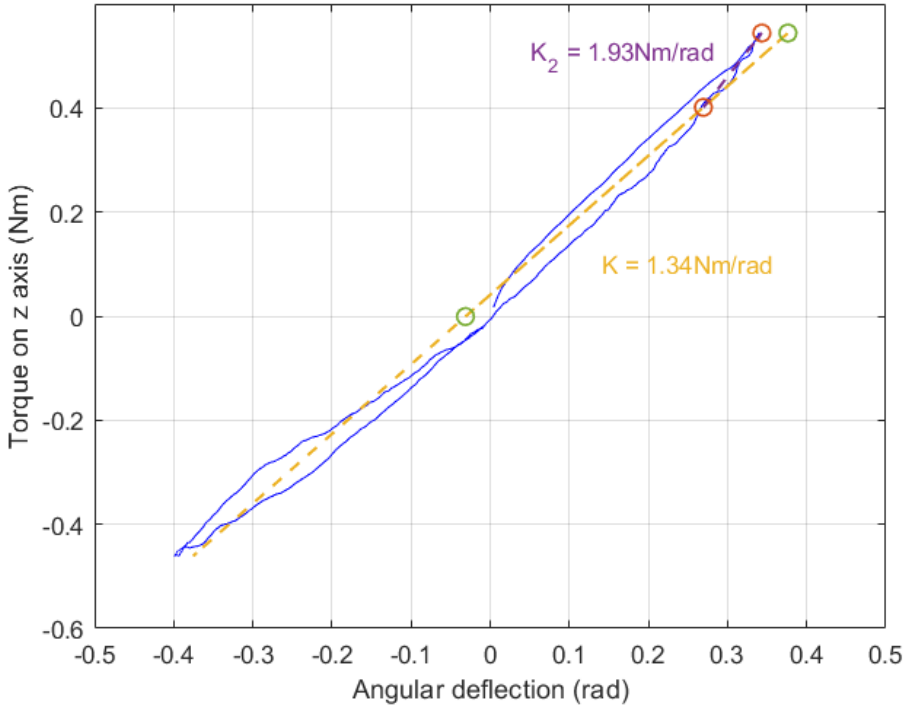

Figure B.5: Torque-deflection plot of 0.03m configurations from measurements.

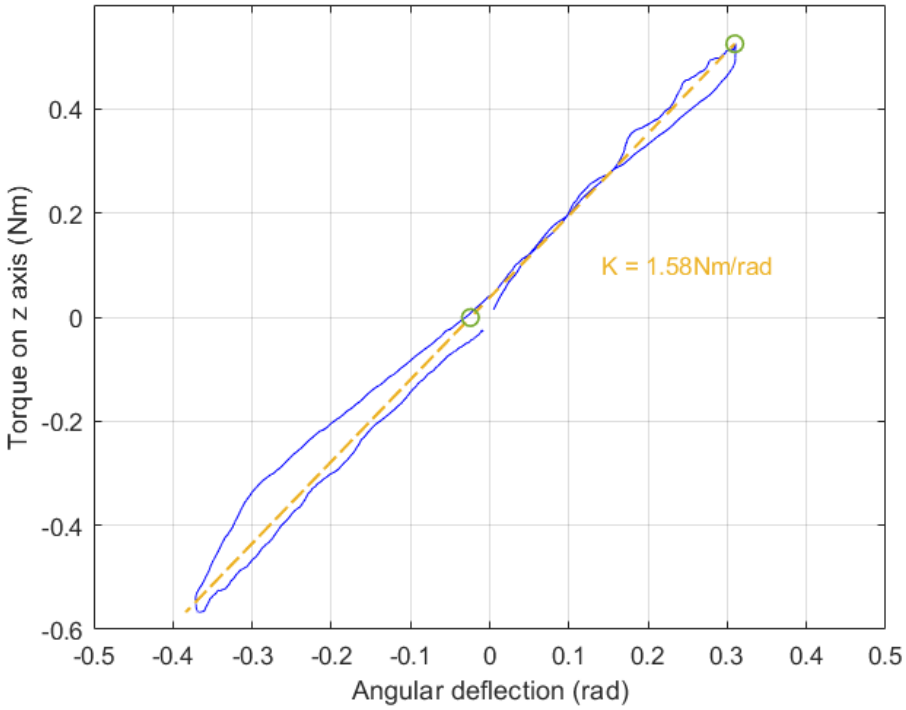

Figure B.6: Torque-deflection plot of 0.04m configurations from measurements.

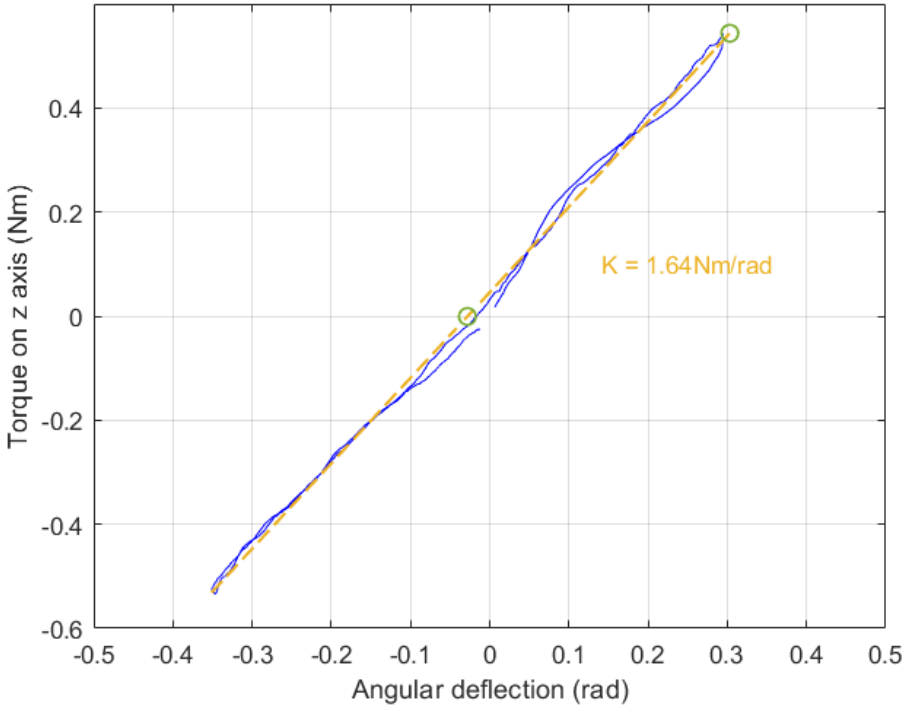

Figure B.7: Torque-deflection plot of 0.05m configurations from measurements.

B.2 Modulation of stiffness and torque from nonlinear stiffness elastic element

In figure B.8, the modulation of stiffness can be noticed together with hysteresis. By changing the tensioning unit's configuration, The stiffness is altered when the cable has more tension. The stiffness and torque magnitude is different due to the property of stiffness is changed. Moreover, the hystereses are also altered, wider hysteresis when compared with linear stiffness material.

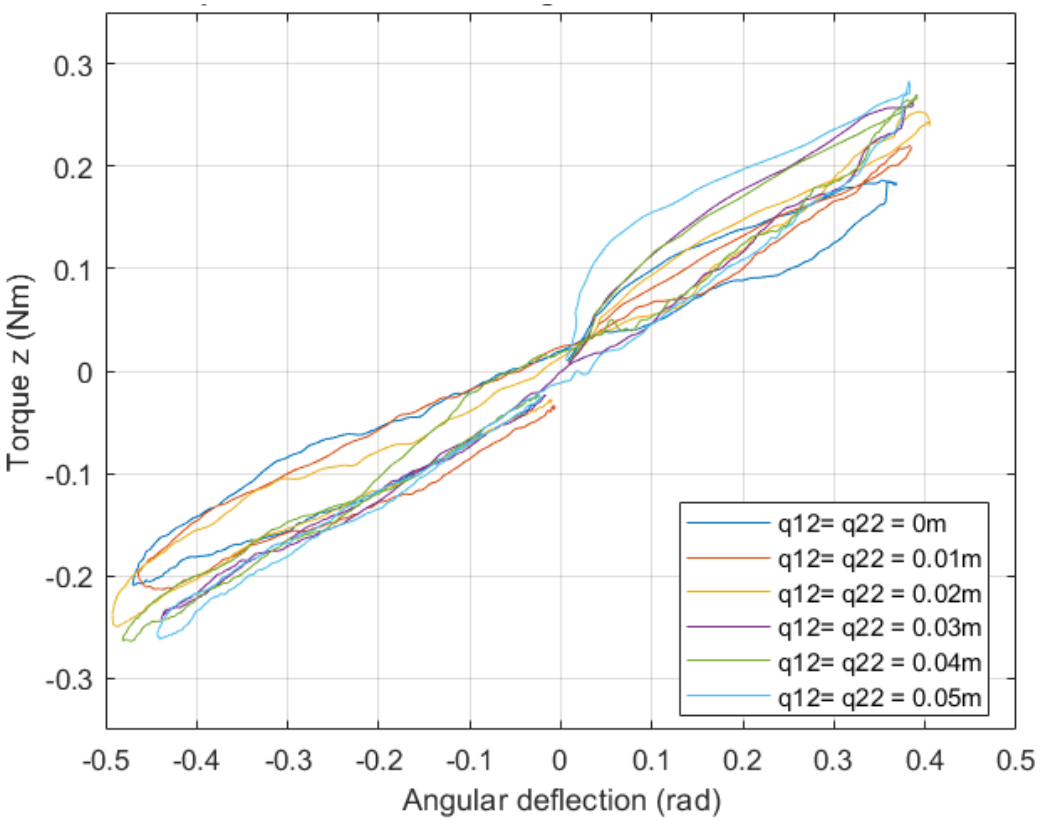

Figure B.8: The modulation of stiffness which presented as the overlaid torque-deflection plot from nonlinear stiffness element. Each configuration is labelled by colors

The torque- deflection plots of each configuration are shown below which are results from the five measurements showing in the averaged data of torque and angular deflection, exhibited with the labelled stiffness and stiffnesses in some cases.

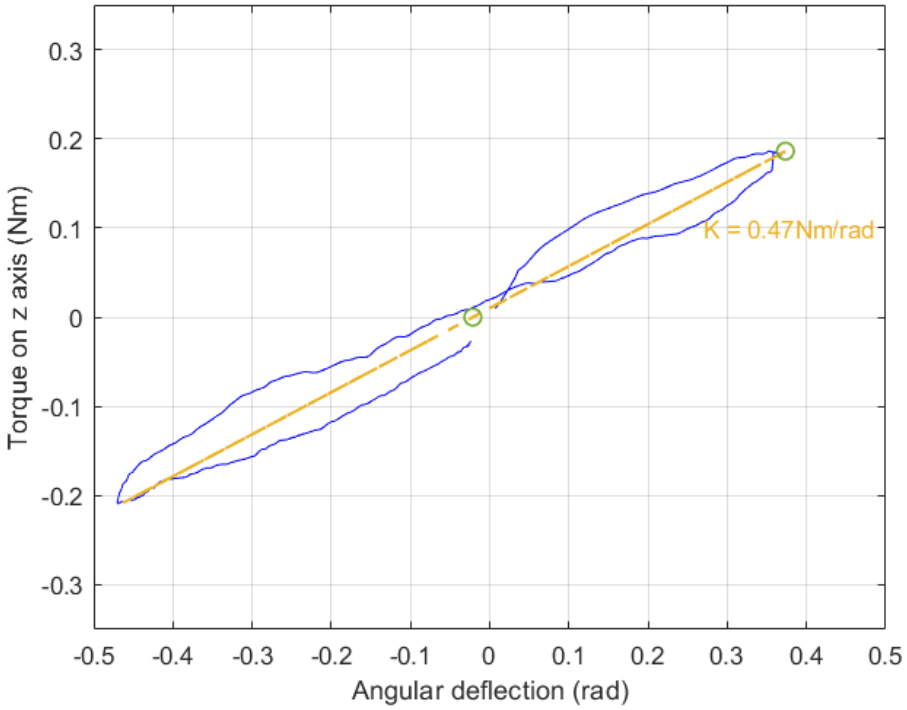

Figure B.9: Torque-deflection plot of 0m configurations from nonlinear stiffness element measurements.

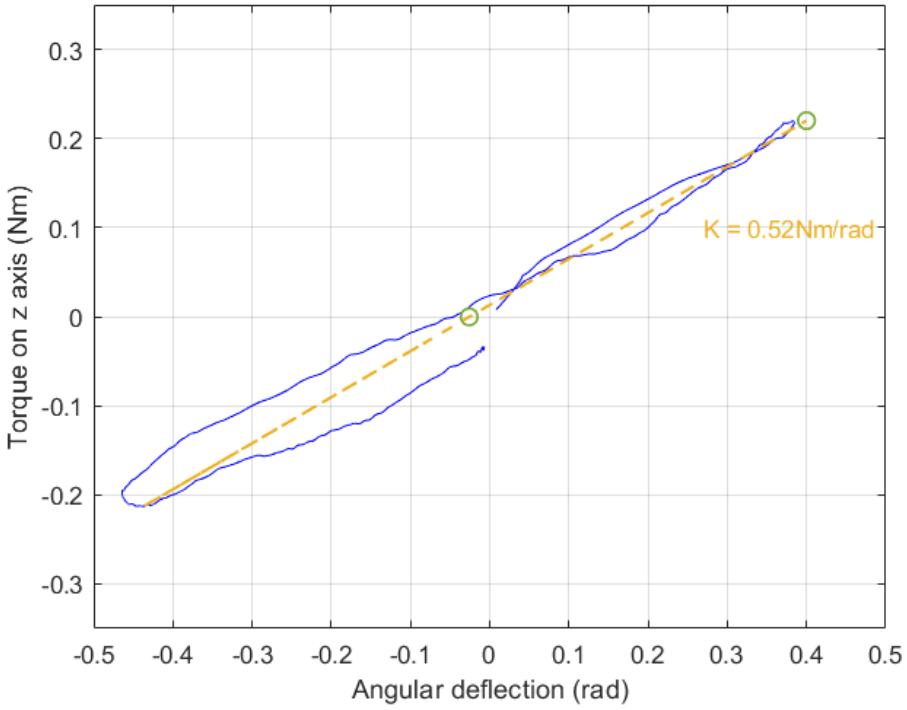

Figure B.10: Torque-deflection plot of 0.01m configurations from nonlinear stiffness element measurements.

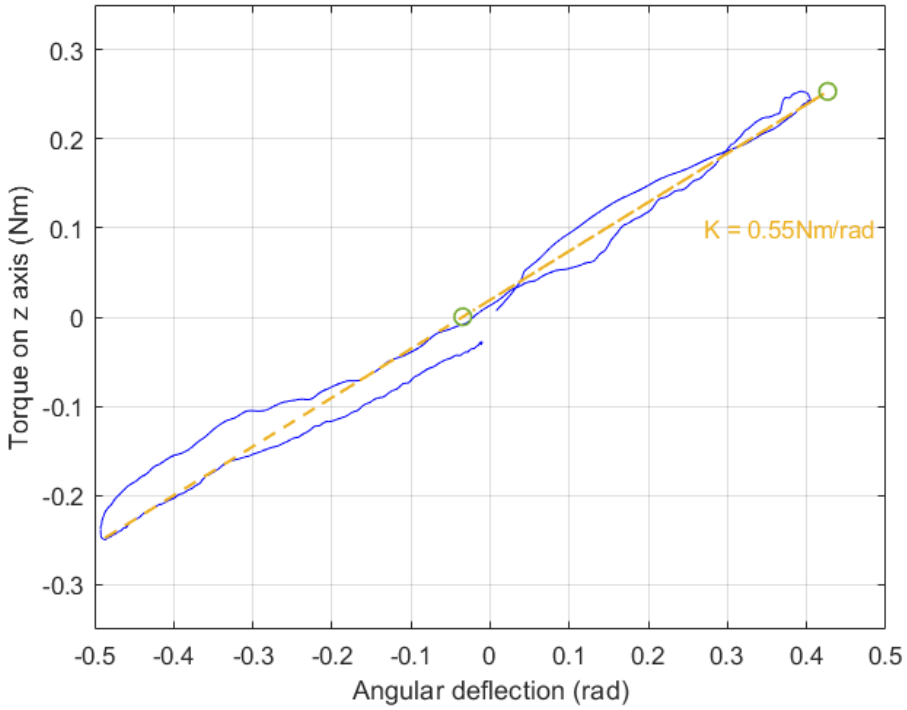

Figure B.11: Torque-deflection plot of 0.02m configurations from nonlinear stiffness element measurements.

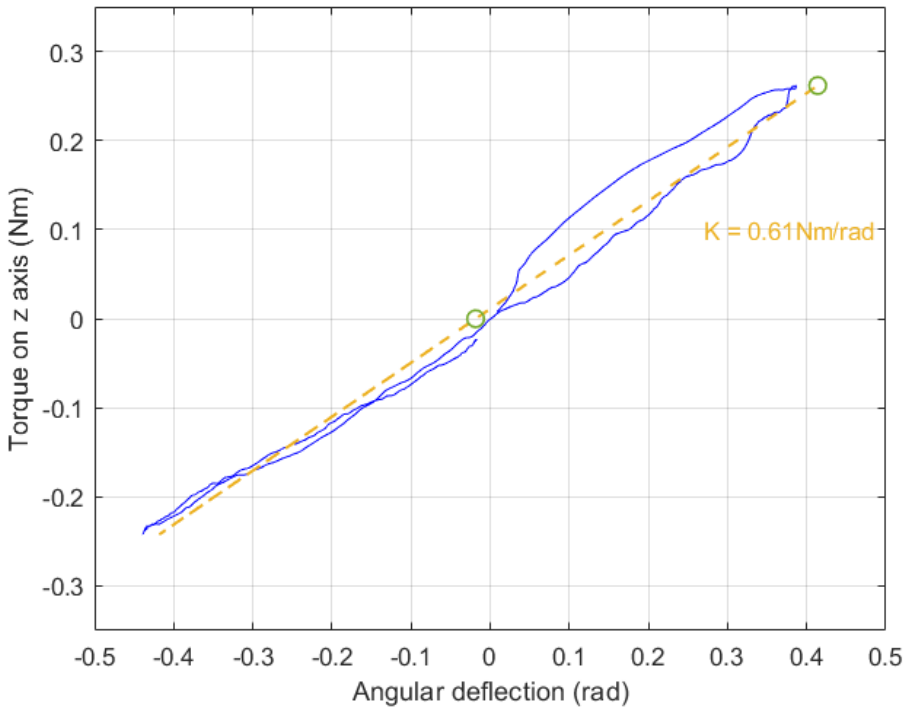

Figure B.12: Torque-deflection plot of 0.03m configurations from nonlinear stiffness element measurements.

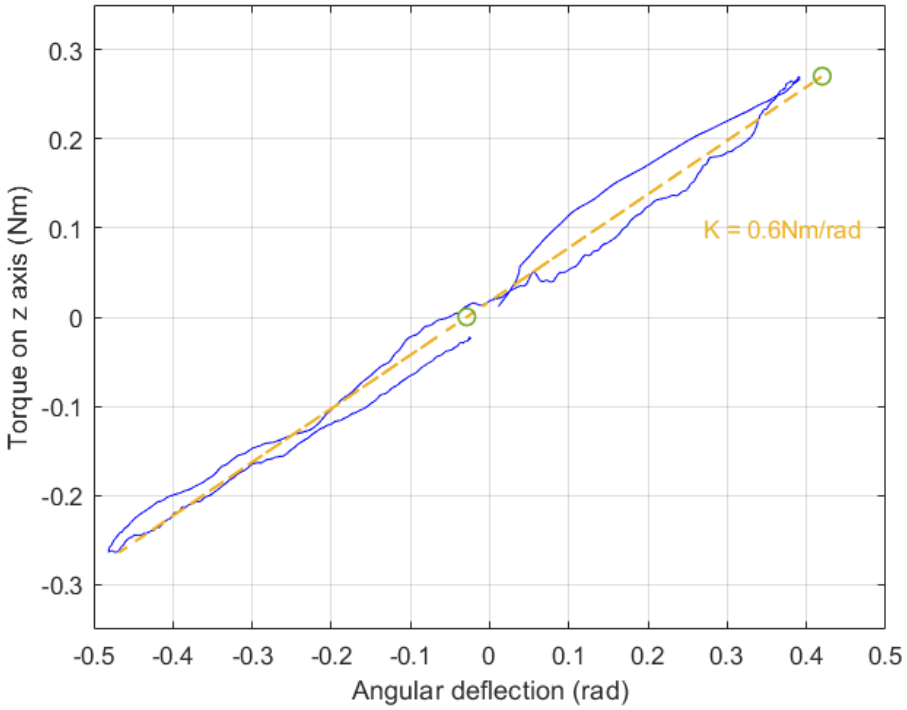

Figure B.13: Torque-deflection plot of 0.04m configurations from nonlinear stiffness element measurements.

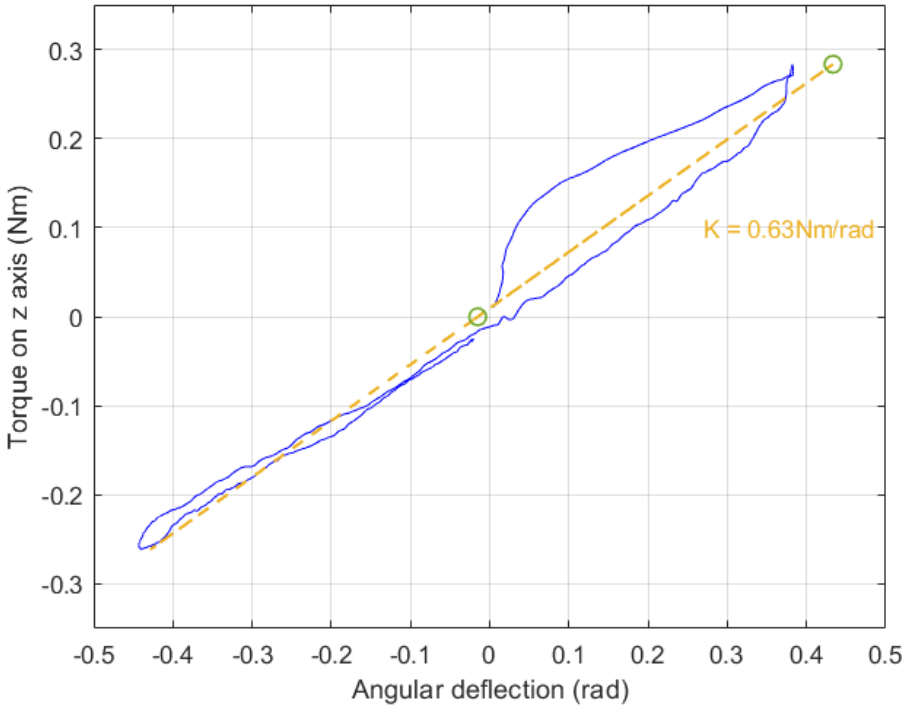

Figure B.14: Torque-deflection plot of 0.05m configurations from nonlinear stiffness element measurements.

Appendix C

CAD of the cable-driven variable stiffness mechanism test bed

In this appendix, the CAD of the cable-driven variable stiffness mechanism is shown for clarifying the prototype mechanical design. In figure C.1, the overview of the prototype is presented in different views; (A) the isometric view, (B) top view and (C) front view. In addition, since the tensioning unit plays a big role in this mechanism, varying the output stiffness. In figure C.2, different perspectives of the unit are exhibited; (A) isometric view, (B) top view and (C) front view. As can be seen, the output in figure C.1 show unclear the components in the output. In figure C.3, the close-up view of output in various perspectives are shown; (A) isometric view, (B) top view and (C) front view.

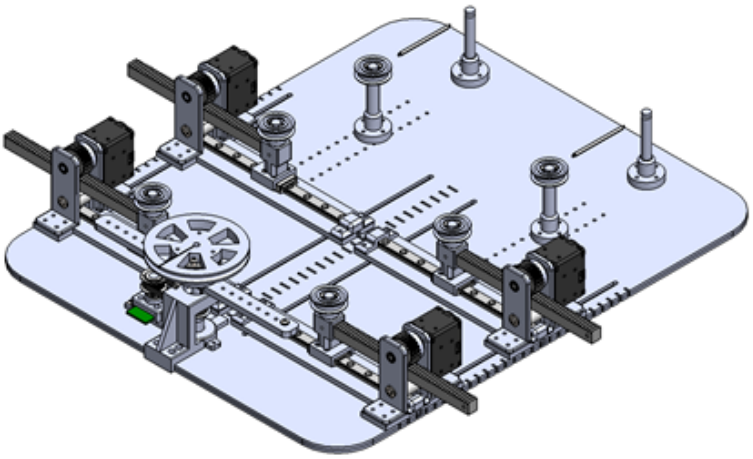

(A)

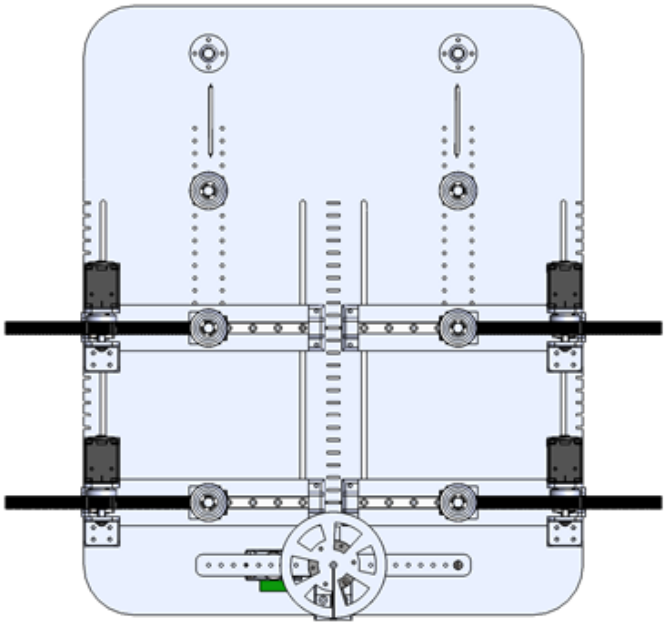

(B)

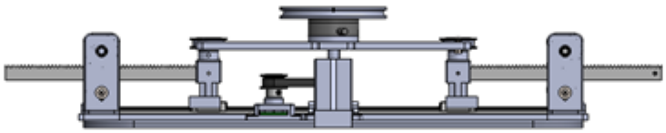

(C)

Figure C.1: CAD of protytype with 1:5 scale;(A) the isometric view, (B) top view and (C) front view

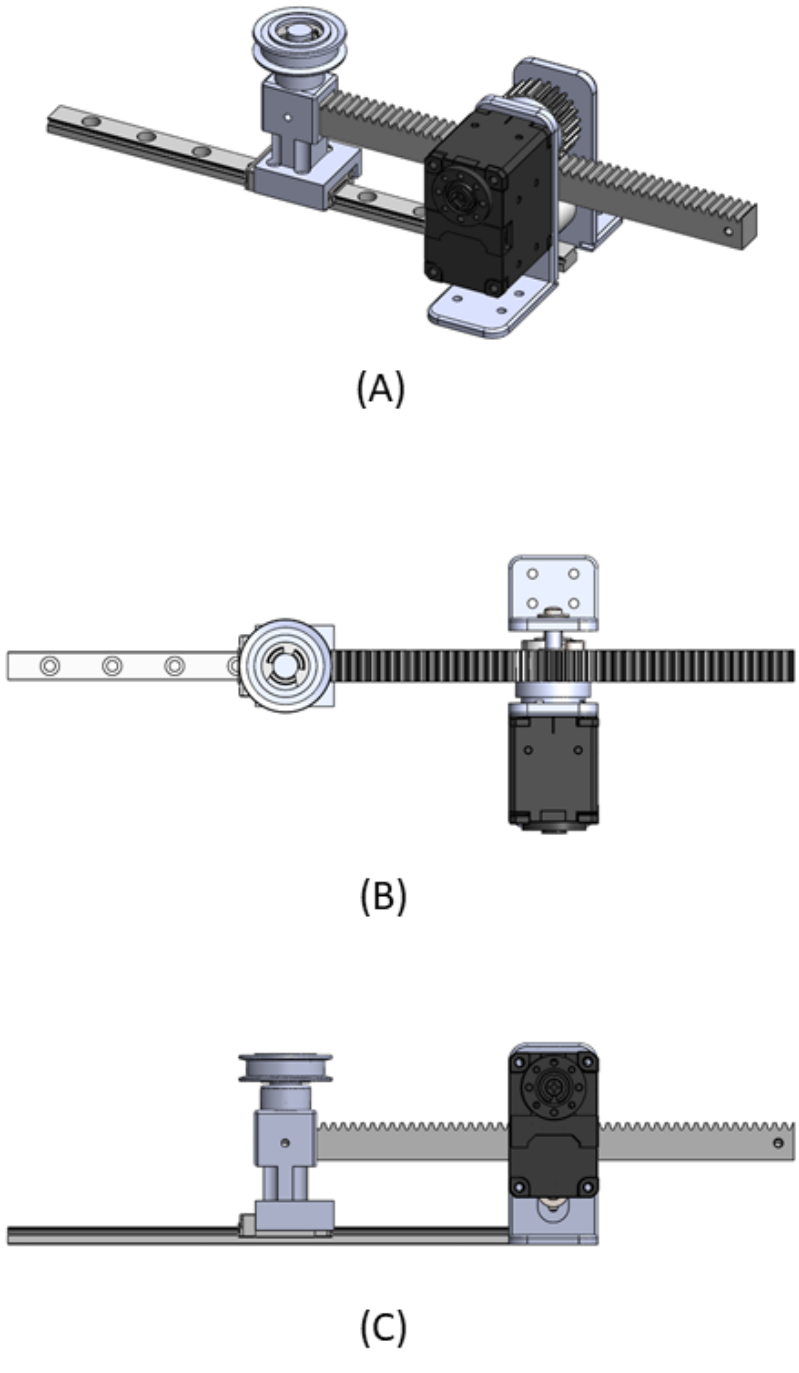

Figure C.2: CAD of tensioning unit part with 1:2 scale;(A) the isometric view, (B) top view and (C) front view

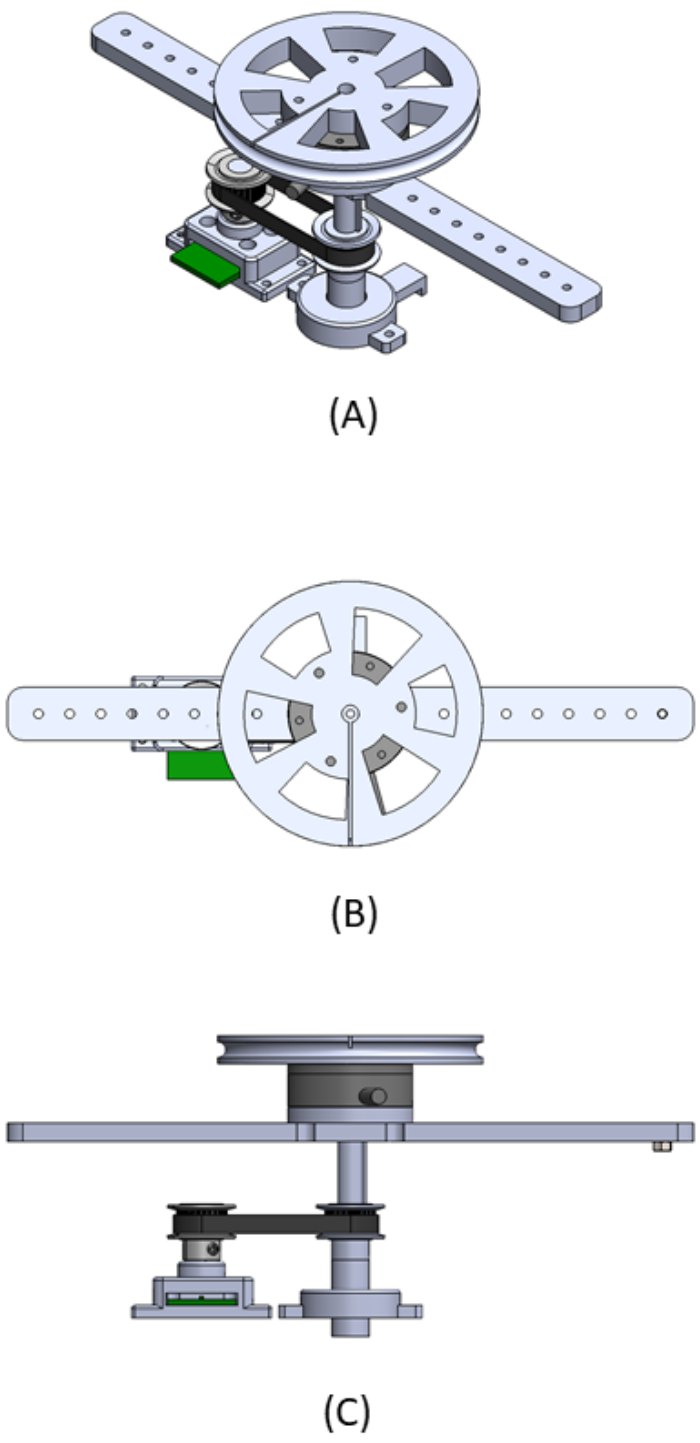

Figure C.3: CAD of output in close-up showing in front view with 1:2 scale;(A) the isometric view, (B) top view and (C) front view